Scholars' Mine

Fall 2007

Quantum dot photolithography

Raghuveer Reddy Gadipalli

Recommended Citation

QUANTUM DOT PHOTOLITHOGRAPHY

by

RAGHUVEER REDDY GADIPALLI

A DISSERTATION

Presented to the Faculty of the Graduate School of the

UNIVERSITY OF MISSOURI-ROLLA

In Partial Fulfillment of the Requirements for the Degree

DOCTOR OF PHILOSOPHY

in

PHYSICS

2007

_____   _____
Massimo F. Bertino, Advisor   John G. Story

_____   _____
George D. Waddill   Alexey G. Yamilov

_____
Nicholas Leventis

PUBLICATION DISSERTATION OPTION

This dissertation has been prepared in the style used by <u>Applied Physics Letters</u>, <u>Journal of Sol-Gel Science and Technology</u>, <u>Nanotechnology</u> and <u>Nano Letters</u>. Pages 40-50 have been published in <u>Applied Physics Letters</u>. Pages 51-91 have been published in <u>Journal of Sol-Gel Science and Technology</u>. Pages 92-112 have been published in <u>Nanotechnology</u>. Pages 113-129 are to be submitted for publication in <u>Nano Letters</u>.

ABSTRACT

This dissertation presents a simple method for the photolithographic patterning of silica hydrogel monoliths and planar substrates with quantum dots and inorganic semiconductor nanoparticles. We developed a method for surface patterning and bulk (3D) patterning of silica hydrogel monoliths and surface patterning of planar substrates with CdS, CdSe, PbS and PbSe quantum dots using infrared light, ultraviolet light, X-rays, and multi-photon ionization radiation. Precursor combinations were prepared which can readily dissociate with IR, UV, X-rays, and multi-photon ionization radiation. Different capping agents were used for improving quantum dot size distribution. The luminescence quantum yield of the composites can be increased to up to 30% with photoactivation. A masking technique was developed with which we can photolithograph sophisticated patterns with CdSe quantum dots on the surface of silica hydrogels that are highly luminescent without any further photoactivation. These are bottom-up methods, water-based, use readily available reagents and need only a few simple processing steps. These are attractive features for applications, and we anticipate that the technique may be employed for large-scale production of quantum dots in the near future.

ACKNOWLEDGMENTS

TABLE OF CONTENTS

LIST OF ILLUSTRATIONS

LIST OF TABLES

1. INTRODUCTION

1.1. LOW-DIMENSIONAL NANOCRYSTALS

Nanostructured semiconductors with a size range of 1-100 nm have been the focus of recent scientific research because of their important nonlinear optical properties,[1] luminescent properties,[2,3] quantum size effects,[4,5] and other important physical and chemical properties.[6] In the past decade, low-dimensional materials such as nanometer-size inorganic dots, tubes, and wires have been discovered which exhibited a wide range of electronic and optical properties that depend sensitively on both size and shape, and are of both fundamental and technological interest.[7-9] They are potentially ideal building blocks for nanoscale electronics and optoelectronics. The ability to control the shapes of semiconductor nanocrystals affords an opportunity to further test theories of quantum confinement and yields samples with desirable optical characteristics from the point of view of application.[10,11]

The existing emerging important applications of low-dimensional semiconductor nanocrystals include using Quantum dots in biological assays,[12-15] building blocks for assembly of semiconductor nanodevices,[16] hybrid nanorod-polymer solar cells that combine semiconducting polymers and nanoparticles in useful photovoltaic devices with relatively high conversion efficiencies,[17] room-temperature ultraviolet lasing using ZnO nanowire (NW) arrays,[18] light-emitting diodes (LEDs),[9] and nanosensors for biological and chemical species.[19-21]

1.2. QUANTUM SIZE CONFINEMENT

The interest of this subject stems from two main desires. The first is the desire to understand the transition from molecular to bulk electronic properties, while the other is the prospect of practical application of these materials to optoelectronic devices, photocatalysts, and chemical sensors. Perhaps the most striking property of nanoscale semiconductors is the massive change in optical properties as a function of size due to quantum confinement. This is most readily manifest as a blue shift in the absorption spectra with the decrease of the particle size. The variation of the energy gap in semiconductors with size can also result in different emission wavelengths for different sizes of nanoparticles. One example is shown in Fig. 1.1[15] for ZnS-capped CdSe nanoparticles with different sizes which display a fluorescence rainbow of blue-green-orange-yellow-red with the emission maxima at 443, 473, 481, 500, 518, 543, 565, 587, 610, and 655 nm, respectively.

Figure1.1. Ten different emission colors of different size ZnS-coated CdSe nanoparticles excited with a near-UV lamp. From left to right (blue to red), the emission maxima are 443, 473, 481, 500, 518, 543, 565, 587, 610, and 655 nm, respectively. Reprinted with permission from [15], M. Y. Han et al., *Nature Biotechnol.* **19**, 631 (2001).

For a semiconductor crystal, electronic excitation consists of a loosely bounded electron-hole pair (the Mott-Wannier exciton[22]), usually delocalized over a length much longer than the lattice constant. The exciton Bohr radius is a useful parameter in quantifying the quantum confinement effects in semiconductor physics. The Bohr radius (a_B) of an exciton in semiconductors may be calculated by[23]

$$a_B = \frac{\hbar^2 \varepsilon}{e^2} \left[\frac{1}{m_e^*} + \frac{1}{m_h^*} \right] \qquad (1)$$

where ε is the dielectric constant, $\hbar$ is the Planck constant, and m_e^* and m_h^* are the electron and hole effective masses respectively. As the particle size is reduced to approach the exciton Bohr radius, there are drastic changes in the electronic structure and physical properties. These changes include shifts of the energy levels to higher energy, the development of discrete features in the spectra, and the concentration of the oscillator strength into just a few transitions (Fig. 1.2)[23], which can be observed as a blue-shift in the optical band gap as well as an enhancement in the absorption cross section. This observed blue-shift of exciton energy (or optical band gap) with decreasing cluster size occurs because the energy band of a cluster with a finite number of atoms is discrete. For CdS, the quantum size effect occurs as the cluster diameter is comparable to or smaller than the exciton diameter of ~60Å (~3000-4000 atoms). For PbS, this size effect can be observed for a cluster as large as 180Å, which contains over 10^5 atoms.

This problem was first treated by Efros *et al.*[24], who considered a simple particle in a box model. This model assumes that the energy band is parabolic in shape, equivalent to the so-called effective mass approximation. The shift in absorption threshold, ΔE, is dependent upon the value of the cluster radius R, Bohr radius of the

electron, $a_e (= \hbar^2 \varepsilon / m_e^* e^2)$, and Bohr radius if the hole, $a_h (= \hbar^2 \varepsilon / m_h^* e^2)$. When (1)

$R \ll a_h$ and $R \ll a_e$, and (2) $a_h \ll R \ll a_e$,

$$\Delta E = \frac{\hbar^2 \pi^2}{2R^2} \left[\frac{1}{m_e^*} + \frac{1}{m_h^*} \right] \qquad (2)$$

When (3) $a_h \ll R$ and $a_e \ll R$

$$\Delta E = \frac{\hbar^2 \pi^2}{2R^2} \frac{1}{\left[m_e^* + m_h^* \right]} \qquad (3)$$
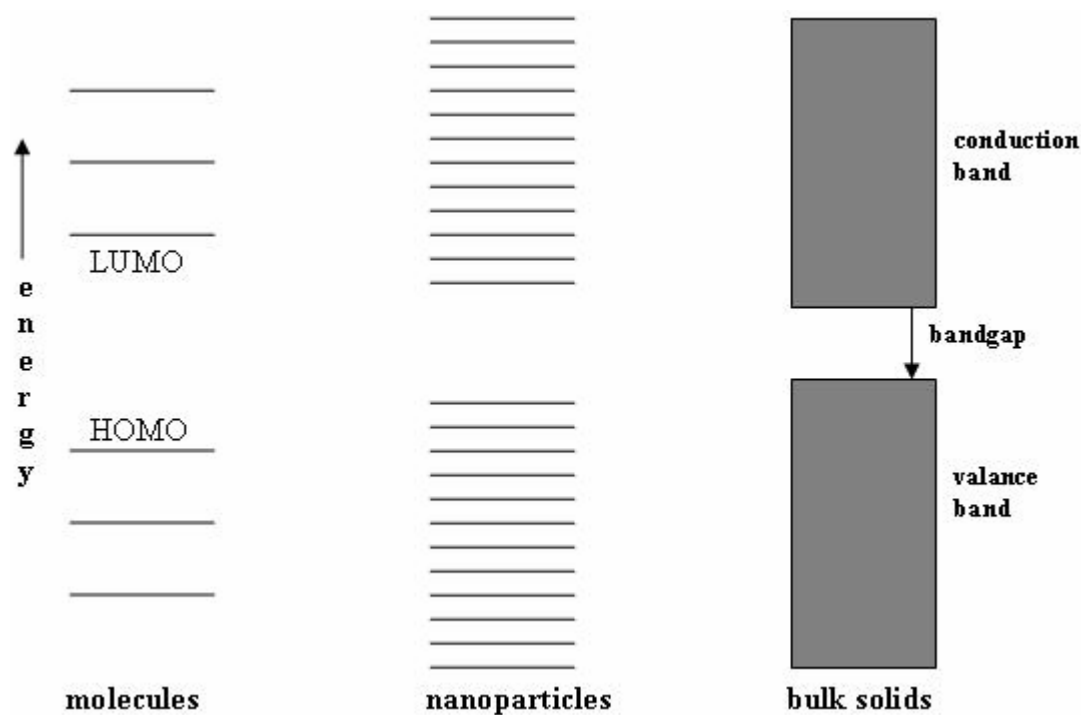
Figure 1.2. A schematic model for the energy structures of bulk solids, nanoparticles, and isolated molecules.

The model by Efros *et al.* ignores the Coulomb interaction and the correlation effect between electrons and holes. This is subsequently remedied by Brus[25] and

Kayanma[26]. For the strongly confined cases (1) and (2), the size-dependent shift of the

exciton energy of a small cluster can be derived as

$$\Delta E = \frac{\hbar^2 \pi^2}{2R^2} \left[\frac{1}{m_e^*} + \frac{1}{m_h^*} \right] - \frac{1.786 e^2}{\varepsilon R} - 0.248 E_{R_y}^* \qquad (4)$$

Where R is the cluster radius and $E_{R_y}^*$ is the effective Rydberg energy,

$e^4 /[2\varepsilon^2 \hbar^2 (1/m_e^* + 1/m_h^*)]$. The first term in Eq. (4) represents the particle in box quantum

localization energy and has a simple $1/R^2$ dependence[24], the second term is the Coulomb

energy with a 1/R dependence[25], and the third term is a result of the spatial correlation

effect[26]. This last size-independent term is usually small, but can become significant for

semiconductors with a small dielectric constant.

In both regimes the main experimental effects of confinement are the appearance

of a structured absorption spectrum due to the presence of discrete energy levels and the

blueshift of the absorption edge, which is roughly proportional to the inverse of the

square of the particle radius. However, some electronic properties such as electron-hole

interactions are expected to be modified only in the strong confinement regime. This is

due to the increase of the spatial overlap of the electron and hole wavelength functions

with decreasing size. As a consequence, the splitting between the radiative and

nonradiative exciton states is enhanced largely in the strong confinement regime.

Four basic dimensionality systems are listed in Table 1.1.

Table 1.1. The number of degrees of freedom D_f in the electron motion, together with the extent of the confinement D_c, for the four basic dimensionality systems.

System	D_c	D_f
Bulk	0	3
Quantum well	1	2
Quantum wire	2	1
Quantum dot	3	0

Quantum confinement not only causes an increase of the energy gap (blueshift of the absorption edge) and the splitting of the electronic states but also changes the density of states (DOS). Many novel physical properties and potential applications of low-dimensional semiconductors and many of the differences between the electronic behavior of the bulk and of quantum-confined low-dimensional semiconductors are due to their differences in the density of states. Fig. 1.3 shows the variation of the DOS with dimensionality.[27]
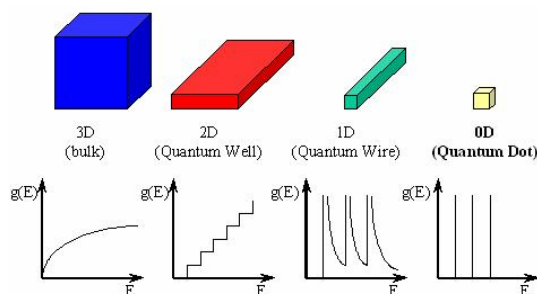
Figure 1.3. Profiles of the density of states of three-dimensional bulk semiconductors, a two-dimensional quantum well, a one-dimensional quantum wire, and zero-dimensional quantum dots. Reprinted with permission from [28], A.P. Alivisatos, J. Phys. Chem. **100**, 13226 (1996).

The dimensionality of the system describes the number of dimensions of free transport of an electron gas, thus quantum wells are two-dimensional structures, quantum wires are one-dimensional, and quantum dots are considered zero-dimensional because electrons are confined in all spatial dimensions. Passing from three dimensions to two dimensions the density of states $\rho(E)$ changes from a continuous dependence, where $\rho(E) \sim E^{1/2}$, to a steplike dependence. Thus the optical absorption features are different for the bulk and for the quantum well structure. The optical absorption edge for a quantum well is at higher photon energy than for the bulk semiconductor and, above the absorption edge, the spectrum is stepped rather than smooth, the steps corresponding to allowed transitions between valence-band states and conduction-band states. In addition, at each step sharp peaks appear corresponding to confined electron-hole (exciton) pair states. In the case of lower dimensional systems (quantum dots, nanocrystallites, clusters, nanoparticles, colloids, etc.), the DOS becomes more discrete as the dimensionality decreases, and large optical absorption coefficients are observed.[28] The low-dimensional structure has proven to be very promising in applications to semiconductor lasers, due mainly to the quantum confinement of the carriers and the variation of the density of states with dimensionality.[29] The changes in the DOS lead to a change in the gain profile, a reduction of threshold current density, and a reduction of the temperature dependence of the threshold current. Owing to the steplike density of states, high gain with a lower spontaneous emission rate has been realized in a GaAs/AlGaAs GRIN-SCH SQW laser.[30] Thus low-dimensional structured materials are interesting, for both basic research and practical applications.

The density of states changes in moving from the bulk (3D) crystal to a quantum well (2D), there is further change in the density of states on moving to quantum wires (1D) and quantum dots (0D). The density of states is defined as the number of states per unit energy per unit volume of real space, which is expressed mathematically as

$$\rho(E) = \frac{dN}{dE} \tag{5}$$

In the bulk crystal, the three degrees of freedom for the electron momentum mapped out a sphere in k-space, while in quantum wells the electron momenta fill successively large circles. Continuing this argument for quantum wire with just one degree of freedom, the electron momenta that fill states along a line. Therefore the total number of states N is then equal to the length of the line in k-space (2k), divided by the length occupied by one state $\left(\frac{2\pi}{L}\right)$, and divided by the length in real space,[31] i.e.

$$N^{1D} = 2 \times 2k \frac{1}{(2\pi/L)} \frac{1}{L} = \frac{2k}{\pi} \tag{6}$$

Then the density of states for a one-dimensional wire can be defined as

$$\rho^{1D}(E) = \frac{dN^{1D}}{dE} = \frac{dN^{1D}}{dk} \frac{dk}{dE}$$

but $\dfrac{dk}{dE} = \left(\dfrac{2m^*}{\hbar^2}\right)^{\frac{1}{2}} \dfrac{E^{-\frac{1}{2}}}{2}$ finally the density of states for a 1D wire is

$$\rho^{1D}(E) = \left(\frac{2m^*}{\hbar^2}\right)^{\frac{1}{2}} \frac{1}{\pi E^{\frac{1}{2}}} \tag{7}$$

where the energy E is measured upwards from a subband minimum. Therefore on comparing the density of states for bulk (3D), quantum wells (2D) and quantum wires

(1D), it can be seen that successive reductions in degrees of freedom for the electron

motion, lead to reductions in the functional form of $\rho(E)$ by factors of $E^{1/2}$.[31]

Table 1.2. The density of states for reduced dimensionality systems, rewritten in a standard form.

Dimensionality	$\rho(E)$
3D	$\dfrac{1}{2\pi^2}\left(\dfrac{2m^*}{\hbar^2}\right)^{3/2} E^{1/2}$
2D	$\dfrac{1}{2\pi}\left(\dfrac{2m^*}{\hbar^2}\right)^{1} E^{0}$
1D	$\dfrac{1}{\pi}\left(\dfrac{2m^*}{\hbar^2}\right)^{1/2} E^{-1/2}$

If there are many (n) confined states within the quantum wire with subband minima E_i, then the density of states at any particular energy is the sum over all the subbands below that point, which can be written as:

$$\rho^{1D}(E) = \sum_{i=1}^{n}\left(\frac{2m^*}{\hbar^2}\right)^{1/2}\frac{1}{\pi(E-E_i)^{1/2}}\Theta(E-E_i) \qquad (8)$$

where Θ is the unit step function. In contrast to the bulk and 2D cases, quantum wires show maxima in the density of states at around the subband minima, i.e. at around the point at which charge would be expected to accumulate. Therefore, interband (electron-hole) recombination will have a narrower linewidth than that of the 2D and 3D cases.[31]

The situation for quantum dots is quite different. As the particles are confined in all directions, then there are no dispersion curves, and thus the density of states is just dependent upon the number of confined levels. One single isolated quantum dot would

therefore offer just two (spin-degenerate) states at the energy of each confined level, and a plot of the density of states versus energy would be a series of δ-functions,[31] i.e. in quantum dots, the parabolic density of states of a 3D system is replaced by a series of discrete energy levels, similar to those seen in atomic physics. These levels are distinct if their separation is larger than that of thermal broadening. This condition sets an upper limit on the size of a quantum dot and is obviously more restrictive for devices that operate at room temperature. The lower limit to the size of a quantum dot depends on the material which is used to form it and on the depth of the confining potential. At least the lowest confined energy level must lie within the potential well of the dot.[32]

If we consider a QD artificial atom as a building block, we can create QD arrays. Electrons in QD arrays can move around and interact with each other through the coulomb interaction, and many interesting effects manifest themselves in magnetic, transport, and optical properties. When QDs are arranged on a periodic lattice and are coupled to each other coherently, a band structure is obtained. This type of dot lattice or artificial crystal was first proposed by Sakaki[33] and it is called quantum dot superlattice (QDSL). It is analogous to quantum well superlattices,[34] in which a sequence of semiconductor layers with different bandgaps produces new materials and devices. The energy spectrum of the superlattice is determined by the artificial periodicity and the coupling between quantum wells (dots) rather than by the properties of the individual semiconductor materials.

1.3. QUANTUM DOTS

Quantum dots (QDs) are very small semiconductor materials which contain tens to a few hundreds of atoms with sizes of a few nanometers but only a small number of electrons (≤ 100) are free. Quantum dots are electrostatically or structurally isolated from the outside and are small regions defined by well defined confining potentials in semiconductor materials, in which electrons are confined and the number of electrons can vary between one and several hundreds and whose size is comparable to the Fermi wavelength of the electrons. First it was realized in 1932 by H. P. Rocksby that the red or yellow color of some silicate glasses could be linked to microscopic inclusions of CdSe and CdS.[35] Such red and yellow colored glasses have been commercially available as color filters for decades. In 1985 Ekimov *et al.*[36] experimentally proved and theoretically modeled that these changes in color were linked to the density of states (DOS) determined by the size of the crystalline material. Below a certain size, the properties of the crystalline material start to deviate significantly from bulk properties and became strongly dependent on size. Finite size of the micro crystallites confines the motion of the quasiparticles (electron, hole and exciton) within their physical boundary. This is called *quantum confinement*. Quantum confinement modifies the DOS which in turn leads to discretization as well as enlarged spacing between the energy levels of electron and hole states. Thus one can observe an increase in the band gap as the optical absorption onset occurs at higher energies (*blue-shift*) in case of nanocrystals.[36, 37] Because QD's are analogous to atoms, they are often referred to as artificial atoms. Unlike real atoms, though, current and voltage leads can be attached to probe a QD's electronic state. The interplay between quantum confinement and charging effects

manifests itself in a wide range of physical phenomena.[38-40] The single electron charging effect is one of the more important of these. When the charging energy of a small quantum dot is larger than the thermal energy, electrons in the lead cannot transfer into the dot (Coulomb blockade effect). By coupling several quantum dots, we can create artificial molecules. An important feature of these artificial molecules is that the couplings between different dots can be tuned by changing gate voltages or interdot distances. This tunability allows us to achieve various interesting phenomena, ranging from the formation of a "chemical bond" between two coupled dots to the manipulation of a single electron in "turnstiles" and "pumps".[41]

Quantum boxes can be thought of as simply a generalization of the rectangular cross-section quantum wires, in which there are confinements along all the three x, y and z-axes. These three confinements remove all degrees of freedom in the particle's momentum and localize it in all directions. Here the particle in consideration is an exciton. Thus the energy levels are now known as sublevels.[31]
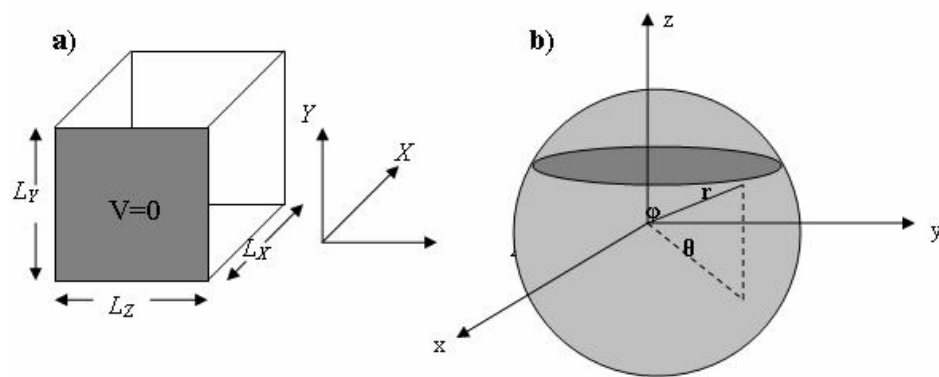
Figure 1.4. (a) Schematic illustration of a quantum box with side L_X, L_Y and L_Z and (b) Schematic illustration of a spherical quantum dot.

Considering the case of an infinite potential separating the inside of the box from the outside, the 3D Schrödinger equation within the box is

$$\frac{-\hbar^2}{2m^*}\left(\frac{\partial^2}{\partial x^2}+\frac{\partial^2}{\partial y^2}+\frac{\partial^2}{\partial z^2}\right)\Psi(x,y,z)=E_{x,y,z}\Psi(x,y,z) \tag{9}$$

Writing the total energy $E_{x,y,z}$ as a sum of the three terms E_x, E_y and E_z , then the 3D equation can be decoupled into three 1D equations:

$$-\frac{\hbar^2}{2m^*}\frac{\partial^2}{\partial x^2}\Psi(x)=E_x\Psi(x) \tag{10.1}$$

$$-\frac{\hbar^2}{2m^*}\frac{\partial^2}{\partial y^2}\Psi(y)=E_y\Psi(y) \tag{10.2}$$

$$-\frac{\hbar^2}{2m^*}\frac{\partial^2}{\partial z^2}\Psi(z)=E_z\Psi(z) \tag{10.3}$$

The confinement energy within this quantum box is

$$E_{x,y,z}=\frac{\hbar^2\pi^2}{2m^*}\left(\frac{n_x^2}{L_x^2}+\frac{n_y^2}{L_y^2}+\frac{n_z^2}{L_z^2}\right) \tag{11}$$

The 3D nature of the confinement requires three quantum numbers, i.e., n_x, n_y and n_z to label each state.[31]

In spherical Quantum dots as the potential is spherically symmetric, then the wave function would also be expected to have spherical symmetry, then the Schrödinger equation for a constant effective mass is[42]

$$-\frac{\hbar^2}{2m^*}\left[\frac{1}{r^2}\frac{\partial}{\partial r}\left(r^2\frac{\partial}{\partial r}\right)+\frac{1}{r^2}\left(\frac{1}{\sin\theta}\frac{\partial}{\partial\theta}\sin\theta\frac{\partial}{\partial\theta}+\frac{1}{\sin^2\theta}\frac{\partial^2}{\partial\phi^2}\right)\right]\Psi(\vec{r})+V(\vec{r})\Psi(\vec{r})=E_r\Psi(\vec{r}) \tag{12}$$

For a free-particle (exciton) the Schrödinger equation is

$$-\frac{\hbar^2}{2m^*}\left[\frac{1}{r^2}\frac{\partial}{\partial r}\left(r^2\frac{\partial}{\partial r}\right)+\frac{1}{r^2}\left(\frac{1}{\sin\theta}\frac{\partial}{\partial\theta}\sin\theta\frac{\partial}{\partial\theta}+\frac{1}{\sin^2\theta}\frac{\partial^2}{\partial\phi^2}\right)\right]\Psi(r,\theta,\phi)=E\Psi(r,\theta,\phi) \tag{13}$$

Solving equation (13) by separation of variables. Substituting the product form $\Psi(r,\theta,\phi)=R(r)\Theta(\theta)\Phi(\phi)$. Function R(r) describes how wave function Ψ varies along the radius vector from the center, with θ and ϕ constant. Function $\Theta(\theta)$ describes

how the wave function Ψ varies with zenith angle with r and ϕ constant. Function

$\Phi(\phi)$ describes how wave function Ψ varies with azimuth angle with r and θ

constant(Fig. 1.4(b)).[31] Multiplying by Eq. (11) with $r^2 / R\Theta\Phi$ [42]

$$\frac{1}{R}\frac{d}{dr}\left(r^2\frac{dR}{dr}\right) - Er^2 + \frac{1}{\Theta\sin\theta}\frac{d}{d\theta}\left(\sin\theta\frac{d\Theta}{d\theta}\right) + \frac{1}{\Phi\sin^2\theta}\frac{d^2\Phi}{d\phi^2} = 0 \quad (14)$$

Angular part

Multiplying Eq. (14) by $\sin^2\theta$, the last term, $\frac{1}{\Phi}\left(\frac{d^2\Phi}{d\phi^2}\right)$, only involved ϕ (whereas the

first two terms only depend on r and θ), and so must be a constant which we called

$-m^2$, i.e.

$\frac{1}{\Phi}\frac{d^2\Phi}{d\phi^2} = -m^2$. The solution was $\Phi(\phi) = e^{im\phi}$, with m an integer (in order that the solution

was the same for ϕ and $\phi + 2\pi$). Substituting into Eq. (14) gives

$$\frac{1}{R}\frac{d}{dr}\left(r^2\frac{dR}{dr}\right) - Er^2 + \frac{1}{\Theta\sin\theta}\frac{d}{d\theta}\left(\sin\theta\frac{d\Theta}{d\theta}\right) - \frac{m^2}{\sin^2\theta} = 0 \quad (15)$$

the 3rd and 4th terms in Eq. (15) are only a function of θ (where the first two terms only

depend on r), and must therefore be a constant which was $l(l+1)$, i.e.

$\frac{1}{\Theta\sin\theta}\frac{d}{d\theta}\left(\sin\theta\frac{d\Theta}{d\theta}\right) - \frac{m^2}{\sin^2\theta} = -l(l+1)$, this can be written as

$$\frac{1}{\sin\theta}\frac{d}{d\theta}\left(\sin\theta\frac{d\Theta}{d\theta}\right) + \left(l(l+1) - \frac{m^2}{\sin^2\theta}\right)\Theta = 0 \quad (16)$$

with the substitution $x = \cos\theta$, Eq. (16) becomes

$$\frac{d}{dx}\left[(1-x^2)\frac{d\Theta(x)}{dx}\right] + \left(l(l+1) - \frac{m^2}{1-x^2}\right)\Theta(x) = 0 \quad (17)$$

Eq. (17) is the Associated Legendre equation, so the solution is $\Theta(x) = P_l^m(x)$ ($x = \cos\theta$)

where the $P_l^m(\cos\theta)$ are Associated Legendre Polynomials and $l = 0,1,2,......$, and m runs

over integer values from $-l$ to l.[42] If l is not an integer one can show that the solution of

Eq. (16) diverges for $\cos\theta = 1$ or -1 ($\theta = 0$ or π). Generally we require the solution to

be finite in these limits, and this is the reason why we write the separation constant is Eq.

(16) as $l(l+1)$ with l an integer. The functions Θ and Φ are often combined into a

Spherical harmonic, $Y_l^m(\theta,\phi)$, where

$$Y_l^m(\theta,\phi) = \sqrt{\frac{(2n+1)}{4\pi}\frac{(n-m)!}{(n+m)!}}P_l^m(\cos\theta)e^{im\phi} \tag{18}$$

The spherical harmonics are orthogonal and normalized, i.e.

$\int\limits_0^{2\pi} d\phi \int\limits_0^{\pi} d\theta \sin\theta\, Y_l^{m*}(\theta,\phi)\, Y_{l'}^{m'}(\theta,\phi) = \delta_{l,l'}\delta_{m,m'}$ which equals to unity when $l = l'$ and

$m = m'$. As the Spherical harmonics are complex, we need to take the complex conjugate

of one of them in this orthogonality/normalization relation.

The first few spherical harmonics are

$$Y_0^0(\theta,\phi) = \sqrt{\frac{1}{4\pi}} \qquad\qquad Y_1^1(\theta,\phi) = -\sqrt{\frac{3}{8\pi}}\sin\theta\, e^{i\phi}$$

$$Y_1^0(\theta,\phi) = \sqrt{\frac{3}{4\pi}}\cos\theta \qquad Y_1^{-1}(\theta,\phi) = \sqrt{\frac{3}{8\pi}}\sin\theta\, e^{-i\phi}$$

For the case of $m = 0$, i.e. no dependence on the azimuthal angle ϕ, we have $\Phi(\phi) = 1$

and also $P_l^m(\cos\theta) = P_l(\cos\theta)$, where the $P_l(x)$ are Legendre Polynomials. Hence

$$Y_l^0(\theta,\phi) = \sqrt{\frac{(2n+1)}{4\pi}\frac{(n-m)!}{(n+m)!}} \tag{19}$$

The first few Legendre Polynomials are $P_0(x) = 1, P_1(x) = x, P_2(x) = \frac{1}{2}(3x^2 - 1)$ [42]

Radial part

From Eq.s (15) and (16)

$$\frac{1}{r^2}\frac{d}{dr}(r^2\frac{dR}{dr}) + [\frac{2mE}{\hbar^2} - \frac{l(l+1)}{r^2}]R = 0 \tag{20}$$

With the substitution $E = \frac{\hbar^2 k^2}{2m}$ and $x = kr$ the above r-dependence equation becomes

"spherical Bessel differential equation"

$$\frac{d^2}{dx^2}R(x) + \frac{2}{x}\frac{dR(x)}{dx} + \left[1 - \frac{l(l+1)}{x^2}\right]R(x) = 0 \tag{21}$$

which is Bessel's equation of order $l + (1/2)$. The solutions are $J_{l+(1/2)}(x)$ and $N_{l+(1/2)}(x)$

Spherical Bessel functions

This ordinary linear equation for the radial function R has two linearly independent solutions. They are called spherical Bessel and Neumann functions and are denoted conventionally by the symbols $j_l(x) = \sqrt{(\pi/2x)}J_{l+(1/2)}(x)$ and

$n_l(x) = \sqrt{(\pi/2x)}N_{l+(1/2)}(x)$ respectively. The first few orders of these functions are

$$j_0(x) = \frac{\sin x}{x} \qquad\qquad n_0(x) = -\frac{\cos x}{x}$$

$$j_1(x) = \frac{\sin x}{x^2} - \frac{\cos x}{x} \qquad\qquad n_1(x) = -\frac{\cos x}{x^2} - \frac{\sin x}{x}$$

$$j_2(x) = \left(\frac{3}{x^3} - \frac{1}{x}\right)\sin x - \frac{3}{x^2}\cos x \qquad\qquad n_2(x) = -\left(\frac{3}{x^3} - \frac{1}{x}\right)\cos x - \frac{3}{x^2}\sin x$$

The spherical Bessel functions $\{j_l\}$ are the solutions appropriate to the Schrodinger equation inasmuch as they are not singular anywhere.[43]

Then the eigenstates and eigenenergies of the free-particle Hamiltonian in spherical coordinates are

$$\Phi_{klm} = j_l(kr) Y_l^m(\theta, \phi) \tag{22.1}$$

$$E_k = \frac{\hbar^2 k^2}{2m} \tag{22.2}$$

The orthonormality of this sequence $\{\Phi_{klm}\}$ is given by the relation

$$\langle lmk | l'm'k' \rangle = \int_{4\pi} d\Omega \left[Y_l^m(\theta, \phi) \right]^* Y_{l'}^{m'}(\theta, \phi) \int_0^\infty j_l(kr) j_{l'}(k'r) r^2 dr$$

$$= \delta_{ll'} \delta_{mm'} \frac{\pi}{2k^2} \delta(k - k') \tag{23}$$

The vector **r** has the spherical coordinates (r, θ, ϕ). The projection $\langle r\theta\phi | lmk \rangle = j_l(kr) Y_l^m(\theta, \phi)$ gives the coordinate representation of the ket vector $|lmk\rangle$.[43]

The spherical well

We consider a particle (exciton) of mass M confined to the interior of a spherical well with impenetrable walls. In the domain $r \geq R$, the wave function vanishes. In the domain $r < R$, the time-independent Schrodinger equation is given by

When $\hat{p}_r^2 = -\hbar^2 \frac{1}{r^2} \frac{\partial}{\partial r} r^2 \frac{\partial}{\partial r}$ and $\hat{L}^2 = -\hbar^2 \left[\frac{1}{\sin\theta} \frac{\partial}{\partial\theta} \left(\sin\theta \frac{\partial}{\partial\theta} \right) + \frac{1}{\sin^2\theta} \frac{\partial^2}{\partial\phi^2} \right]$

then the Hamiltonian was

$$\hat{H} = \frac{\hat{p}_r^2}{2m} + \frac{\hat{L}^2}{2mr^2} = \frac{-\hbar^2}{2m^*} \left[\frac{1}{r^2} \frac{\partial}{\partial r} \left(r^2 \frac{\partial}{\partial r} \right) + \frac{1}{r^2} \left(\frac{1}{\sin\theta} \frac{\partial}{\partial\theta} \sin\theta \frac{\partial}{\partial\theta} + \frac{1}{\sin^2\theta} \frac{\partial^2}{\partial\phi^2} \right) \right]$$

then the Schrödinger equation for a free particle was $\frac{1}{2m} \left(\hat{p}_r^2 + \frac{\hat{L}^2}{r^2} \right) \Phi_{klm} = E_{klm} \Phi_{klm}$

with general solutions given by

$$\Phi_{klm}(r,\theta,\phi) = j_l(kr) Y_l^m(\theta,\phi) \qquad (24.1)$$

$$E_k = \frac{\hbar^2 k^2}{2m} \qquad (24.2)$$

To impose boundary conditions $\Phi(r=R)=0$ we set $j_l(kR)=0$, which has an infinite number of solutions. To delineate these values we return to the notation $x \equiv kr$ in terms of which $j_l(kR)=0$ becomes $j_l(x_{ln})=0$ where x_{ln} is the nth zero of $j_l(x)$. Eigenfunctions and eigenenergies for the spherical well are then given by

$$\Phi_{nlm}(r,\theta,\phi) = j_l\left(\frac{x_{nl}r}{R}\right) Y_l^m(\theta,\phi) \qquad (25.1)$$

$$E_{nl} = \frac{\hbar^2 x_{ln}^2}{2MR^2} \qquad (25.2)$$

Orthogonality of spherical Bessel functions is given by

$$\int_0^R dr\, r^2\, j_l\left(\frac{x_{nl}r}{R}\right) j_l\left(\frac{x_{nl}'r}{R}\right) = \frac{R^3}{2}\left[j_{l+1}(x_{nl})\right]^2 \delta_{nn'}$$ which indicates the nature of normalization

of the functions. Note that the continuous spectrum of k values for the free particle (exciton) in spherical coordinates translates to the discrete spectrum of the quantum number n for the finite spherical well problem.[43]

The ground-state wavefunction and eigenenergy for the spherical well are given by

$$\Phi_G(r,\theta,\phi) = \sqrt{\frac{1}{2\pi R^3}} \frac{1}{j_l(\pi)} j_0\left(\frac{\pi r}{R}\right) \qquad (26.1)$$

$$E_G = \frac{\hbar^2 \pi^2}{2MR^2} \qquad (26.2)$$

The confinement energy decreases as the size of the quantum dot increases.[43]

1.4. APPLICATIONS

Light emitting diodes (LEDs) from organic polymer and II-VI semiconductor nanocrystals have attracted considerable attention because polymer nanoparticle composites combine key properties required for flat-panel displays (FPDs) including low weight, low power, low voltage, low cost and compact size.[44] FPDs were replacing CRT displays in military applications and in civilian technologies, such as information processing. Nanoparticle LEDs can provide improved brightness and multicolor capabilities compared to many of the existing flat-panel displays. The extremely small size of nanoparticles creates the prospect of displays with unprecedented resolution.[44]

The temperature dependence of semiconductor nanoparticle luminescence properties can be used for thermometry applications.[45] This is a non-contact thermometry which has many advantages over other thermometry methods.[46] As the temperature of the phosphor changes, the intensity of the fluorescence, the decay lifetime of the fluorescence, the excitation spectra of the fluorescence, and the wavelength of the fluorescence may all change. Because the fluorescence can be both excited and measured optically, fluorescence-based temperature sensors are advantageous compared to contact temperature sensors in applications where electromagnetic noise is strong or it is physically difficult to connect a wire. Emissivity does not affect the fluorescence signals, and wavelengths for fluorescence can be found for which glass and water are relatively transparent.

Physical and chemical properties of nanoparticles suggest that the photophysical behavior of these tiny particles may be more finely tunable than that of dyes and, thus, may offer a promising way to solve some critical problems with biological labeling.

Nanoparticle biological probes are easier to make and are potentially less expensive than organic dyes. In comparison with conjugates formed with organic dyes, this new class of luminescent probes is 20 times as bright, 100 times as stable against photobleaching, and 1/3 as wide in spectral width.[47]

Fluorescence resonance energy transfer (FRET) is the transfer of the excited-state energy between two different luminescent molecules (or nanoparticles), from the initially excited donor (D) to an acceptor (A). FRET can occur when the donor molecules emit at wavelengths that overlap with the absorption spectrum of the acceptor. Energy transfer occurs without the appearance of a photon and is the result of long-range dipole-dipole interactions between the donor and acceptor. An important characteristic of FRET is that the transfer rate is highly dependent on the distance between the donor acceptor. The distance at which FRET is 50% efficient, called the Förster distance, is typically 20-60 Å.[48] FRET is widely used as a sensing mechanism for molecular level distance and binding event detection.[49] The stability of nanoparticles under UV and visible light makes possible not only high-contrast multiplexed imaging but also a long-term monitoring of the environment.

Using nanoparticles or QDs as a storage medium offers tremendous potential. Enhanced, cost-effective storage of information requires ultrahigh packing densities as well as inexpensive self-assembling techniques and fast methods for writing and retrieving the information. Semiconductor quantum dots, which involve a few thousand atoms, may offer an attractive path toward achieving these goals. Single-electron storage has been suggested as a possibility with quantum dots.[50]

Nanoparticles such as TiO_2,[51] iron oxide,[52,53] cadmium sulfide,[54-56] and clay[57] have been incorporated into polymer systems such as poly (sodium 4-styrenesolfonate), polysaccharides such as κ-carrageenan and cellulose sulfate, PMMA, polystyrene, and sodium bis(2-ethylhexyl) sulfosuccinate (AOT)/isooctane organogels. The applications of these nanocomposites range from photovoltaics, catalysts, sensors and reverse osmosis membranes.[58] One of the major applications of semiconductor nanoparticle/polymer composites is in the field of photovoltaics. Akimov et al. first demonstrated synthesis of conductive polymer nanocomposites containing 2 to 50 nm CdS nanocrystals, which were prepared in poly (vinyl alcohol), poly(vinylpyridine), and photographic gelatin. The composites exhibited good photosensitivity and photoconductivity. Also, nonlinear optical properties of quantum confined semiconductors are enhanced in polymer systems.[58]

Porous glasses prepared by the sol–gel technique have a variety of applications when incorporated by photonic materials: tunable lasers, sensors, luminescence solar concentrators, semiconductor quantum dots, and biological markers.[59]

Super critically dried silica hydrogels are called aerogels and find applications in acoustic insulation, Cherenkov counters, batteries, capacitor electrodes, dielectric materials, piezoelectric materials, cosmic dust collection, inertial confinement fusion (ICF), nuclear waste storage, and catalysis.[60]

Oxidized copper selenide quantum dots in sol-gel glasses can be used for nonlinear optical applications and laser applications.[61] The poly(N-vinyl-2-pyrrolidone) capped CdS quantum dots synthesized by a sol-gel method can be used for electroanalysis of myoglobin.[62] The luminescence quenching effect of oxygen concentration on the

photoluminescence of CdSe/ZnS quantum dots around 520 nm can be used in preparing optical fiber luminescent oxygen sensors.[63] ZnSe quantum dots embedded in SiO_2 thin films which are prepared from H_2SeO_4 and $Zn(Ac)_2.H_2O$ by the sol-gel process has the potential application of preparation of optical composite thin films.[64]

Photolithographic patterning of sol-gel materials is important for optical and electronic applications, and for data storage and encryption. Surface patterning can be employed to realize electrical contacts,[65] and diffraction gratings.[66,67] Quantum dot lasers can be fabricated based on quantum dots embedded in a titania sol-gel matrix,[68] PbS and CdS nanoparticles embedded in silica gels can be considered for waveguides, optical amplification, passive Q-switching, refractive index modification, light converting devices and non-linear applications.[69,70] Composites of silica gel and cytochrome-tagged Au nanoparticles were reported and they have applications in biotechnology.[71] Patterning of sol-gel materials with regularly spaced arrays of nanoparticles allows production opto-electronic components and devices such as gratings,[72] photonic crystals,[73] and optical memories.[74]

1.5. PHOTOLITHOGRAPHY

Photolithography which is also called lithography, is a method of printing on a smooth surface that can be used to print text or artwork onto paper or another suitable material. Lithography was invented by a Austro-German, Alois Selefelder, in 1798. Lithography is actually developed for the semiconductor industry which is the creation of a pattern in a resist layer, usually an organic polymer film, on a substrate material. A latent image, consisting of a chemical change in the resist is created. The pattern is

developed by selectively removing either the exposed areas (for a positive resist) or the unexposed areas (for a negative resist). Electrons, ions and photons can all be used for exposure in the lithography process.

Photolithography is the use of photons for high resolution of the lithographic exposure which is a broad field that includes most of the lithography in use today. This is the technique most widely used by the semiconductor industry and illustrates the general technique of lithography. It can be taken to include infrared lithography, deep and near-ultraviolet photolithography, X-ray lithography and multi-photon ionization lithography. Only the shortest wavelengths are directly relevant to high resolution of the fabrication. The projection and proximity printing processes to be described are analogous to processes that could be used at nanometer dimensions for parallel printing with electrons or ions. The diffraction limit for the minimum resolvable grating period is usually taken as the Rayleigh criterion for the overlap of the diffraction peaks, which is approximately minimum line resolvable spacing

$$\approx \frac{\lambda}{NA} \tag{27}$$

where λ is the wavelength and NA is the numerical aperture of the optical system, which is of the order of one. The shortest wavelength to be used with conventional optics is about 193 nm from an excimer laser source. The use of wavelengths much shorter than this is limited by absorption in optical materials. While the technology constantly improves, with better optics, and sources of shorter wavelength, the limit of far-field diffraction is a fundamental one that prevents its use for feature sizes smaller than the wavelength of light. Photolithography is essentially ruled out for fabrication at dimensions below 100 nm.

Projection systems employing X-rays would reduce diffraction effects, but the problem of fabricating optics to use in the X-ray region remains. Work in this area is advancing, with the development of multilayer mirrors and X-ray mask technology.

Proximity patterning allows the 1:1 replication of a mask pattern. The effects of near field diffraction can be arbitrarily reduced by decreasing the distance between mask and substrate. Qualitatively, the minimum line width is $d \approx \sqrt{\lambda s}$ where s is the separation between mask and substrate.

Proximity patterning can be done effectively by X-ray exposure where the shorter wavelengths, of the order of 1 nm, allow much greater mask-substrate separation. With short wavelength X-rays, diffraction can effectively be ignored for attainable gaps of the order of a few micrometers. Perhaps the most significant problem with X-ray printing is the creation of a durable and stable mask of high contrast. An absorbing metal, such as gold supported on a thin film such as SiN_4, is one type of mask. Some of the smallest features replicated by X-rays were 17.5 nm in extent, fabricated by using edge-evaporated metal as a mask. Some other high-resolution process is necessary to generate the mask features, in most cases this means electron beam lithography.[75]

1.6. QUANTUM DOT PHOTOLITHOGRAPHY

Rapid progress in nanoscale fabrication technology ("Nanotechnology") has enabled us to make various types of semiconductor devices using quantum dots (QDs) using various fabrication methods. The emergence of quantum semiconductor physics and improved epitaxial crystal growth techniques led to the successful development of semiconductor quantum wells in the late 1970s. Early on, there were predictions that

optical devices made from quantum wires and quantum dots would show improved performance over quantum wells.

In optics, this first phase in the development of quantum dots and wires stalled. Most importantly, the lithographic top-down techniques used to fabricate quantum dots and wires were not sufficiently precise and free from defects to make structures useful for optics applications, especially at room temperature. These top-down approaches met with limited success simply because they could not make useable structures that were small enough. After 15 years of further development the top-down lithographic approaches are still not adequate to make structures as small as needed. In addition, optical techniques used to characterize and understand these structures typically probed ensembles of dots or wires. The detailed information needed to understand dots and wires was masked by inhomogeneous broadening from the sample distribution.

Requirements for realizing useful quantum dot and wire optical devices[76] include: (1) making the structures small enough that the level splitting is larger than several k_BT, a GaAs/AlGaAs dot must be 10 nm or smaller in lateral dimension to operate at room temperature; (2) making the structure large enough to ensure that at least one electron and one hole state are bound inside the nanostructure, a GaAs/AlGaAs dot must be 5 nm or larger in lateral dimension; (3) size fluctuations small enough that the inhomogeneous broadening is less than k_BT; and (4) a high density of dots or wires for applications, such as lasers and light-emitting diodes (LED), that need a large number of emitters. If the lateral confinement is provided by surfaces or interfaces, then high-quality damage-free surfaces or interfaces are needed to minimize nonradiative recombination.

The smallest dot made with a top-down approach is 30 nm wide,[77] still too large to be quantum at room temperature. Most dots were larger. Photoluminescence (PL)[77-79] and cathodoluminescence (CL)[80-82] revealed only small blue shifts of the emission that could be attributed to lateral confinement. The emission peaks had large inhomogeneous broadening, indicative of a large distribution of dot sizes. These earliest results for the first dots made[83] pointed out important needs: to fabricate smaller structures to reach the quantum limit; to better characterize structures, investigating single dots to eliminate inhomogeneous broadening; to identify the relaxation pathways; and to further reduce nonradiative recombination at surfaces. The deep-etched QDs directly through the quantum well typically had poor luminescence due to nonradiative recombination and trapping at etch-induced damage near the side walls. Deep-etched QDs made with low-damage etching such as electron cyclotron resonance etching[84,85] and wet chemical etching,[86] had luminescence efficiencies comparable to the corresponding quantum well luminescence efficiencies. For example, Bestwick et al.[85,89] fabricated 25-60 nm GaAs/AlGaAs QDs using electron cyclotron resonance etching. They got 5% size uniformity in samples with 57-nm-wide QDs. The linewidth for the QD PL from these samples was almost the same as for the quantum well PL (3 meV). For these QDs there was negligible blue shift between the QD and quantum well peaks, as one would expect for QDs five times bigger than the exciton.[80] These dots, with minimal sidewall damage, had luminescence efficiencies greater than for the unprocessed well. As the dot size decreased, the line width increased by a factor of two, indicative of size fluctuations for smaller dots. The exciton energy in 25 nm dots shifted by 7 meV due to the confinement. This is the magnitude of shift expected when the dot and exciton have the same size.[80]

Lithographic top-down approaches have not yet routinely provided the dot and wire structures needed. Essentially, the lithographic capabilities needed are still beyond the current state of the art. Etched structures were typically either too big to be useful as quantum structures at room temperature, had too much surface damage to provide adequate quantum efficiency, or did not have enough uniformity from structure to structure to provide the desired control. Alternatives such as barrier modulation and stressors provided weak confinement. Enhanced interdiffusion provided size reduction at the cost of reducing the barrier for confinement.

With development using top-down fabrication stalled, it became clear in the early 1990s that precision epitaxial growth techniques should be exploited for the bottom-up fabrication of wires and dots directly in quantum well structures. Quantum wells could be grown with monolayer precision down to a few monolayers in thickness. Comparable techniques were needed for dots and wires.

In the last 12 years, the development of quantum dots and wires has entered a second phase marked by more rapid and successful advancement. The development of quantum wire and dot structures was revitalized by the realization that comparable processes were needed to grow wires and dots from the bottom-up, ideally with the same precision and size control as achieved in the growth of quantum wells. Over the past decade, much progress has been made in realizing controlled bottom-up fabrication of dots and wires. This had led to dot and wire structures that now show real promise of providing much-enhanced integrated optical device structures for lasers and modulators. Such techniques as cleaved edge overgrowth (CEO), growth on nonplanar surfaces, and growth of self-assembled dot (SAD) structures have provided much smaller quantum

wires and dots with sufficiently controlled size and free from significant defects and good quality interfaces that do not degrade the luminescence. Lasing has been demonstrated with both wires and dots made with bottom-up growth techniques. These dots and wires have proven ideal for careful studies of the confined electrons, the effect of Coulomb interactions between trapped electrons and holes, and the coherent dynamics of the electrons in these structures. These achievements have led to well-developed fabrication techniques, early prototype quantum dot and wire laser structures.

The applications in traditional optics for dots and wires have been developed based on having a high density of dots or wires to provide a large optical response. At the same time, it has been assumed that the nanostructures are far enough apart to remain independent. In these optics applications, controlled positioning of the dots and wires is not important. However, other applications are being developed where position control will be increasingly important. For example, photonic crystals are arrays of dielectric scatterers carefully arranged to control photon dispersion, just as atoms in a lattice modify electron dispersion. Photonic crystals can be made, for example, by etching a regular array of holes into a quantum well system or etching away all of the structure except for a regular array of posts, each with an embedded quantum well. The typical dimension that defines the size of the hole or post and their separation is the wavelength of light. This is typically a few hundred nanometers for light propagation through semiconductor systems. Such dimensions are easily achieved by lithographic methods. It would be attractive to position optically active elements in each dielectric scatterer to provide optical gain, absorption, or nonlinear response.[88] That would require fabrication of nanostructures precisely positioned to have the same lattice structure as the intended

photonic crystal. As another example, applications in quantum technology that require controlled transfer of quantum information between quantum bits in different nanostructures will also require controlled positioning of these structures. Growth directly on substrates patterned by lithography can also be used to control the positions of the wires and dots.

While substantial work is still being done to engineer quantum dots and wires for traditional optics applications, the study of dots and wires has recently entered a new phase focusing on single quantum dot photonics. The characterization of single quantum wires and dots has become nearly routine, and detailed information about the optics of individual structures has been obtained. This has led to fundamental experiments in quantum optics such as antibunching and photon interference. In parallel, quantum dots are now being intensely investigated as sources for the operational quantum bits (qubits) and single photon sources needed for quantum information processing. These nontraditional applications in quantum technology are motivating much of the work now being done to develop structures with position control. Moreover, these applications in quantum technology are stimulating extensive work to extract detailed information about the quantum coherent dynamics and manipulation of optical excitations (the qubits) in quantum dots.

In addition, methods to provide position control of the growth are being pursued now. Such control is needed to fabricate complex structures such as photonic crystals with the dots or wires embedded in the periodic lattice to provide an attractive medium, and quantum dot structures for applications in quantum technology.[89]

Our quantum dot photolithography is a bottom-up photochemical method that allows us to synthesize various inorganic semiconductor quantum dots and nanoparticles at a precisely controlled physical location and with a precisely controlled size in porous materials and on planar substrates. This technique allows patterning of porous materials and planar substrates with electronically active materials. In our technique, the porous matrix was washed with a solution of the precursors, which react to form nanoparticles in the exposed regions with infrared (IR), ultraviolet (UV), X-rays and multi-photon ionization radiation.[90-95] Planar substrates like glass slides and silicon wafers can be patterned by spin coating a thin film of precursor solution on the substrate and by illuminating the selected region with the laser radiation. After exposure to the focused laser beam, quantum dots were formed in the illuminated regions. Both porous matrices and planar substrates were washed immediately with water to remove unreacted precursors. The patterned quantum dots were found to adhere reasonably well to the substrate, and were not washed out.[90-92] By focusing the beam of a Nd:YAG laser, quantum dots can be placed photolithographically on the surfaces and also in the bulk (3D) of silica hydrogels, and on the surfaces of planar substrates like glass slides.[91-93] Bulk (3D) patterning of silica hydrogels was also realized with multi-photon ionization radiation. IR patterning was focused on the photolithography of CdS nanoparticles on the surface and in the bulk of silica hydrogels and on the surface of planar substrates by using $CdNO_3$, NH_4OH and thiourea as precursors. By varying the type and concentration of capping agents like sodiumhexametaphosphate, 2-mercaptoethanol and thioglycerol, the size of the quantum dots-and therefore the quantum confinement effects-can be controlled at will.[91] Using 2-mercaptoethanol as a capping agent and focusing an infrared

beam inside the silica hydrogel allowed for 3D patterning. ultraviolet patterning uses CdSO$_4$ and 2-mercaptoethanol as precursors for CdS patterning and cadmiumperchlotate hexahydrate, selenourea, thioglycerol and sodium citrate for CdSe patterning. This method allowed us to pattern with a spatial resolution of a few microns. This represents a significant improvement over the infrared method, where resolution was not better than 40 μm, probably due to heat diffusion effects. The resolution could be further improved by employing more elaborate photolithographic equipment. This UV method also allowed patterning of planar substrates which is an extremely relevant feature, since it removes the need for a porous matrix to limit the nanoparticle size, and may allow planar fabrication of quantum dot devices. The UV method allowed using masks for sophisticated patterns. Recently we showed that (i) photodissociation can be made more efficient by using a different set of precursors like cadmiumperchalorate hexahydrate, selenourea, thioacetamide, 2-mercaptoethanol, thioglycerol and sodium citrate allowing production of complex patterns by masking, (ii) the quantum yield of the composites can be increased to up to about 30% by photoactivation, and (iii) quantum dots can be produced with X-ray lithography.[93,94] X-ray lithography paved the way to ultra-high spatial resolution. In our experiments, comparatively hard X-rays (8.5keV) were employed, for which masks can be realized which have a resolution of tens of microns. However, soft X-rays can be employed, for which masks can be fabricated with a resolution well below 1 μm. Features produced with X-ray lithography penetrated into the bulk of the monoliths for as much as 12 mm. These structures have an aspect ratio of around 200 and could conceivably be employed as waveguides. In fact, materials such as PbS have a much higher index of refraction (n=4.1) than the matrix (n=1.1 to 1.5) for

silica gels. Addition of PbS in a concentration as little as 0.1% by volume to a silica gel increases the index of refraction of the composite by $\Delta n \approx 5 \times 10^{-3}$, which is sufficient for waveguide applications.[93] The 3D fabrication of semiconductor nanoparticles using multi-photon ionization radiation is of potential relevance for 3D fabrication of contacts, electronic devices, quantum dot devices and 3D optical integrated circuits[95]. This method paved the way for the realization of 3D opto-electronic circuitry that includes passive and active components. An additional benefit is that the nanoparticles produced with this technique are in the quantum confinement regime, thus the technique could conceivably be employed for 3D fabrication of quantum dot devices.

Our techniques are unique because (i) they are of bottom-up character, (ii) they allow us access to a wide number of semiconductor materials for patterning, (iii) they are compatible for porous matrices and planar substrates, (iv) they are compatible with photolithographic fabrication methods, (v) sophisticated masks can be employed and (vi) 3D patterning is possible.

1.7. REFERENCES

[1.] M. G. Bawendi, M. L. Steigerwald, and L. E. Brus, *Annu. Rev. Phys. Chem.* **41**, 477 (1990).

[2.] M. G. Bawendi, W. L. Wilson, L. Rothberg, P. J. Carroll, T. M. Jedju, M. L. Steigerwald, and L. E. Brus, *Phys. Rev. Lett.* **65**, 1623 (1990).

[3.] W. Hoheisel, V. L. Colvin, C. S. Johnson, and A. P. Alivisatos, *J. Chem. Phys.* **101**, 8455 (1994).

[4.] A. P. Alivisatos, *Science*, **271**, 933 (1996).

5. H. Weller, *Angew. Chem. Int. Ed. Engl.*, **32**, 41 (1993).

6. S. Mann, *Nature*, **322**, 119 (1988).

7. J. Hu, T. W. Odom, and C. M. Lieber, *Acc. Chem. Res*. **32**, 435 (1999).

8. C. M. Leiber, *Solid State Commun*. **107**, 607 (1998).

9. X. Duan, Y. Huang, Y. Cui, J. Wang And C. M. Lieber, *Nature,* **409**, 66 (2001).

10. K. Leung , S. Pokrant, and K. B. Whaley, *Phys. Rev.B,* **57**, 12291 (1998).

11. X. Peng, L. Manna, W. Yang, J. Wickham, E. Scher, A. Kadavanich and A. P. Alivisatos, *Nature*, **404**, 59 (2000).

12. G. P. Mitchell, C. A. Mirkin, R. L.Letsinger, *J. Am. Chem. Soc*. **121**, 8122 (1999).

13. M. J. Bruchez, M. Maronne, P. Gin, S. Weiss, and A. P. Alivisatos, *Science*, **281**, 2016 (1998).

14. W. C. W. Chen, and S. M. Nie, *Science*, **281**, 2016 (1998).

15. M. Y. Han, X. H. Gao, J. Z. Su, and S. M. Nie, *Nat. Biol*. **19**, 631 (2001).

16. Y. Cui, and C. M. Lieber, *Science*, **291**, 851 (2001).

17. W. U. Huynh, J. J. Dittmer, and A. P. Alivisatos, *Science*, **295**, 2425 (2002).

18. P. Yang, In "*Global Photonics Applications and Technology*," World Markets Series, Business Briefing, P. 42. (2002).

19. Y. Cui, Q. Wei, H. Park, and C. M. Lieber, *Science*, **293**, 1289 (2001).

20. M. Law, H. Kind, B. Messer, F. Kim, and P. Yang, *Angew. Chem. Int. Ed*. **41**, 2405 (2002).

21. P. Yang, H. Yan, S. Mao, R. Russo, J. Johnson, R. Saykally, N. Morris, J. Pham, R. He, and H.-J. Choi, *Adv. Funct. Mater*. **12**, 323 (2002).

22. R. S. Knox, "*Theory of Excitons*", Solid State Physics Supplement 5, Academic Press, New York, (1963).

23. Y. Wang, In "Advances In Photochemistry" (D.C. Neckers, D.H. Volman, And G. Von Bunau, Eds.), Vol. **19**, P. 179. Willey, New York, (1995); A. I. Ekimov, Al. A. Efros, and A. A. Onuschenko, *Solidi State Commun*. **56**, 921 (1985).

24. (a) Al. L. Efros, and A. L. Efros, *Fiz. Tech. Poluprovodn*. **16,** 1209 (1982) [*Sov. Phys. Semicond*. **16**, 772 (1982)], (b) A. I. Ekimov, and A. A. Onushchenko, *Zh. Eksp. Teor. Fiz*. **40**, 337 (1984) [*JETP Lett*. **40**, 1136(1984)].

25. L. E. Brus, *J. Chem. Phys*. **80**, 440 (1984).

26. Y. Kayanuma, *Phys. Rev. B* **38**, 9797 (1988).

27. A. P. Alivisatos, *J. Phys. Chem*. **100**, 13226 (1996).

28. D. M. Mittleman, R. W. Schoenlein, J. J. Shiang, V. L. Clovin, A. P. Alivisatos, and C. V. Shank, *Phys. Rev. B*, **49**, 14435 (1994).

29. Y. Arakawa, and H. Sakaki, *Appl. Phys. Lett*. **40**, 939 (1982).

30. T. Fujji, S. Yamakoshi, K. Nabu, O. Wada, and S. Hiyamiza, *J. Vac. Sci. Technol*. **2**, 259 (1984).

31. *Quantum Wells, Wires And Dots, Second Ed.* By Paul Harrison, Wiley- Interscience, John Wiley & Sons, Ltd, (2005).

32. L. E. Burs, *J. Chem. Phys*., **80**, 4403 (1984).

33. H. Sakaki, *Japan J. Appl. Phys*. **28**, L314 (1989).

34. L. Esaki, and T. Tsu, *IBM J. Res. Develop*. **14**, 61 (1970).

35. H. P. Rocksby, *J. Soc. Glass Tech*. **16**, 171 (1932).

36. A. I. Ekimov, Ai. L. Efros, and A. A. Onushchenko, *Solid State Communications* **56**, 921 (1985).

37. A. I. Ekimov, A. A. Onushchenko, A. G. Plyukhin, and A. L. Efros, *Zhurnal Eksperimental'noi I Teoreticheskoi Fiziki*, **88**, 1490 (1985).

38. H. Van Houten, C. W. J. Beenakker, And A. A. M. Staring, In "Single Charge Tunneling". (H. Grabert And M. H. Devoret, Eds.), Vol. **294** of *Nato Asi Series*, P. 167. Plenum Press, New York, (1992).

39. L. P. Kouwenhoven, C. M. Markus, P. L. Mceuen, S. Tarucha, R. M. Westervelt, and N. S. Wingreen, In "Mesoscopic Electron Trasnport." (L. L. Sohn, L. P. Kouwenhoven, And G. Schön, Eds), Vol. **345** of *Nato Asi Series*, P. 105. Kulwer Academic, Dordrecht, (1997).

40. U. Meirav, and E. B. Foxman, *Semicond. Sci. Technol*. 10, 255 (1995).

41. A. Zrenner, E. Beham, S. Stufler, F. Findeis, M. Bichler, and G. Abstreiter, *Nature*, **418,** 612 (2002).

42. *Mathematical Methods for Physicists*, 4th Ed., G. B. Arfken, and H. J. Weber, Academic Press, (1995).

43. *Introductory Quantum Mechanics*, 4th Ed., by Richard l. Liboff, by Pearson Education (Singapore) Pte. Ltd. (2003).

44. T. P. Cassagneau, B. Sweryda-Karwiec, and J. H. Fendler, *Mater. Res. Soc. Bull.* **25**, 40 (2000).

45. S. Wang, S. L. Westcott, and W. Chen, *J. Phys. Chem. B*, **106**, 11203 (2002).

46. S. W. Allison, and G. T. Gillies, *Rev. Sci. Instrum*., **68**, 2615 (1997).

47. W. C. Chen, and S. M. Nie, *Science*, **281**, 2016 (1998).

48. D. L. Dexter, *J. Chem. Phys*. **21**, 836 (1953).

49. J. R. Lakowicz, "**Principles of Fluorescence Spectroscopy**", 2nd Ed. Kulwar Academic/Plenum, New York, (1999).

50. S. Tiwari, F.Rana, H. Hanafi, A. Hartstein, E. F. Crabbe, and K. Chen, *Appl. Phys. Lett*. **68**, 1377 (1996).

51. Y. Liu, and R. O. Claus, *Proc. SPIE,* **3242**, 118 (1997).

52. F. Jones, H. Colfen, and M. Antonietti, *Colloid Polym. Sci*., **278**, 491 (2000).

53. K. E. Gonsalves, H. Li, and P. Santigo, *J. Mater. Sci*. **36**, 2461 (2001).

54. S. C. Farmer, and T. E. Patten, *Chem. Mater*. **13**, 3920 (2001).

55. F. M. Pavel, and R. A. Mackay, *Langmuir*, **16**, 8568 (2000).

56. B. Simmons, S. Li, V. T. John, G. L. Mcpherson, C. Taylor, D. K. Schwartz, and K. Maskos *Nano Lett*. *(Letter)*, **2**, 1037 (2002).

57. Q. Zhou, S. Wang, X. Fan, J. Mays, R. Advincula, G. Sakellariou, S. Pispas, and N. Hadjichristides, *Polym. Preprint Acs Div. Polym. Chem*, **42**, 59 (2001).

58. S.-Y. Kwak, S. H. Kim, and S. S. Kim, *Env. Sci. Tech*. **35**, 2388 (2001).

59. R. Reisfeld, T. Saraidarov, and B. Jasinska, *Optical Materials*, **26**, 181 (2004).

60. A. C. Pirre, and G. M. Pajonk, *Chem. Rev*. **102**, 4243 (2002).

61. K. V. Yumashev, V. S. Gurin, P. V. Prokoshin, V. B. Prokopenko, and A. A. Alexeenko, *Physica Status Solidi B: Basic Research*, **224**, 815 (2001).

62. Z. Li, L. Meichuan, C. Yuxiao, L. Ping, Z. Chenglin, and J. Litong, *Huaxue Chuanganqi*, **25**, 51 (2005).

63. P. A. S. Jorge, M. Mayeh, R. Benrashid, P. Caldas, J. L. Santos, and F. Farahi, *Applied Optics*, **45**, 3760 (2006).

64. J. Haiqing, Y. Xi, C. Jun, W. Minqiang, and K. Fantao, *Ceramics International*, **30**, 1685 (2004).

65. T. Deng, F. Arias, R. F. Ismagilov, P. J. A. Kenis, and G. M. Whitesides, *Anal. Chem.*, **72**, 645 (2000).

66. M. Fukushima, H. Yanagi, S. Hayashi, N. Suganuma, and Y. Taniguchi, *Thin Solid Films* , **438**, 39 (2003).

67. E. W. Bohannan, X. Gao, C. Sotiriou-Leventis, K. R. Gaston, C. D. Doss, and N. Leventis, *J. Sol-Gel Sci. Tech.*, **23**, 235 (2002).

68. V.C. Sundar, H.J. Eisler, and M.G. Bawendi, *Adv. Mater.*, **14**, 739 (2002).

69. B. Capoen, T. Gacoin, J. M. Nedelec, S. Turrell ,and M. Bouazaoui, *J. Mater. Sci.*, **36**, 2565 (2001).

70. N. Tohge, M. Asuka, and T. Minami, *SPIE*, **1328**, 125 (1990).

71. J. M. Wallace, J. K. Rice, J. J. Pietron, R. M. Stroud, J. W. Long, and D. R. Rolison, *Nano Lett.*, **3**, 1463 (2003).

72. M. Fukushima, H. Yanagi, S. Hayashi, N. Suganuma, and Y. Taniguchi, *Thin Solid Films*, **438**, 39 (2003).

73. S. A. Maier, M. D. Friedman, P. E. Barclay, and O. Painter, *Appl. Phys. Lett*. **86**, 1103 (2005).

74. F. Stellacci, C. A. Bauer, T. Meyer-Friedrichsen, W. Wenseleers, V. Alain, S. M. Kuebler, S. J. K. Pond, Y. Zhang, S. R. Marder, and W. J. Perry, *Adv. Mater.*, **14**, 194 (2002).

75. Harisingh Nalwa, "*Encyclopedia of Nanoscience And Nanotechnology*", American Scientific Publishers Vol. **4**, Page # 49

76. K. Vahala, *IEEE J. Quantum Elect*., **24**, 523 (1988).

77. H. Temkin, G. J. Dolan, M. B. Panish, and S. N. G. Chu, *Appl. Phys. Lett*., **50**, 43 (1987).

78. M. A. Reed, R. T. Bate, K. Bradshaw, W. M. Duncan, W. R. Frensley, J. W. Lee, and H. D. Shih, *J. Vac. Sci. Technol*. **B**, **4**, 358 (1986).

79. K. Kash, A. Scherer, J. M. Worlock, H. G. Craighead, and M. C. Tamargo, *Appl. Phys. Lett.* **49**, 1043 (1986).

80. G. W. Bryany, *Phys. Rev. B*, **37**, 8763 (1988).

81. P. M. Petroff, J. Cibert, A. C. Gossard, G. J. Dolan, and C. W. Tu, *J. Vac. Sci. Technol. B*, **5**, 1204 (1987).

82. J. Cibert, and P. M. Petroff, *Phys. Rev. B*, **36**, 3243 (1987).

83. An Excellent Review Of Work Done Until 1990 Is Given By K Kash, *J. Lumin*., **46**, 69 (1990).

84. L. Davis, K. K. Ko, W.-Q. Li, H. C. Sun, Y. Lam, T. Brock, S. W. Pang, P. K. Bhattacharya and M. J. Rooks, *Appl. Phys. Lett*., **62**, 2766 (1993).

85. T. D. Bestwick, M. D. Dawson, A. H. Kean, and G. Duggan, *Appl. Phys. Lett*. **66**, 1382 (1995).

86. O. Schilling, A. Forchel, M. Lebedev, Ph. Pagond-Rossaiaux, and L. Goldstein, *Superlatt. Microstruct*. **16**, 261 (1994).

87. C. A. Verschure, T. D. Bestwick, M. D. Dawson, A. H. Kean, and G. Duggan, *Phys. Rev. B*, **52**, 8640 (1995).

88. S. Watanabe, E. Pelucchi, B. Dwir, M. H. Baier, K. Leifer, and E. Kapon, *Appl. Phys. Lett.* **84**, 2907 (2004).

89. G. W. Bryant, and G. S. Solomon "*Optics Of Quantum Dots And Wires*" Artech House, Inc. 685 Canton Street, Norwood, Ma 02062, (2005).

90. M. F. Bertino, R. R. Gadipalli, J. G. Story, C. G. Williams, G. Zhang, C. Sotiriou-Leventis, A. T. Tokuhiro, S. Guha, and N. Leventis, *Appl. Phys. Lett*. **85**, 6007 (2004).

91. R. R. Gadipalli, L. A. Martin, B. Heckman, J. G. Story, M. F. Bertino, P. Fraundorf, S. Guha, and N. Leventis, *J. Sol-Gel Sci. Tech*. **40**, 101 (2006).

92. M. F. Bertino, R. R. Gadipalli, L. A. Martin, J. G. Story, B. Heckman, S. Guha, and N. Leventis *J. Sol-Gel Sci. Tech*. **39**, 2999 (2006).

93. M. F. Bertino, R. R. Gadipalli, L. A. Martin, L. E. Rich, A. Yamilov, B. R. Heckman, N. Leventis, S. Guha, J. Katsoudas, R. Divan, and D. C. Mancini, *Nanotechnology* **18**, 315603 (2007).

94. M. F. Bertino, R. R. Gadipalli, L. A. Martin, B. Heckman, N. Leventis, S. Guha, J. Katsoudas, R. Divan, and D. C. Mancini, "X-ray lithography of metal and semiconductor nanoparticles", *JVST B* (accepted).

95. R. R. Gadipalli, L.A.Martin, L. Rich, J. G. Story, A. Yamilov, M. F. Bertino, B. Heckman, N. Leventis, S.Guha, "*Three-Dimensional Semiconductor Patterning*" (To Be Submitted).

PAPER - I

2. LASER WRITING OF SEMICONDUCTOR NANOPARTICLES AND QUANTUM DOTS

M. F. Bertino,[1] R. R. Gadipalli,[1] J. G. Story,[1] C. G. Williams,[1] G. Zhang,[2] C. Sotiriou-Leventis,[2] A. T. Tokuhiro,[3] S. Guha,[4] and N. Leventis[5]

[1]Department of Physics, University of Missouri-Rolla, Rolla, MO 65409.

[2] Department of Chemistry, University of Missouri-Rolla, Rolla, MO 65409.

[3]Department of Nuclear Engineering, University of Missouri-Rolla, Rolla, MO 65409.

[4]Department of Physics, University of Missouri-Columbia, Columbia, MO 65211.

[5]NASA Glenn Research Center, Materials Division/Polymers Branch, 21000 Brookpark Road, Cleveland, OH 44135.

2.1. ABSTRACT

Silica aerogels were patterned with CdS using a photolithographic technique based on local heating with infrared (IR) light. The solvent of silica hydrogels was exchanged with an aqueous solution of the precursors $CdNO_3$ and NH_4OH, all pre-cooled to a temperature of 5 ^0C. Half of the bathing solution was then replaced by a thiourea solution. After thiourea diffused into the hydrogels, the samples were exposed to a focused IR beam from a continuous wave, Nd-YAG laser. The precursors reacted in the spots heated by the IR beam to form CdS nanoparticles. We successfully lithographed features with a diameter of about 40 μm, which extended inside the monoliths for up to 4 mm. Samples were characterized with transmission electron microscopy and optical absorption, photoluminescence and Raman spectroscopies. Spots illuminated by the IR

beam were made up of CdS nanoparticles dispersed in a silica matrix. The CdS nanoparticles had a diameter in the 4-6 nm range in samples exposed for four minutes to the IR beam, and of up to 100 nm in samples exposed for ten minutes.

Photolithographic patterning of sol-gel materials is becoming increasingly important for optical and electronic applications, and for data storage and encryption. Surface patterning can be employed to realize electrical contacts[1] and diffraction gratings.[2,3] Patterning can also have a more three-dimensional character, and the lithographed features can extend from the surface deep into the bulk of the materials.[4] "True" three-dimensional patterning, i.e., formation of patterns in the bulk of the materials but not on their surface, is achieved with multiphoton ionization techniques.[5,6]

Patterning with these techniques is attained in two simple steps, impregnation of the matrices with a solution of metal ions followed by photoreduction. However, patterns can be produced only out of materials accessible to photoreduction, noble and semi-noble metals. Patterning of sol-gel materials with electronically active components like semiconductors and magnetic materials usually requires multiple steps. The (pre-formed) active phase is added during gelification of the matrix,[7-9] or synthesized by calcination of precursors.[10-13] The resulting composites are homogeneously loaded with the active phase, and patterning is achieved by etching.

We report here a photolithographic technique that allows patterning of porous materials with electronically active materials. In our technique, the porous matrix is washed with a solution of the precursors, which react to form nanoparticles in the spots heated by an infrared (IR) laser. The experiments described here focus on

photolithography of CdS nanoparticles inside a silica hydrogel. The mean size of the CdS nanoparticles can be increased from a few nm to about 100 nm by increasing the exposure to the IR beam. The hydrogel is subsequently dried in supercritical CO_2 to form an aerogel. Our technique, however, is more general. It can produce patterns of metals and magnetic materials, and can probably be extended to other porous matrices. For example, we have successfully patterned silica aerogels with Ag by irradiating solutions of $AgNO_3$ and formaldehyde, and with Fe (and Fe oxides) by irradiating solutions of Fe-triethanolamine complexes and hydrazine.[14] These results will be reported in a forthcoming publication.[15]

Silica hydrogels were prepared with a conventional base-catalyzed route.[4,16] The hydrogels were then washed in methanol and in water, and placed in a refrigerator kept at $5\ ^0C$. CdS was synthesized by hydrolyzing thiourea in basic solution.[17-21] Hydrogels were bathed in a pre-cooled aqueous solution of $CdNO_3$ (1 mol·l^{-1}) and NH_4OH (4 mol·l^{-1}). After about two hours, half of the bathing solution was removed from the vial, and was replaced by a 1 mol·l^{-1} thiourea solution. The samples were left in the refrigerator for an additional hour to let thiourea diffuse inside the monoliths. Cooling was necessary, since hydrogels loaded with the precursors turned pale yellow within about one hour when kept at room temperature. The monoliths did not change their color appreciably when refrigerated. The samples were then rapidly removed from the refrigerator, placed in a glass cuvette, and exposed to the light of a continuous wave Nd-YAG laser. The IR power on the sample was typically 1.8 W. Nanoparticle formation was monitored with transmission electron microscopy (TEM) and by observing the coloration of the illuminated spots. Nanoparticles started forming and the spots started becoming yellow

after an irradiation time of about four minutes. The spots kept becoming darker (and the particles somewhat larger, and more densely distributed) for another 6 minutes. We did not notice any relevant changes afterwards. We then compared this reaction time with the reaction time of hydrogels that were loaded with the precursors and placed in a constant temperature bath. The reaction time was about 10 minutes at temperatures below 35 ^{0}C, and a few seconds at temperatures higher than 60 ^{0}C. We thus estimated that the local temperature was between 35 and 60^{0}C. After exposure, the samples were immediately washed several times in cold distilled water to quench any further reaction of the precursors. To produce aerogels, the hydrogels were washed in methanol and in acetone, and were then dried in supercritical CO_2.
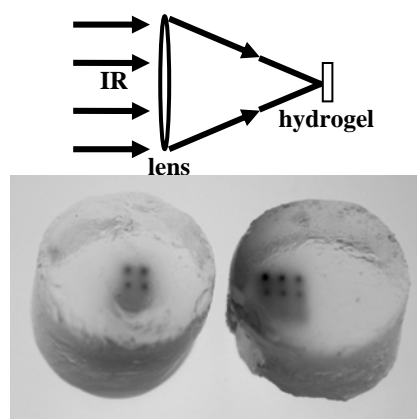
Figure 2.1. Top: Schematic representation of the illumination arrangement. Bottom: digital camera image showing arrays of CdS spots photolithographed in two aerogel monoliths. The diameter of the aerogel monoliths was about 7 mm, and the diameter of the circular spots was about 400 μm.

Arrays of circular spots photolithographed with our technique are shown in Fig. 2.1. By varying the focal length of the lens and the distance between the hydrogel surface and the lens focus, the diameter of the spots was varied between 40 and 400 μm, and the penetration depth from a few microns to a few millimeters. The size and color of the spots did not change upon washing and supercritical drying, indicating that CdS was neither chemically altered nor removed by the washings, in agreement with our previous patterning experiments.[4] After drying, regions lithographed with CdS were carved out of the matrix and crushed. The powder was analyzed with TEM. Typical micrographs of samples exposed for four minutes to the IR beam are reported in Fig. 2.2a and 2.2b. CdS nanoparticles appeared as dark spots, and were fairly uniformly distributed within the silica matrix. Energy-dispersive X-ray chemical analysis showed that the composition of the particles was 55% Cd - 45% S, comparable to the composition of the bathing solution. High magnification micrographs (Fig. 2.2b) showed that particles with a typical diameter of 20 nm coexisted with a large number of particles with a diameter of a few nm. A size distribution histogram is reported in Fig. 2.2c. The mean particle size was around 7 nm. With increasing exposure to the IR beam, the nanoparticles became larger (~ 100 nm) and more densely packed, as shown in figure 2.2d. This indicated that growth of pre-formed particles prevailed on nucleation of new particles, consistent with our previous findings on the synthesis of Ag nanoparticles in silica aerogels[16]. Preliminary results show that the size of the nanoparticles did not depend strongly on laser power within the range accessible to our instrument (1 to 7 W, measured at the sample). This is probably because the reaction time was of the order of a few minutes for all powers

employed. A complete investigation of the factors affecting nanoparticle size will be reported in a separate publication[15].
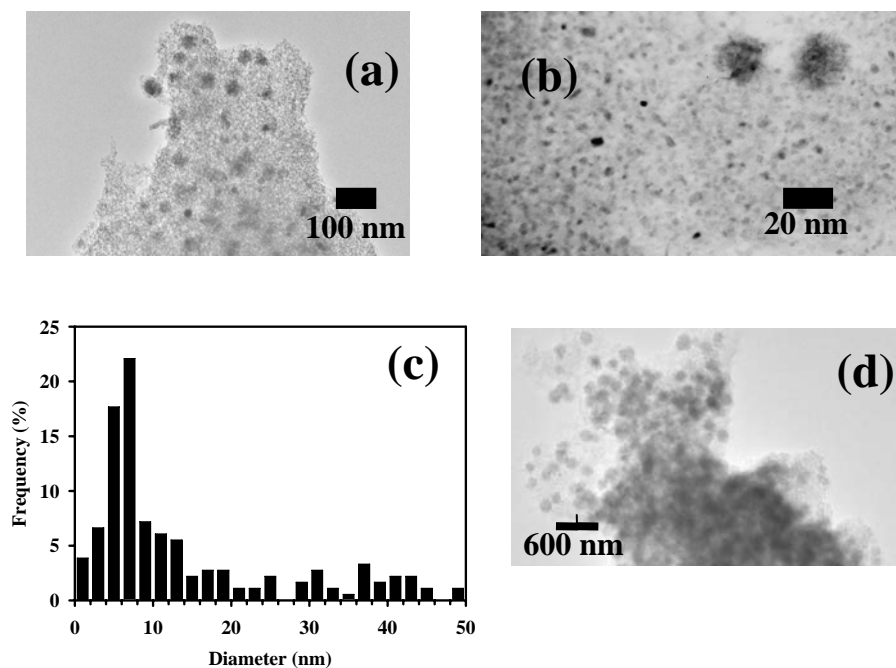
Figure 2.2. (a), (b) Bright field micrographs of CdS-patterned silica aerogels. IR exposure was four minutes. (c) Corresponding size distribution histogram. (d) Same as above for an IR exposure of ten minutes.

Samples were additionally characterized with optical absorption, photoluminescence and Raman spectroscopies. Room temperature absorption and photoluminescence (PL) spectra are reported in Fig. 3a. The absorption spectrum exhibited an excitonic shoulder at about 440 nm, characteristic of CdS nanoparticles with a diameter in the 4-4.5 nm range.[22] Photoluminescence spectra exhibited a peak around 475 nm and a shoulder around 520 nm. A peak around 475 nm has been found in CdS/silica composites with a CdS nanoparticle diameter between 4 and 5 nm.[23-25] The

shoulder at 520 nm was probably due to particles with a larger diameter,[24] but may also be due to recombination at surface defects.[23,25] Formation of defects at the surface of CdS nanoparticles is not surprising, since the nanoparticles are probably nucleated and remain in contact with the pore walls.[26,27] Spots exposed for long times to the IR beam were optically dense, and their absorption spectrum could not be measured. Photoluminescence intensity from these samples was absent or below the detection limit of our instrumentation. Raman spectra, shown in Fig. 2.3b, exhibited a peak at 298 cm^{-1}. This frequency was in good agreement with previous Raman measurements of CdS/silica composites,[28] and corresponded to the first-order LO phonon frequency of CdS. The full width at half maximum (FWHM) of the Raman peak was 36 cm^{-1}, which was found to correspond to a mean particle size of about 3 nm in CdS/silicon dioxide films.[29]
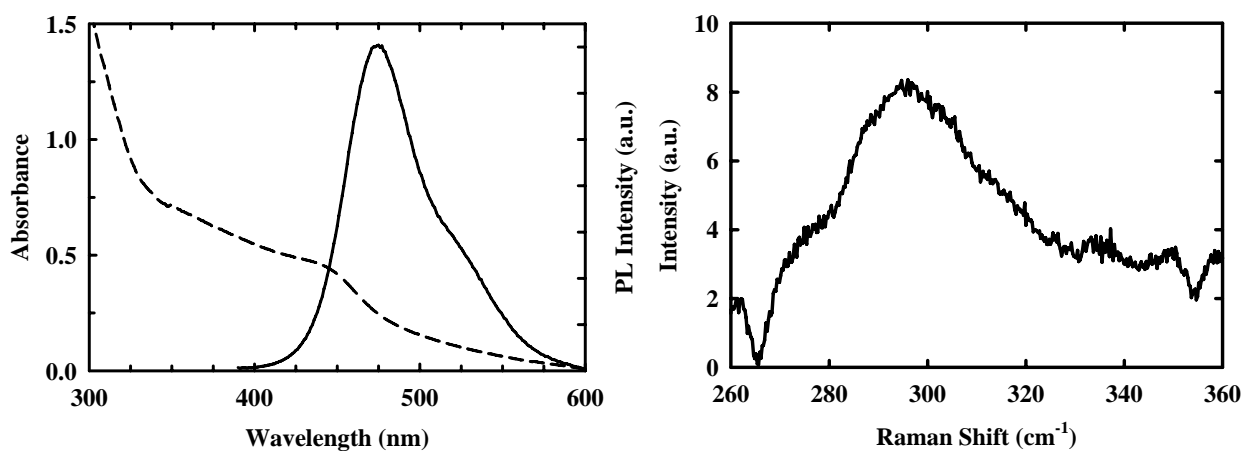
Figure 2.3. (a) Room temperature absorption (dashed line) and photoluminescence (solid line) of silica aerogel samples patterned with CdS. PL was excited at 350 nm. (b) Room temperature Raman spectra of silica aerogel samples patterned with CdS. IR exposure was four minutes for all samples.

Optical characterization confirmed the chemical identity of the CdS nanoparticles. It also showed that a relevant fraction of nanoparticles exhibited quantum confinement effects in samples exposed for a short time to the IR beam. The mean particle size determined with linear optical spectroscopies was between 3 and 5 nm. The difference with the TEM mean size (~7 nm) is not irreconcilable, since the TEM size determination procedure was probably skewed towards large sizes. Small CdS particles could hardly be distinguished from the silica matrix, and we counted only particles with regular shapes which showed a large contrast. Mean sizes determined with optical spectroscopies also have a fairly large uncertainty, the main sources of error being polydispersity and surface defects.[25,30]

In conclusion, we have shown a simple method to pattern silica aerogels with CdS. Our method is quite general, and can be extended to other semiconductors, to magnetic materials, to metals, and also to other porous matrices. Size control is reasonable, and can probably be improved by adding surfactants to the bathing solution, or by employing matrices with a uniform pore size like MCM-41[13] or porous anodized alumina[28]. The main challenge of our technique concerns the choice of the precursors. These must not react rapidly at room temperature, otherwise the composites will be uniformly loaded with the active phase. The reaction cannot require too high temperatures, because these need high laser powers, which can damage the host matrix. In the experiments described here, the reaction rate is tuned by varying the NH_4OH concentration. When the concentration of NH_4OH is too low, most of the Cd precipitates as $Cd(OH)_2$, and does not diffuse inside the hydrogel. $Cd(OH)_2$ also catalyzes hydrolysis of thiourea, and CdS forms rapidly even in cold samples. At high NH_4OH concentrations,

$Cd(NH_3)_4^{2+}$ complexes are formed. These complexes are water soluble, and they diffuse inside the matrix. They also do not catalyze hydrolysis of thiourea as strongly as $Cd(OH)_2$. Temperatures of the order of 35-60 ^{0}C are required to hydrolyze thiourea at an appreciable rate,[17] and these temperatures are easily reached with IR irradiation.

2.2. REFERENCES

[1] T. Deng, F. Arias, R. F. Ismagilov, P. J. A. Kenis, and G. M. Whitesides, *Anal. Chem.* **72**, 645 (2000).

[2] M. Fukushima, H. Yanagi, S. Hayashi, N. Suganuma, and Y. Taniguchi, *Thin Solid Films* **438 –439**, 39 (2003).

[3] E. W. Bohannan, X. Gao, C. Sotiriou-Leventis, K. R. Gaston, C. D. Doss, and N. Leventis, *J. Sol-Gel Sci. Techn*. **23**, 235 (2002).

[4] M. F. Bertino, J. F. Hund, J. Sosa, G. Zhang, C. Sotiriou-Leventis, N. Leventis, A. T. Tokuhiro, and J. Terry, J. *Non-Cryst. Solids* **333,** 108 (2004).

[5] P.-W. Wu, W. Cheng, I. B. Martini, B. Dunn, B. J. Schwartz, and E. Yablonovitch, *Adv. Mater*. **12**, 1438 (2000).

[6] F. Stellacci, C. A. Bauer, T. M. Friedrichsen, W. Wenseleers, V. Alain, S. M. Kuebler, S. J. K. Pond, Y. Zhang, S. R. Marder, and J. W. Perry, *Adv. Mater*. **14**, 194 (2002).

[7] C. A. Morris, M. L. Anderson, R. M. Stroud, C. Merzbacher, and D. R. Rolison, *Science* **284**, 622 (1999).

[8] N. Leventis, I. A. Elder, G. J. Long, and D. R. Rolison, *Nano Lett*. **2,** 63 (2002).

9. V. I. Klimov, A. A. Mikhailovsky, S. Xu, A. Malko, J. A. Hollingsworth, C. A. Leatherdale, H. J. Eisler, and M. G. Bawendi, *Science* **290**, 314 (2000).

10. Y. Zhang, N. Raman, J. K. Bailey, C. J. Brinker, and R. M. Crooks, *J. Phys. Chem*. **96**, 9098 (1992).

11. A. V. Rao, G. M. Pajonk, N. N. Parvathy, *Mater. Chem. and Phys*. **48**, 234 (1997).

12. S. Besson, T. Gacoin, C. Ricolleau, C. Jacquiod, and J. P. Boilot, *Nano Lett*. **2**, 409 (2002).

13. W. Xu, Y. Liao, and D. L. Akins, *J. Phys. Chem*. B **106**, 11127 (2002).

14. R. S. Sapieszko, and E. Matjevic, *J. Colloid Interf. Sci*. **74**, 406 (1980).

15. M. F. Bertino, R. R. Gadipalli, J. G. Story, C. Sotiriou-Leventis, S. Guha, J. A. Switzer, and N. Leventis, (unpublished).

16. J. F. Hund, M. F. Bertino, G. Zhang, C. Sotiriou-Leventis, N. Leventis, A. Tokuhiro, and J. Farmer, *J. Phys. Chem. B* **107**, 465 (2003).

17. I. Kaur, D. K. Pandya, and K. L. Chopra, *J. Electrochem. Soc*. **127**, 943 (1980).

18. N. C. Sharma, R. C. Kainthla, D. K. Pandya and K. L. Chopra, *Thin Solid Films* **60**, 55 (1979).

19. S. C. Sahu , and S. N. Sahu, *Thin Solid Films* **235**, 17 {1993).

20. P.C. Rieke, and S. B. Bentjen, *Chem. Mater*. **5**, 43 (1993).

21. G. A. Kitaev, A. A. Uritskaya, and S. G. Mokrushin, *Zhurnal Fizicheskoi Khimii*, **38**, 2065 (1965).

22. P.E. Lippens, and M. Lannoo, *Phys. Rev. B* **39**, 10935 (1989).

23. N. De La Rosa-Fox, M. Pinero, R. Litran, and L. Esquivias, *J. Sol-Gel Sci. Techn*. **26**, 947 (2003).

24. T. Iwami, K. Tadanaga, M. Tatsumisago, and T. Minami, *J. Am. Ceram. Soc*. **78**, 1668 (1995).

25. B. Capoen, T. Gacoin, J. M. Nedelec, S.Turrell, and M.Bouazaoui, *J. Mater. Sci*. **36**, 2565 (2001).

26. V. Hornebecq, M. Antonietti, T. Cardinal, and M. Treguer-Delapierre, *Chem. Mater*. **15**, 1993 (2003).

27. D. Lawless, S. Kapoor, P. Kennepohl, D. Meisel, and N. Serpone, *J. Phys. Chem*. **98**, 9619 (1994).

28. A. Balandin, K.L. Wang, N. Houklin, and S. Bandyopadhyay, *Appl. Phys. Lett*. **76**, 137 (2000).

29. A.G. Rolo, L.G. Vieira, M. J. M. Gomes, J. L. Rebeiro, M .S. Belsley,   and M. P. Dos Santos, *Thin Solid Films* **312**, 348 (1998).

30. M. Guglielmi, A. Martucci, G. C. Righini, and S. Pelli, *Sol-Gel Optics* **2288**, 174 (1994).

PAPER - II

3. PATTERNING POROUS MATRICES AND PLANAR SUBSTRATES WITH QUANTUM DOTS

M.F.Bertino[1], R. R Gadipali[1], L. A. Martin[1], J. G. Story[1], B. Heckman[1], S. Guha[2],

N. Leventis[3]

[1]Department of Physics, University of Missouri-Rolla, MO 65409, USA

[2]Department of Physics, University of Missouri-Columbia, Columbia, MO 65211, USA

[3]NASA Glenn Research Center, Materials Division/Polymers Branch, 21000 Brookpark Road, Cleveland, Ohio 44135 & Department of Chemistry , University of Missouri-Rolla, MO 65409, USA

3.1. ABSTRACT

Silica hydrogels and planar substrates were patterned with CdS nanoparticles using a photolithographic method based on the photo dissociation of thiols and cadmium-thiolate complexes. Silica hydrogels were prepared via a standard base-catalyzed route. The solvent was exchanged with an aqueous solution of $CdSO_4$ and 2-mercaptoethanol, and the samples were then exposed to a focused ultraviolet beam. Planar substrates were patterned by illuminating a precursor solution spin coated on the substrates. CdS nanoparticles formed in the illuminated spots, and had a diameter below about 2 nm. The diameter of the spots illuminated by the UV beam could be varied from a few hundred to a few μm, on both hydrogels and planar substrates. Samples were characterized with transmission electron microscopy, X-ray photoelectron spectroscopy, X-ray diffraction, and optical absorption, photoluminescence and Raman spectroscopies. All these

techniques confirmed the chemical identity of the CdS nanoparticles. To investigate the mechanism of nanoparticle formation, we took absorption spectra of the precursor solution as a function of UV irradiation time. In unirradiated solutions, we noticed a maximum at 250 nm, characteristic of Cd-thiolate complexes. The absorption at 250 nm decreased with increasing UV exposure. A new band appeared at 265 nm for exposures around 5 minutes, and that band shifted to 290 nm in samples exposed for 10 minutes. A yellow precipitate formed after about 30 minutes. XRD showed that the precipitate was cubic CdS, with a mean particle size of 1.4 nm. We attribute formation of CdS to the photodissociation of the thiols and of the Cd-thiolates. UV irradiation of these precursors yields a series of species that can react with Cd^{2+}, such as $RS^{\cdot}$, S^{2-} and H_2S. Small CdS nanoparticles form in the initial stages of illumination, and present absorption bands in the 265 – 290 nm region. These CdS aggregates grow, coalesce and precipitate for longer irradiation times.

3.2. INTRODUCTION

Quantum dot-based technologies are moving from the laboratory into commercial applications. Kits for labeling biomolecules and cells with quantum dots, but also composites of quantum dots and polymers are now commercially available.[1] Quantum-dot based composites are especially attractive materials, and can be used for a variety of applications. For example, quantum dot lasers have been fabricated based on quantum dots embedded in a titania sol-gel matrix,[2] and PbS and CdS nanoparticles embedded in silica gels are being considered for waveguide and non-linear optical applications.[3,4] A major issue preventing widespread application of quantum dot composites is cost, which

derives mainly from the relatively complex synthetic procedures employed to produce composites made up of high quality quantum dots.[2] Cost issues become even more relevant if one considers that in microfabrication a large fraction of a quantum dot film may have to be etched away and discarded. It would therefore be desirable to develop techniques that allowed rapid and inexpensive fabrication of high quality quantum dots and quantum dot composites.

Our group has recently developed a method that alleviates, in part, these fabrication issues, and is also compatible with commonly employed photolithographic technologies.[5] According to our methodology, the solvent of silica hydrogels is exchanged with a solution of quantum dot precursors. Typically, one of the precursors is a group II metal chelate, and the second precursor is a sulfur-containing molecule like thiourea. Local heating with an infrared (IR) laser beam dissociates the chelate and the sulfur precursor and small, quantum confined sulfide nanoparticles are formed within the illuminated area.

In this manuscript, we present an alternate method that follows the same general principles of the IR approach, and uses a UV light to generate CdS inside a porous matrix. The main difference is that the new precursors are cadmium-thiolate complexes and thiols that are photodissociated by ultraviolet light. Operating with ultraviolet light has allowed us to pattern with a spatial resolution of a few microns. This represents a significant improvement over the IR technique, where resolution was not better than 40 μm, probably due to heat diffusion effects. The resolution could be further improved by employing more elaborate photolithographic equipment. Our technique also allows patterning of planar substrates by exposing glass slides spin coated with the precursor

solution to UV light. Patterning of planar substrates is an extremely relevant feature, since it removes the need for a porous matrix to limit the nanoparticle size, and may allow planar fabrication of quantum dot devices.

3.3. EXPERIMENTAL

3.3.1. Gel synthesis and patterning procedure. Silica hydrogels were prepared following a conventional base-catalyzed route.[6] The hydrogels were then washed several times in methanol and in water. The hydrogels were cut into small cylinders of about 7 mm in diameter, and 5-7 mm in length. The cylinders were then bathed in 20 ml of a solution of $CdSO_4$ and 2-mercaptoethanol, $HOCH_2CH_2SH$, for about 2 hours. Several precursor concentrations were tested; the best results were obtained by using a thiol concentration of at least 10 times higher than the metal ion concentration, and by adding NH_4OH to reach a pH of at least 7.5, e.g., $[CdSO_4]$ = 0.1 mol·l^{-1} (M), $[HOCH_2CH_2SH]$ = 1 M, $[NH_4OH]$ = 4 M. We also worked without adding a base, but with a thiol concentration at least 500 times higher than the metal ion concentration, e.g., $[CdSO_4]$ = 0.005 M, and $[HOCH_2CH_2SH]$ = 7 M. The minimum UV exposure times necessary to produce nanoparticles as well as the physical characteristics of the nanoparticles did not depend strongly on the composition of the precursor solution and on the pH. The hydrogel samples were placed in a glass cuvette filled with the bathing solution for index matching, and were exposed to ultraviolet light. The light source was either a high pressure, 100 W Hg arc discharge lamp, or the 351.1 nm excitation wave of a continuous wave Ar ion laser (Coherent Innova). The laser power at the sample was on the order of 50 mW, and the illuminated spots had a diameter between about 3 and 100 μm. To ensure

that only the ultraviolet light was initiating the chemical reaction and that visible and infrared light did not play any role, samples were also illuminated with (A) an Ar ion laser emitting only in the visible part of the spectrum with a power of ~ 1 W and (B) a continuous wave infrared laser, also with a power of about 1 W. CdS did not form in any of these control experiments, confirming that only ultraviolet light induced reaction of the precursors. To pattern planar substrates, we spin coated glass slides or silicon wafers with the precursor solution, and exposed them to focused ultraviolet light.

3.3.2. Characterization. Samples were characterized with transmission electron microscopy (TEM, and high resolution TEM), with UV-Vis optical absorption spectroscopy, photoluminescence spectroscopy, X-ray diffraction (XRD), and X-ray photoelectron spectroscopy (XPS). TEM micrographs were taken with a Zeiss EM 109, operated at 80 kV. HREM micrographs were taken using Philips 430ST TEM at an accelerating voltage of 300 kV. Samples for TEM were prepared by carving illuminated spots out of a monolith with a razor blade. The carved out regions were then crushed in methanol, and a drop of the suspension was placed on a 300 mesh lacey carbon grid.

UV-Vis optical absorption spectra of parent solutions and hydrogel monoliths were taken using a CARY 5 UV-Vis-NIR spectrophotometer. Characterization of the parent solutions was difficult, since they presented a strong absorption below about 280 nm. The absorption probably originated from Cd-thiolate complexes, which have an absorption maximum at 250 nm,[7,8] and from RS$^-$ anions, which absorb around 240 nm.[9] 2-mercaptoethanol has a pK$_a$ of 9.5,[10] and we estimate that [RS$^-$] = 5 ×10^{-5}M in a [RSH] = 7M solution. Because of the large absorption, the parent solutions could be characterized spectroscopically only after dilution by a factor 800 to 1000.

Photoluminescence spectra were taken using a JY-Horiba Fluorolog 3-22 Fluorometer. Raman spectra were obtained using the 514.5 nm line of an Ar^+ laser and a SPEX 0.85 m double spectrometer equipped with a liquid N_2 cooled charge coupled device array detector. X-ray diffraction (XRD) analysis of the powder was performed using a Scintag XDS200 diffractometer with a Cu radiation source and a liquid nitrogen cooled Ge detector. Crystallite sizes were estimated via the Scherrer equation using the MDI Jade 5.0 software. A Gaussian correction was applied for the instrumental line broadening utilizing NIST standard silicon powder SRM 640B. X-ray photoelectron spectroscopy (XPS) was carried out on a KRATOS AXIS 165 scanning spectrometer equipped with a 225-W Mg X-ray source, producing photons with an average energy of 1253.6 eV.

3.4. RESULTS AND DISCUSSION

3.4.1. Formation of CdS upon illumination of precursor solutions. Our patterning technique is based on ultraviolet illumination of solutions of Cd^{2+} and a thiol (RSH) like 2-mercaptoethanol. Cd^{2+} ions in the presence of thiols form polynuclear species complexed with RS^- with the formula $\{Cd(RS_5Cd_3)_n\}^{(n+2)+}$.[11] Hayes *et al.* investigated the pH and concentration dependence of the complexes.[7] Cd thiolates form at a pH higher than 6.0 when the $[RSH]/[Cd^{2+}]$ ratio is close to 3 (e.g., $[Cd^{2+}] = 1.25 \times 10^{-4}M$, $[RSH] = 5 \times 10^{-4}M$). The pH threshold shifts to lower values with increasing $[RSH]/[Cd^{2+}]$ ratio. For a $[RSH]/[Cd^{2+}]$ ratio of around 5, the minimum pH necessary to form Cd-thiolate complexes is around 3.5. In our experiments, we worked at $[RSH]/[Cd^{2+}]$ ratios of about 10 (adding NH_4OH to keep the solution at a pH$\geq$8), and at $[RSH]/[Cd^{2+}]$ ratios higher than 500 at a pH of around 3. The characteristics of the resulting materials did not depend

strongly on precursor concentration and pH. Figure 3.1 reports the dependence of the absorption spectrum of a precursor solution, with a composition of $[CdSO_4] = 0.1M$, $[RSH] = 1M$ and $[NH_4OH] = 4M$, diluted 800 times (see also Experimental Section) on irradiation time. In the unirradiated solution (solid line), a maximum at 250 nm was evident, which originated from Cd-thiolate complexes.[7,8] Upon irradiation with ultraviolet light, the intensity of the peak at 250 nm decreased. After an exposure of 5 minutes to the UV beam, a second (shifted) absorption band appeared around 265 nm. This band shifted to about 290 nm in samples exposed for 10 minutes to the UV beam. The appearance of bands in the 265-290 nm region is consistent with previous reports of radiolysis of Cd-thiolate complexes, and can be reconciled with the formation of very small CdS nanoparticles.[7,8]
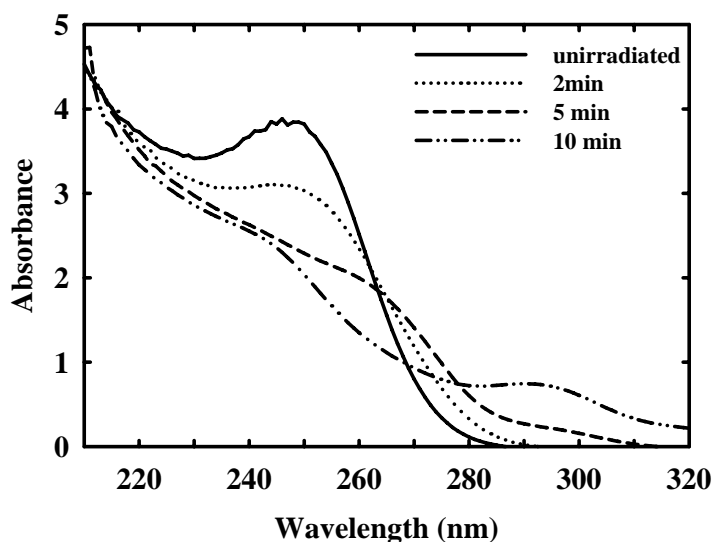
Figure 3.1. Optical absorption of an aqueous solution with $[CdSO_4] = 0.1M$, [2-mercaptoethanol] = 1M, and $[NH_4OH] = 4M$, diluted 800 times. The solutions were illuminated with a high pressure, 100 W Hg lamp for the indicated times.

In samples irradiated for more than 30 minutes, we noticed a yellow precipitate. That precipitate was filtered and analyzed with XRD. The corresponding spectrum is reported in Figure 3.2, and showed that the precipitate was cubic CdS. Debye-Scherrer analysis of the peak widths indicated an average crystallite size of about 1.4 nm. The formation of CdS precipitates confirms our attribution of the bands in the 265-290 nm to small CdS aggregates.
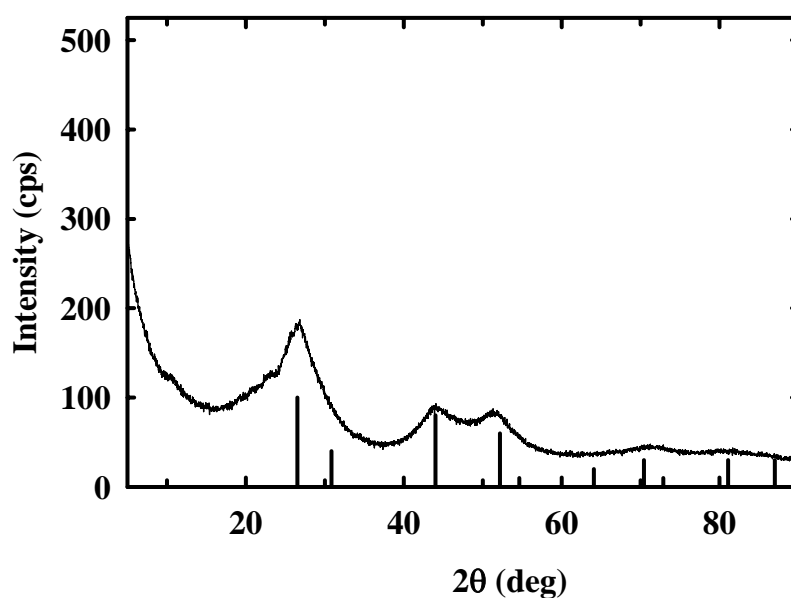
Figure 3.2. X-ray diffraction of precipitates formed after exposure of $CdSO_4$ (0.005M) and 2-mercaptoethanol (7M) solution to ultraviolet light for one hour. Debye-Scherrer analysis indicated a mean particle size of 1.4 nm. The vertical lines indicate the position of the reflections of bulk cubic CdS, and their length the relative intensity.

Formation of CdS in our experiment is due to photodissociation of the thiols and of the Cd-thiolate complexes. Exposure of thiols like 2-mercaptoethanol to ultraviolet light yields thiyl radicals, RS·, and eventually disulfides, RSSR, RS⁻ and S^{2-} anions.[10,12,13]

Photodissociation of Cd-thiolates can also originate species that can react with Cd^{2+}. For example, UV irradiation of Cd-benzenethiolate complexes yields benzenethiolate radicals and H_2S.[14,15] Thiols adsorbed on the surface of CdS nanoparticles can be desorbed and oxidized by UV irradiation.[16] Several of these photogenerated species can react with the metal ions and form CdS. S^{2-} and H_2S are the most reactive species, but recent experiments have also shown that $RS^{\cdot}$ radicals can react with divalent cations to form sulfides.[17,18] Fig. 3.3 summarizes the likely reactions leading to the formation of CdS nanoparticles, and compares the UV patterning technique with the IR photolithographic technique developed previously by our groups.[5] Both UV and IR techniques yield sulfide nanoparticles; however, their mechanisms are widely different. The IR technique is based on hydrolysis of thiourea. The hydrolysis reaction occurs very slowly at room temperature, and is greatly accelerated by a temperature increase, thus photolithography can be carried out with infrared light. In the UV technique, sulfur-containing radicals and anions are liberated by photodissociation of the sulfur precursors. The precursors do not react when heated, at least within the range of temperatures covered by our control experiments (up to about 100 ^0C).

UV Photolithography.

- Mechanism: photodissociation of thiols.

$$RSH + h\nu \rightarrow RS^{\cdot}$$

$$Cd^{2+} + RS^{\cdot} \rightarrow CdS + products.$$

- Precursor solution (typ.) [2-mercaptoethanol] = 1-7 $mol \cdot l^{-1}$, $[Cd^{2+}] < 0.05$ $mol \cdot l^{-1}$

IR photolithography.

- Mechanism: thermal dissociation of chelates and chalcogenide precursors [19-21].

$$(H_2N_2)CS + OH^- \rightarrow HS^- + products.$$

$$HS^- + [Cd(NH_3)_n]^{2+} \rightarrow CdS + products.$$

- Precursor solution (typical): [Thiourea] = 0.5 $mol \cdot l^{-1}$; $[Cd^{2+}]$ = 0.5 $mol \cdot l^{-1}$, $[NH_4OH]$ = 4 $mol \cdot l^{-1}$.

Figure 3.3. Proposed reaction schemes for the UV and IR photolithographic techniques.

3.4.2. Patterning of porous matrices. Silica hydrogels were prepared as described in the experimental section and their solvent was exchanged with a solution of Cd^{2+} and 2-mercaptoethanol. Ultraviolet light was focused on selected regions of the samples, as shown schematically in Figure 3.4 a), top. To pattern planar substrates, the precursor solution was spin coated on the support (typically a glass slide, or a silicon wafer), and a region was illuminated as shown in Figure 3.4 b), top. Yellowish spots started forming after illuminating samples with the Hg lamp for 20-30 minutes. Illumination times were a few minutes when the Ar ion laser was employed. The diameter of the photolithographed spots could be varied from a few to ~100 μm by changing the distance between the sample and the focal point. Typical patterned regions are shown in Figure 3.4a), bottom (hydrogels) and 3.4b), bottom (planar substrates). Patterns extended into the bulk of

hydrogels; the penetration depth could be varied from a few microns to about one millimeter by varying the focal length of the lens.

After irradiation, the samples were washed several times in water to remove unreacted precursors. The size and color of the spots was not altered by washing, indicating that CdS was neither chemically altered nor removed, in agreement with our previous patterning experiments.[22] To help confirm the chemical identity of the nanoparticles in the illuminated regions, some samples were washed with acetonitrile. The color and size of the spots was not altered. This ruled out the presence of unreacted Cd-thiolate precursors, which are highly soluble in acetonitrile.[23] Some samples were also washed in acidic (H_2SO_4) solution. The lithographed regions vanished after a few hours, ruling out the presence of elemental sulfur, and strongly suggesting the presence of CdS.
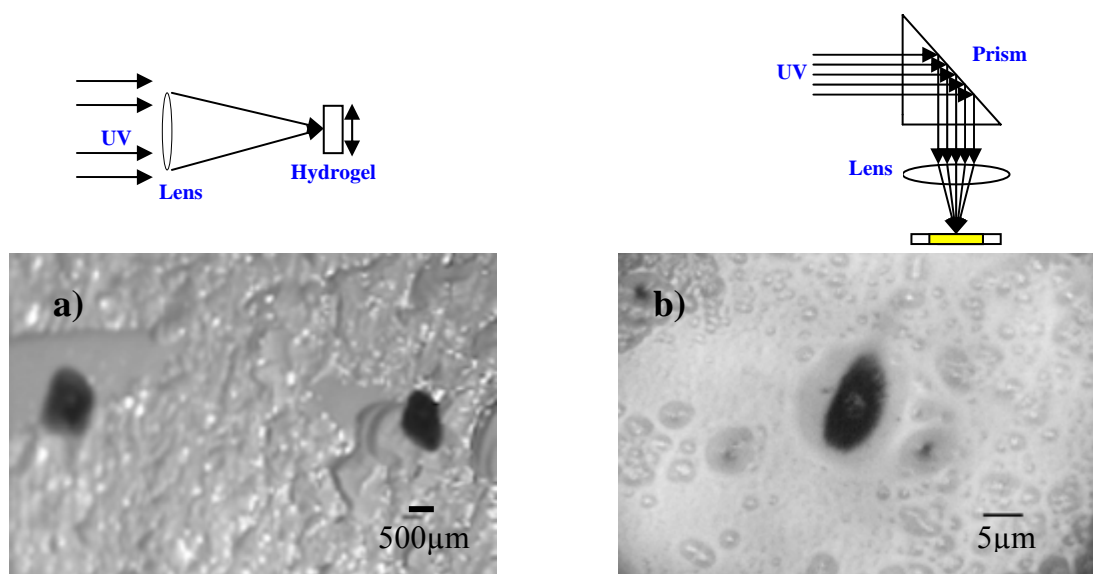
Figure 3.4.Top: Schematic representation of the illumination arrangement employed to pattern: a) hydrogels, b) planar substrates. Multiple regions of a same sample were patterned by translating the sample in front of the beam. Bottom: a) CdS spots photolithographed on the surface of a silica hydrogel. b) CdS spot photolithographed on a glass slide. Samples were illuminated with the 351.1 nm of a continuous wave Ar ion laser. The laser power at the sample was 50 mW, and exposures were between 5 and 10 minutes.

For TEM analysis, UV-illuminated regions were carved out of the hydrogel, crushed in methanol and placed on a lacey carbon copper grid. Figure 3.5(a) shows a typical TEM micrograph. CdS nanoparticles with diameter in the 15-20 nm range were present in all samples, and appeared as dark spots distributed within the light grey silica matrix. High magnification micrographs revealed the presence of a large number of particles in the 2-5 nm size range. Individual particles showed lattice fringes that could be reconciled with the cubic structure observed with XRD (Figure 3.5a, inset).A size distribution histogram is reported in Figure 3.5(b). The histogram, however, is most

probably not highly representative of the actual particle size distribution, since particles smaller than 3 nm could hardly be distinguished from the matrix.[24]
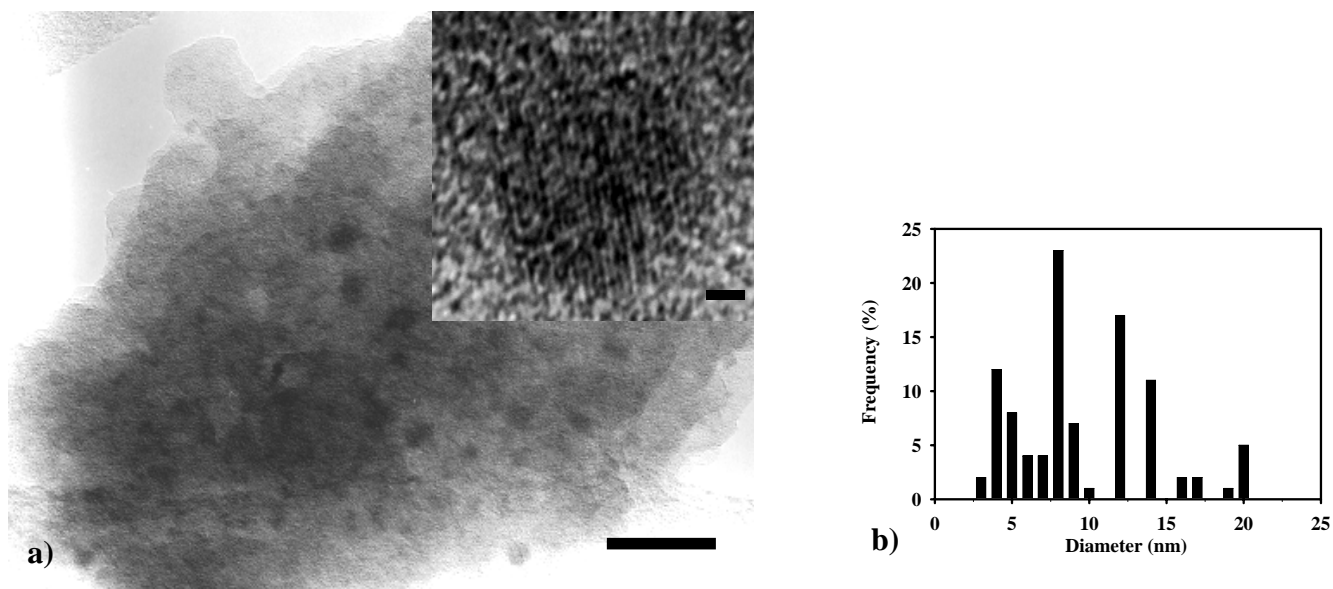
Figure 3.5. a) TEM micrograph showing CdS particles as dark spots embedded in a silica matrix (light grey). The scale bar represents 100 nm. Inset: HRTEM image of a 6 nm diameter CdS nanoparticle. The scale bar represents 1 nm. The lattice fringes are consistent with a cubic crystalline structure. b) Size distribution histogram obtained by measuring about 120 particles. Particles with diameters below about 3 nm could hardly be distinguished from the silica matrix, and the histogram is likely skewed towards large sizes. The precursor concentration in the parent solution was $[CdSO_4] = 0.005$ M, $[RSH] = 7$ M, and the sample was illuminated for 30 minutes with a high pressure, 100 W Hg lamp.

The chemical identity of the samples was further confirmed by absorption, photoluminescence, and Raman spectroscopy. Room temperature absorption spectra

taken as a function of exposure time are reported in Figure 3.6. The spectra exhibited

excitonic shoulders at about 265 nm for an exposure time of 30 minutes. The shoulder

shifted to about 360 nm for exposures of 60 minutes, and did not shift significantly for

longer exposures.   The position of these shoulders can be reconciled with CdS

nanoparticles with a mean diameter of 1.4 nm and 2 nm, respectively.[25,26] The mean

nanoparticle size of the UV technique is therefore a factor 2-3 smaller than the mean

particle size attainable with the IR technique.[5] Recent developments, however, have

shown that the mean particle size can be considerably reduced when a surfactant like a

thiol is added to the precursor solution of the IR technique.[27]
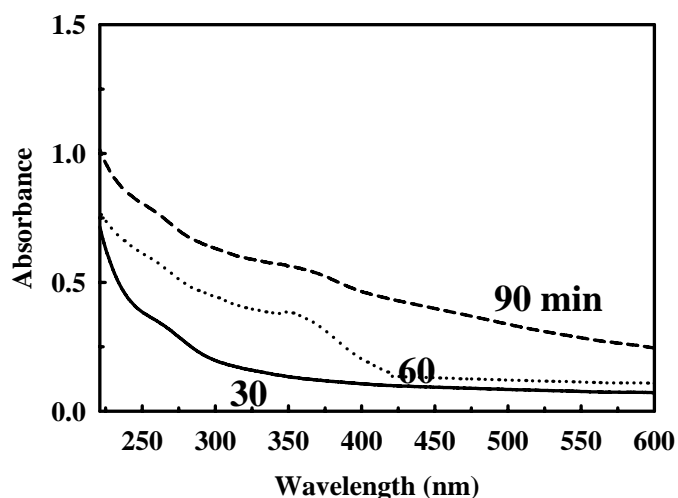
Figure 3.6. Absorption spectra of hydrogels patterned with CdS using UV radiation. The

curves correspond to an exposure time of 30, 60, and 90 min, respectively. The precursor

concentration in the parent solution was $[CdSO_4] = 0.005$ M, $[RSH] = 7$ M. A 100 W

high pressure mercury lamp was used to illuminate the samples.

Room temperature photoluminescence (PL) spectra are reported in Figure 3.7, and

are characterized by broad peaks, indicating that the photoluminescence was dominated

by traps. Particle size could not be determined from the PL spectra due to the broadness of the peaks; however, some trends could be discerned. Luminescence was in general weak, and increased with irradiation time. Peaks in the 400-450 nm region of the spectrum were often detected in samples irradiated for short times, and were probably due to carbon impurities incorporated in the silica matrix during the gel formation process.[28-31] The emission profiles tended to shift towards longer wavelengths with increasing irradiation time, in agreement with the trend prevalent in the absorption spectra (see Figure 3.6). The emission spectra were comparable to the emission of samples obtained with the IR technique with a comparable mean size and capping agent.[27]
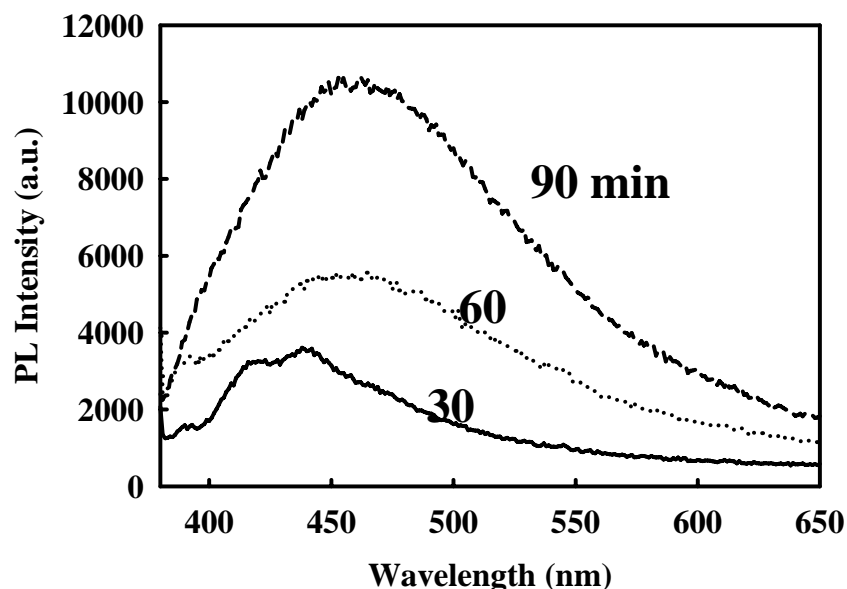
Figure 3.7. Photoluminescence of hydrogels patterned with CdS at the indicated exposures. The precursor concentration in the parent solution was $[CdSO_4] = 0.005$ M, $[RSH] = 7$ M. A 100 W high pressure Hg lamp was used to illuminate the samples. The excitation wavelength was 350 nm.

Raman spectra are shown in Figure 3.8, and exhibited a shift at 306 cm^{-1}. This frequency nearly coincides with the first-order longitudinal-optical phonon frequency of bulk CdS, and is also in good agreement with previous Raman measurements of CdS/silica composites.[32]
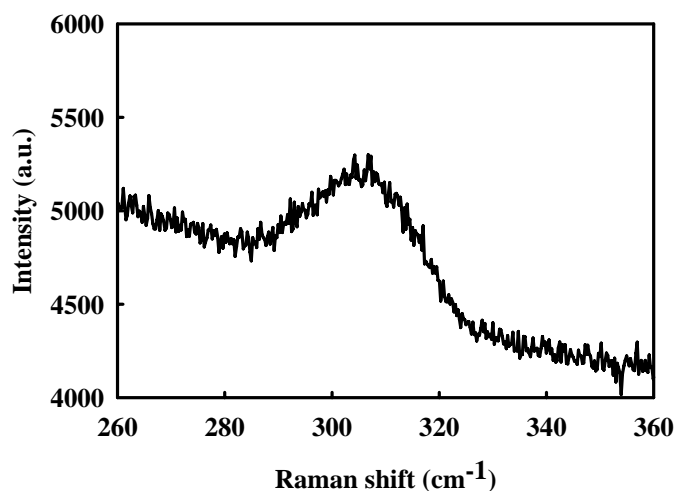
Figure 3.8. Raman spectra of hydrogels patterned with CdS. The precursor concentration in the parent solution was [CdSO$_4$] = 0.005 M, [RSH] = 7 M. The samples were illuminated for 30 minutes with a high pressure Hg lamp.

Thus, optical spectroscopy characterization confirmed the chemical identity of the CdS nanoparticles. The mean particle size determined with optical spectroscopy techniques was between 1.4 and 2 nm, and was consistent with the size measured with XRD. The difference with the TEM mean size (9.67 nm) is not irreconcilable, since particles with a size below about 3 nm could hardly be distinguished from the silica matrix. In a previous study.[5] we also measured a larger (7.5 nm) nanoparticle size with TEM than with optical techniques (4-5 nm). We conclude that TEM should be regarded

only as a rough indicator of the size distribution of nanoparticles embedded in sol-gel matrices.

3.4.3. Patterning of planar substrates. Our methodology can also be applied to the patterning of planar substrates with quantum dots, as shown in Figure 3.4(b). Figure 3.9 shows the absorption and emission spectra of glass slides patterned with CdS. The data were in overall agreement with the data obtained for silica hydrogel patterning. Absorption showed an excitonic shoulder around 380 nm. From the position of the excitonic shoulder a mean size of about 2 nm was calculated, close to the mean size of CdS nanoparticles formed in silica gel matrices for comparable irradiation times. Emission was very broad, as in the case of patterned silica matrices.
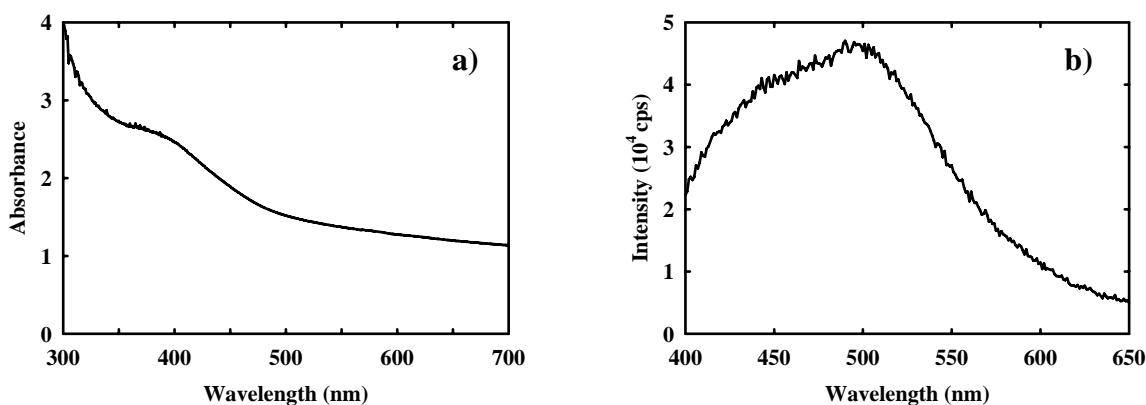
Figure 3.9. a) Optical absorption of a microscope glass slide patterned with CdS. b) Photoluminescence spectra, excited at 350 nm. The precursor concentration in the parent solution was $[CdSO_4] = 0.1M$, and $[RSH] = 1M$. NH_4OH was added to maintain a pH of about 11. The samples were irradiated for 60 min with a 100 W high pressure mercury lamp.

XPS spectra of patterned planar substrates are reported in Figure 3.10. Two Cd peaks were clearly evident, with binding energies of: $Cd_{3d5/2} = 405.5$ eV, and $Cd_{3d3/2} = 412.2$ eV; the sulfur peak had a maximum around 162.5 eV, which corresponded to $S_{2p3/2}$, and a shoulder around 163.5 eV, which corresponded to $S_{2p1/2}$. All these values are in excellent agreement with those previously reported for CdS nanoparticles capped with mercaptoethanol.[33,34]
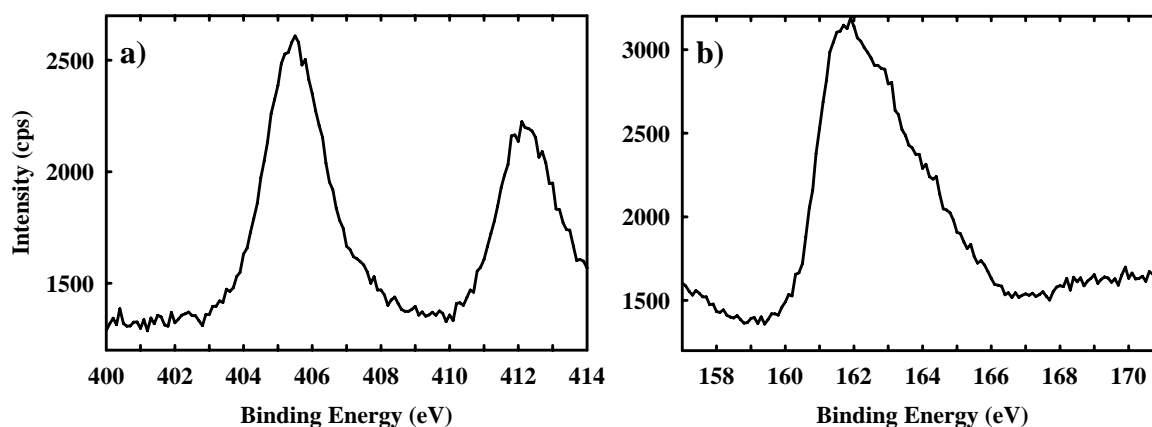
Figure 3.10. XPS spectra of CdS spots photolithographed on Si wafers. a) Cd 3d. b) S 2p. The binding energies of $Cd_{3d5/2}$ (405.5 eV), $Cd_{3d3/2}$ (412.2 eV), $S_{2p3/2}$ (162.5 V), $S_{2p1/2}$ (163.5 eV) nearly coincided with those previously reported for small CdS nanoparticles capped with mercaptoethanol [29,30]. Precursor solution composition and irradiation times were as in Figure 3.9.

3.5. CONCLUSION

In conclusion, we report a new photolithographic method for patterning planar and porous matrices with semiconductor quantum dots. Our approach is based on

photodissociation of metal thiolate precursors of CdS. Numerous characterization techniques were employed, showing that CdS nanoparticles with a mean diameter smaller than 2 nm were indeed produced in the illuminated regions. The minimum spot size attained in our experiments was a few microns. In the future, the spatial resolution could be brought to the diffraction limit by employing more elaborate photolithographic set-ups. The composites could be employed to fabricate highly stable quantum dot ion sensors, since the porous matrix prevents coagulation and leaching of the nanoparticles in the environment, but also more sophisticated devices, such as photonic crystals and quantum dot lasers. Practical applications could be further facilitated by employing a cross-linking technique developed by our group, which increases the mechanical strength of hydrogel monoliths and films [35].

3.6. REFERENCES

[1] For example: *Evident Technologies*, 216 River Street, Suite 200, Troy, New York 12180; *Quantum Dot Corp*. 26118 Research Road Hayward, CA 94545.

[2] V. C. Sundar, H.-J. Eisler, and M. G. Bawendi, *Adv. Mater.* **14**, 739 (2002).

[3] B. Capoen, T. Gacoin, J. M. Nedelec, S. Turrell, and M. Bouazaoui, *J. Mater. Sci*. **36**, 2565 (2001).

[4] N. Tohge, M. Asuka, and T. Minami, *SPIE* **1328**, 125 (1990).

[5] M. F. Bertino, R. R. Gadipalli, J. G. Story, C. G. Williams, G. Zhang, C. Sotiriou-Leventis, A. T. Tokuhiro, S. Guha, and N. Leventis, *Appl. Phys. Lett*. **85**, 6007 (2004).

6   N. Leventis, I. A. Elder, D. R. Rolison, M. L. Anderson, and C. I. Merzbacher, *Chem. Mater*. **11**, 2337 (1999).

7   D. Hayes, O. I. Mitit, M. T. Nenadovit, V. Swayambunathan, and D. Meisel, *J. Phys. Chem*. **93**, 4603 (1989).

8   M. Mostafavi, Y. P. Liu, P. Pernot, and J. Belloni, Radiat. *Phys. Chem*. **59**, 49 (2000).

9   G. Gaspari, and A. Granzow, *J. Phys. Chem*. **74**, 836 (1970).

10   A. R. Knight, *The Chemistry of the Thiol Group, Part 1*; S. Patai, Ed. (John Wiley & Sons Ltd. London, 1974), Chapter 10.

11   H. F. De Brabander, and L. C. Van Poucke, *J. Coord. Chem*. **3**, 301 (1974); F. F. Said, and D. G. Tuck, Inorg. *Chem. Acta*. **59**, 1 (1982).

12   H. Bao, Y. Gong, Z. Li, and M. Gao, *Chem. Mater*. **16**, 3853 (2004).

13   N. A. Rosenthal, and G. Oster, *J. Am. Chem. Soc*. **83**, 4445 (1961).

14   T. Turk, U. Resch, M. A. Fox, and A. Vogler, *Inorg. Chem*. **31**, 1854 (1992).

15   T. Turk, U. Resch, M. A. Fox, and A. Vogler, *J. Phys. Chem*. **96**, 3818 (1992).

16   Ch.-H. Fischer, and A. Henglein, *J. Phys. Chem*. **93**, 5578 (1989).

17   T. Mirkovic, M. A. Hines, P. S. Nair, and G. D. Scholes, *Chem. Mater*. **17**, 3451 (2005).

18   Y. Hasegawa, M. Afzaal, P. O'Brien, Y. Wada, and S. Yanagida, *Chem. Commun*. 242-243 (2005).

19   M. F. Bertino, J. F. Hund, J. Sosa, G. Zhang, C. Sotiriou-Leventis, N. Leventis, A. T. Tokuhiro, and J. Terry, *J. Non-Cryst. Solids* **333**, 108 (2004).

20   I. G. Dance, A. Choy, and M. L. Scudder, *J. Am. Chem. Soc*. **106**, 6285 (1984).

[21]   H. Matsumoto, T. Sakata, H. Mori, and H. Yoneyama *J. Phys. Chem*. **100**, 13781 (1996).

[22]   Y. Nosaka, *J. Phys. Chem*. **95**, 5054 (1991).

[23]   P.E. Lippens, and M. Lannoo, *Phys. Rev. B* **39**, 10935 (1989).

[24]   J. Huang, K. Sooklal, C. J. Murphy, and H. J. Ploehn, *Chem. Mater*. **11**, 3595 (1999).

[25]   W. H. Green, K. P. Le, J. Grey, T. T. Au, and M. J. Sailor, *Science* **276**, 1826 (1997).

[26]   V. Bekiari, and P. Lianos, *Langmuir* **14**, 3459 (1998).

[27]   L. T. Canham, A. Loni, P. D. J. Calcott, A. J. Simons, C. Reeves, M. R. Houlton, J. P. Newey, K. J. Nash, and T. I. Cox, *Thin Solid Films* **276**, 112 (1996).

[28]   A.G. Rolo, L.G. Vieira, M. J. M. Gomes, J. L. Ribeiro, M. S. Belsley, and M. P. dos Santos, *Thin Solid Films* **312**, 348 (1998).

[29]   M. Kundu, A. A. Khosravi, S. K. Kulkarni, and P. Singh, *J. Mater. Sci*. **32**, 245 (1997).

[30]   R. B. Khomane, A. Manna, A. B. Mandale, and B. D. Kulkarni, *Langmuir* **18**, 8237 (2002).

[31]   N. Leventis, C. Sotiriou-Leventis, G. Zhang, and A.-M. M. Rawashdeh, *Nano Lett*. **2**, 957 (2002).

[32]   I. Kaur, D. K. Pandya, and K. L. Chopra, *J. Electrochem. Soc*. **127**, 943 (1980).

[33]   N. C. Sharma, R. C. Kainthla, D. K. Pandya and K. L. Chopra, *Thin Solid Films* **60**, 55 (1979).

[34]   G. A. Kitaev, A. A. Uritskaya, and S. G. Mokrushin, *Zhurnal Fizicheskoi Khimii*, **38**, 2065 (1965).

[35] M.F.Bertino, R.R.Gadipalli, L.A.Martin, B. Heckman, J.G.Story, N.Leventis, P. Fraundorf, and S.Guha, to be submitted to *Jou. of Sol-Gel Sci. Technol.* **40**, 101, (2006).

PAPER - III

4. INFRARED QUANTUM DOT PHOTOLITHOGRAPHY

R.R.Gadipalli[a], L.A.Martin[a], B. Heckman[a], J.G.Story[a], M.F. Bertino[a*], P. Fraundorf[c], S.Guha[d], and N. Leventis[b,*]

[a] *Department of Physics, University of Missouri-Rolla, MO 65409, USA.*

[b] *Department of Chemistry, University of Missouri-Rolla, Rolla, MO 65409, USA*

[c] *Department of Physics, University of Missouri-Saint Louis, MO 63121, USA.*

[d] *Department of Physics, University of Missouri-Columbia, Columbia, MO 65211, USA.*

* Corresponding authors. Tel.: +1-573 341 6221; fax: +1-573 341 4715 (M.B.); +1-573-341-4391 (N.L.).

E-mail address: Massimo@umr.edu (M.F.Bertino); Leventis@umr.edu (N. Leventis)

4.1. ABSTRACT

CdS quantum dots were fabricated photolithographically on the surface and in the bulk of silica hydrogels, as well as on the surface of planar substrates. Silica hydrogels were prepared with a standard base-catalyzed route, and the solvent was exchanged with a cold aqueous solution of $CdNO_3$, NH_4OH, thiourea, and a capping agent, e.g., 2-mercaptoethanol. The samples were then exposed to a focused infrared beam produced by a continuous-wave Nd:YAG laser. The precursors reacted upon heating, and CdS nanoparticles formed in the illuminated regions. Use of capping agents allowed control of the mean particle size, while focusing the beam inside hydrogel monoliths generated nanoparticles in the bulk, but not at the surface. Planar substrates were patterned by illuminating a precursor solution spin-coated on the substrates. The average size of the

CdS nanoparticles could be varied between about 1.5 and 4.5 nm by varying the type and the concentration of the capping agents.

4.2. INTRODUCTION

Embedding nanoparticles in sol-gel materials is becoming increasingly relevant for electro-optical and chemical applications. Quantum dot lasers have been fabricated based on quantum dots embedded in a titania sol-gel matrix,[1] PbS and CdS nanoparticles embedded in silica gels are being considered for waveguide and non-linear optics,[2,3] while composites of silica gel and cytochrome-tagged Au nanoparticles have been reported[4] and they are likely to have applications in biotechnology. Patterning of sol-gel matrices with regularly spaced arrays of nanoparticles allows production of optoelectronic components and devices such as diffraction gratings,[5] photonic crystals,[6] and optical memories.[7]

Very recently, our team has developed a photochemical method that allows to pattern silica hydrogels with metal, oxide and semiconductor nanoparticles.[8] In that method, the gelation solvent is exchanged with a solution of quantum dot precursors, typically a group II metal chelate, and a sulfur source like thiourea. Local heating with an infrared (IR) laser induces hydrolysis of thiourea. The released sulfur ions react with the metal ions forming small, quantum-confined sulfide nanoparticles. Here, we extend that work and show that quantum dots can be synthesized in a precisely controlled physical location and with a precisely controlled size. By focusing the beam of a Nd:YAG laser, quantum dots can be placed photolithographically on the surfaces of silica gels, on planar substrates like glass slides, and also in the bulk of porous matrices. By varying the type

and the concentration of capping agents, the size of the quantum dots – and therefore the quantum confinement effects – can be controlled at will. Despite its simplicity, our technique is versatile, and may become an important tool in the fabrication and miniaturization of optoelectronic devices and sensors based on quantum dot/sol-gel composites.

4.3. EXPERIMENTAL

4.3.1. Preparation of hydrogels. Silica hydrogels were prepared by a modification of previously published procedures[9] in which the contents of vial A (4.514 mL of tetramethoxysilane; 3.839 mL of methanol) and of vial B (4.514 mL of methanol; 1.514 mL of water, and 20 μL of concentrated NH_4OH) were mixed thoroughly and poured in molds. Typical gelation times were around 10-15 min. The gels were left to age at room temperature for ~2 days. Aged gels were removed from their molds and soaked in methanol four times for 12 hours each time. The hydrogels were then soaked in water four times for 12 h each time. The water-washed gels were then cut into cylinders of about 7 mm diameter (which was the diameter of our molds), and 4-5 mm length, and placed in 20 ml of solution containing the quantum dot precursors.

4.3.2. Quantum dot precursors. CdS was synthesized by hydrolyzing thiourea in basic solution.[10-14] Hydrogel slices with a volume of about 2 ml were soaked in a 20 ml of precursor solution with a $CdNO_3$ concentration of 1 $mol \cdot l^{-1}$ (M) and a NH_4OH concentration of 4 M. The samples were then placed in a refrigerator kept at 5 ^{0}C. After about two hours, half of the bathing solution was decanted and replaced with an aqueous solution containing thiourea with a concentration of 1 M, and a capping agent such as

2-mercaptoethanol, thioglycerol, or sodium hexametaphosphate (HMP, average molecular weight = 611.7). The concentration of the capping agents was varied between 0.01 and 0.1 M. The samples were left in the refrigerator for an additional hour to let the thiourea and the capping agents diffuse inside the monoliths. Cooling was necessary, since the precursors react slowly at room temperature. Hydrogels loaded with the precursors turned pale yellow within about one hour when kept at room temperature, but did not appreciably change their color when refrigerated. The samples were then rapidly removed from the refrigerator, placed in a glass cuvette, and exposed to the light of a continuous wave, Nd:YAG laser. Samples were exposed to the IR beam between 4 and 10 minutes, and the estimated power on the sample was about 1.8 W. The local temperature at the illuminated spots was measured by placing a thermocouple immediately below the gel surface. The local temperature was typically between 30 and 40 ^{0}C, and did not exceed 50 ^{0}C even when the laser was operated at high powers (> 5W). After exposure, the samples were immediately washed several times in cold distilled water to avoid any further reaction while the precursors were removed. To pattern planar substrates, a thin film of precursor solution was spin coated on the support (typically a glass slide, or a silicon wafer), and a selected region was illuminated. After an exposure of about 3 minutes to the focused laser beam, yellow spots formed in the illuminated regions; the samples were then immediately washed by submersion in cold water to remove unreacted precursors. The patterned quantum dots were found to adhere reasonably well to the substrate, and were not washed out. The films produced in our proof-of-concept experiments were relatively thick and fairly rough (average thickness: 2 ± 0.5 μm). The quality of the films could probably be improved by using less

concentrated precursor solutions. For three-dimensional patterning, we employed a continuous-wave laser (IPG Photonics YLR-100) emitting at a wavelength of 1065 nm, and with a power of 23 W. The laser beam was focused 6 mm beneath the surface of a hydrogel monolith with a lens of focal length 5 cm.

4.3.3. Characterization. Samples were characterized with transmission electron microscopy (TEM and HREM), with UV-Vis optical absorption spectroscopy, photoluminescence spectroscopy, Raman spectroscopy, and X-ray photoelectron spectroscopy (XPS). TEM micrographs were taken with a Zeiss EM 109 operated at 80 kV. HREM micrographs were taken using a Philips 430ST operated at 300 kV. Samples for TEM were prepared by carving illuminated spots out of a monolith with a razor blade. The carved out regions were then crushed in methanol, and a drop of the suspension was placed on a 300 mesh lacey carbon grid. UV-Vis optical absorption spectra were taken using a CARY 5 UV-Vis-NIR Spectrophotometer. Photoluminescence spectra were taken using a JY-Horiba Fluorolog 3-22 Fluorometer. The Raman measurements were carried out in a perfect backscattering geometry using a fiber optically coupled confocal micro-Raman system (TRIAX 320) equipped with a liquid N_2-cooled charge-coupled detector. The 514.5-nm line of an Ar^+ ion laser was the excitation source. A ×50 microscope objective was used to focus and collect the scattered laser light. The microscope is equipped with a holographic super-notch filter to block the elastically scattered light; for Stokes scattering the filter blocks up to ~300 cm^{-1}. This makes it somewhat inconvenient to measure the first order longitudinal optical (LO) phonon of CdS. However, for anti-Stokes scattering the notch filter cutoff is around -200 cm^{-1}. Although the intensity of anti-Stokes scattering is lower, due to the limitation of the notch filter we use anti-Stokes

Raman scattering to measure the first order longitudinal optical phonon in our CdS quantum dots. X-ray photoelectron spectroscopy (XPS) was carried out on a KRATOS AXIS 165 scanning spectrometer equipped with a 225-W Mg X-ray source, producing photons with an average energy of 1253.6 eV.

4.4. RESULTS AND DISCUSSION

4.4.1. Patterning of porous matrices. Our infrared photolithographic method relies on the hydrolysis of thiourea in basic solution, according to Eq. (1).

$$Cd^{2+} + (H_2N)_2C{=}S + 2OH^- \rightarrow CdS + H_2NCN + 2\ H_2O \tag{1}$$
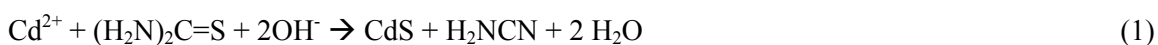
Thiourea has often been employed as the sulfur source to fabricate high-quality metal sulfide thin films, and the reaction kinetics hava been investigated by several authors.[15-17] In most of those studies, the metal ion source was the water-insoluble $Cd(OH)_2$, which was formed by addition of a base to a Cd^{2+} solution. The $Cd(OH)_2$ route is advantageous for thin film deposition purposes, since the hydroxide catalyzes the hydrolysis of thiourea, and reduces the processing temperature.[17] The hydroxide route, however, is not practicable for our purposes, since $Cd(OH)_2$ is a precipitate that would not diffuse inside the hydrogels. Formation of $Cd(OH)_2$ can be prevented by using complexes of Cd^{2+}. For example, Cd^{2+} - amino complexes can be formed by adding large concentrations of ammonium hydroxide to the bathing solution. When $[NH_4OH]{>}1.8$ M (pH ~11), the stable phase is not the insoluble $Cd(OH)_2$, but the water-soluble $[Cd(NH_3)_4]^{2+}$ complex, which ***does*** diffuse into hydrogels. The transition from the hydroxide to the amino complex is quite noticeable: the turbid $Cd(OH)_2$ suspension disappears, and the solution becomes clear. Exposure to an IR beam leads to local heating and dissociation of thiourea according to Eq.(1), leading to CdS formation only in the exposed regions. Reaction (1)

in the unexposed part of the cold gel is negligible, at least for the exposure times of our experiments (up to 15 minutes), and patterning is possible.

A schematic representation of the illumination set-up is shown in Figure 4.1, together with examples of (a) surface and (b) three-dimensional patterning of silica hydrogels, as well as (c) patterning of a planar substrate. Surface patterning of porous monolithic matrices can be achieved routinely with a laser power as low as 1 W, as described in Ref. 8 and shown in Figure 4.1a. The patterned regions in Figure 4.1 had a size between 1 and 3 mm to facilitate digital camera imaging; nevertheless, patterns as small as 40 μm could be obtained. A further development presented here is represented by the three-dimensional patterning shown in Figure 4.1b. Three-dimensional patterns were obtained by focusing the beam inside the monolith with a short focal length (~ 5 cm) lens, and by employing high laser powers (> 5 W). The patterned regions were pale yellow and clearly distinguishable from the matrix. The size of the patterns was controlled by varying the illumination time. For example, the spot marked as i) in Figure 4.1b was obtained after an illumination time of 1 minute, and spot ii), which had a volume about 30% larger, was obtained by illuminating for 2 minutes. After irradiation, the samples were washed several times in cold water to remove unreacted precursors. The size and color of the spots did not change upon washing, indicating that CdS was neither chemically altered nor removed by that processing, in agreement with our previous results.[18]
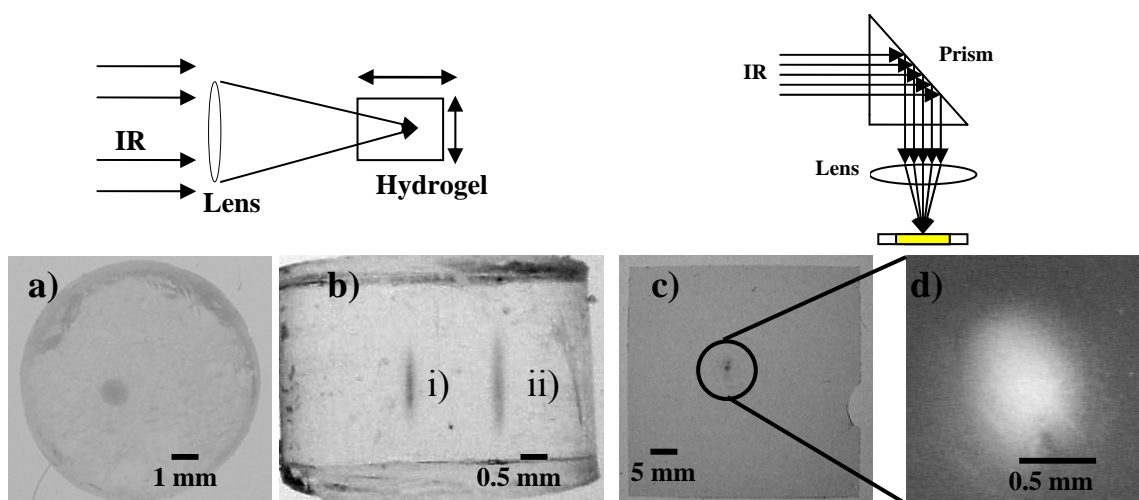
Figure 4.1. Top, left: Schematic representation of the illumination arrangement employed to pattern silica hydrogels. Bottom, a) Surface patterning of a silica hydrogel monolith. b) Bulk, three-dimensional patterning of a silica hydrogel monolith. The dimensions of the features are i) 2.3 mm × 0.3 mm (exposure time: 1 minute), and ii) 3.3 mm × 0.4 mm (exposure time: 2 minutes). Top, right: Schematic representation of the illumination arrangement employed to pattern planar substrates. Bottom, c) Surface patterning of a glass slide spin-coated with a precursor solution. The dimensions of the spot are 0.6 mm × 0.8 mm. d) Higher magnification image of the same region.

For initial confirmation of the chemical identity of the nanoparticles in the illuminated regions, some samples were placed in aqueous acidic solution (H_2SO_4, ca. 0.05 M). The yellow spots vanished after a few hours, ruling out the presence of elemental sulfur and strongly suggesting the presence of CdS. In turn, Figure 4.2 shows a typical TEM micrograph obtained by carving a patterned region out of a hydrogel. Nanoparticles with diameters in the 15-25 nm range were present in all samples, and appeared as dark spots distributed within the light grey silica matrix. High magnification

micrographs revealed the presence of a large number of smaller particles, whose lattice fringes could occasionally be detected, as shown in the inset of Figure 4.2.
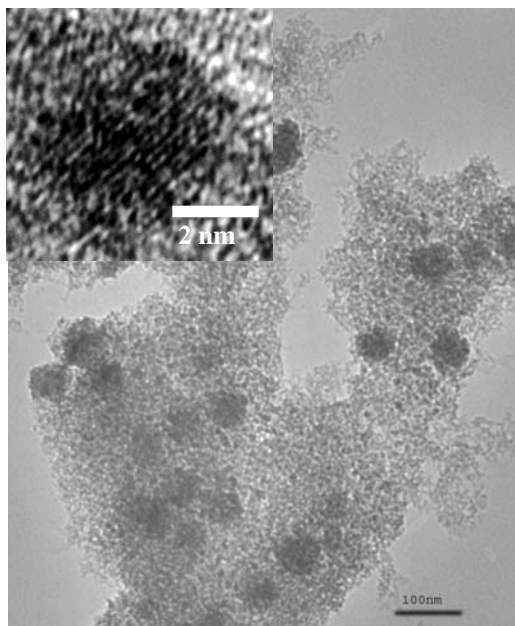
Figure 4.2. TEM micrograph showing CdS particles without any surfactant as dark spots embedded in a silica matrix (light grey). The scale bar represents 100 nm. Inset: HREM image of a 5 nm diameter CdS nanoparticle. The precursor solution contained $CdNO_3$ (0.5 M), NH_4OH (2 M), and thiourea (0.5 M). Gels were illuminated for 5 minutes with a power of 1.8 W.

As we have shown before, in samples exposed for a few minutes small ($\leq$ 5 nm) nanoparticles represent up to 70-80% of the total number of nanoparticles, but they are very difficult to distinguish from the silica matrix with transmission electron microscopy.[8,23] Size distribution histograms were not obtained, and the mean nanoparticle size was inferred from optical absorption spectra such as those reported in Figure 4.3,

which also summarizes data from samples containing different capping agents. When capping agents were not added to the solution, the spectra exhibited an excitonic shoulder around 460 nm, which corresponds to a mean particle size of about 4.5 nm.[19,20] Addition of hexametaphosphate (HMP) as a capping agent did not strongly affect the particle size, and the absorption spectra continued to exhibit an excitonic shoulder around 460 nm. Thiols controlled particle size more effectively. The excitonic shoulder was shifted to around 370 nm for 2-mercaptoethanol as a capping agent, and around 380 nm for thioglycerol. The mean particle size, estimated from the position of the excitonic shoulder,[19,20] was about 2 nm for 2-mercaptoethanol capping and about 2.5 nm for thioglycerol capping. The mean particle size of samples containing thiols are quite comparable, and about a factor 2 smaller than the mean particle size in samples without capping agents. Variation of the thiol concentration between 0.01 and 0.1 M did not affect the position of the excitonic shoulder significantly. For capping agent concentrations higher than about 0.1 M, CdS did not form.

The effect of surfactants on the mean particle size can be explained as follows. The pores of the matrix control nanoparticle size fairly efficiently, as shown by the comparatively small mean particle size (4.5 nm) of samples without capping agents. Addition of relatively weak stabilizing agents, like HMP, only weakly affects the mean size of the CdS nanoparticles. Capping agents that bind strongly to nanoparticles, like thiols (RSH), are more effective than the pore walls in limiting the particle size. The lack of formation of CdS at high capping agent concentrations can be explained by the formation of metal chelates. For example, complexes such as $[Cd(RS_5Cd_3)_n]^{(n+2)+}$ form when 2-mercaptoethanol or other thiols are added to a solution of Cd^{2+} ions.[21-23] These

complexes are highly stable, and probably worse catalysts for the hydrolysis of thiourea than the $[Cd(NH_3)_4]^{2+}$ complexes. For example, parent solutions with $[CdNO_3] = 0.5$ M, [thiourea] = 0.5 M, and [RSH] = 0.1 M are stable for several hours at room temperature. Solutions with [RSH] = 0.2 M must to be heated to 50 ^{0}C before CdS forms, and with [RSH] = 0.3 M CdS forms only near the boiling point. Since the maximum temperature of the regions exposed to the IR beam was around 50 ^{0}C, it is not surprising that patterning was possible only for comparatively small surfactant concentrations.
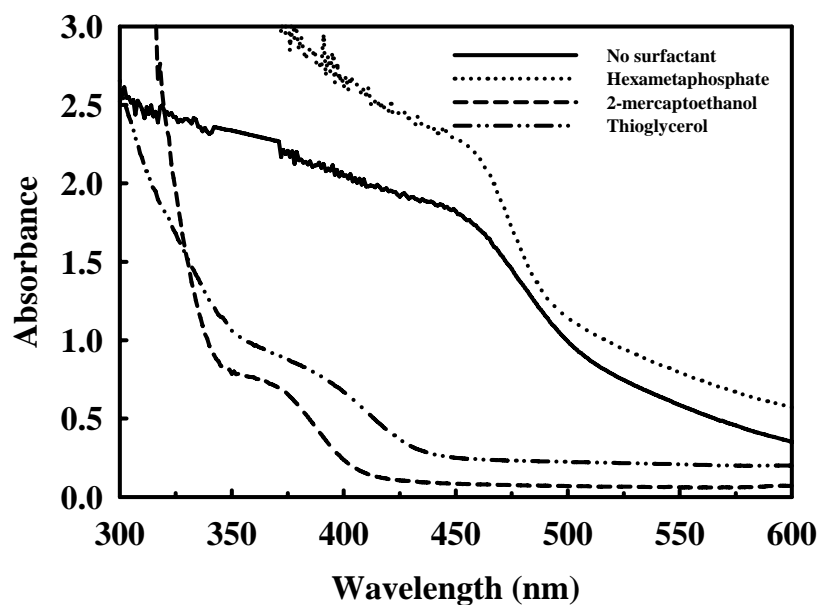
Figure 4.3. Absorption spectra of hydrogels patterned with CdS. The precursor solution contained $CdNO_3$ (0.5 M), NH_4OH (2 M), and thiourea (0.5 M), and the capping agents indicated in the caption at a concentration of 0.1 M. Gels were illuminated for 5 minutes with a Nd:Yag laser at a power of 1.8 W.

Room temperature photoluminescence (PL) spectra are reported in Figure 4.4, and are characterized by broad peaks, indicating the presence of a substantial number of

defects. The mean particle size could not be determined from the PL spectra due to the broadness of the peaks; however, some trends could be discerned. For example, luminescence was in general weak. Features in the 400-450 nm region of the spectrum were often detected, and were attributed to organic impurities remaining in the silica matrix since the gelation step, and, possibly, to CdS precursor residues.[24-27] The luminescence intensity was higher in samples capped with thiols, and increased with the length of the aliphatic chain, in qualitative agreement with recent reports showing that the luminescence quantum yield of CdS nanoparticles increases with the chain length of aliphatic thiols.[28]
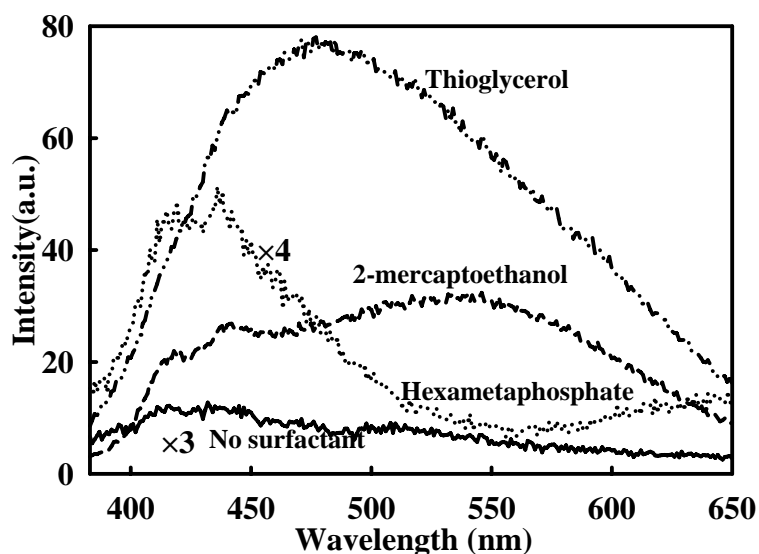
Figure 4.4. Photoluminescence of hydrogels patterned with CdS using IR photolithography. The precursor solution contained $CdNO_3$ (0.5 M), NH_4OH (2 M), and thiourea (0.5 M), and the indicated capping agents in a concentration of 0.1 M. Gels were illuminated for 5 minutes at a power of 1.8 W. The excitation wavelength was 350 nm.

Raman spectra are shown in Figure 4.5, and exhibit a peak at 300 cm^{-1}. This frequency is in good agreement with previously reported Raman shifts in CdS/silica

composites,[29] and corresponds to the first-order longitudinal optical (LO) phonon frequency of CdS. A peak at 600 cm^{-1} was also routinely observed and corresponds to the first overtone.
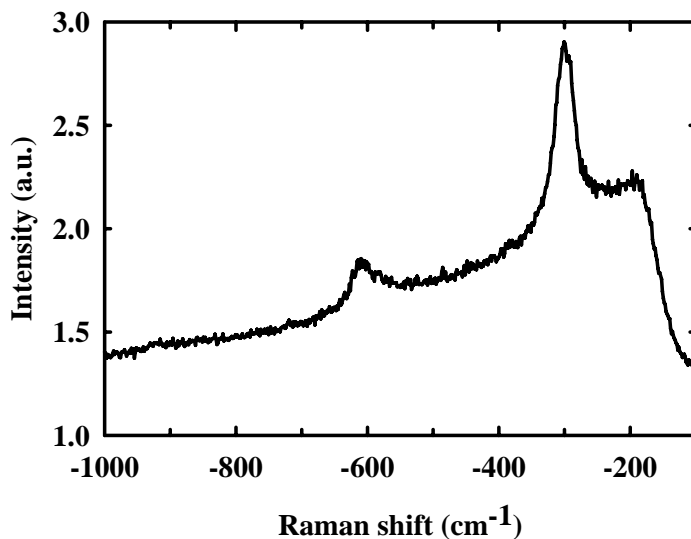
Figure 4.5. Raman spectrum of a silica hydrogel patterned with CdS. The precursor solution contained $CdNO_3$ (0.5 M), NH_4OH (2 M), and thiourea (0.5 M). Gels were illuminated for 5 minutes at a power of 1.8 W.

4.4.2. Patterning of planar substrates. As Figure 4.1 shows, our photolithographic method can also be applied to the patterning of planar substrates with quantum dots. The results obtained for patterning of planar substrates were quite comparable to the results obtained for porous matrices. Figure 4.6 shows the absorption spectra of glass slides patterned with CdS as a function of the concentration of 2-mercaptoethanol. Excitonic shoulders were detected in all samples and were located at about 440 nm in samples without capping agents, and at around 370 nm in samples with a 2-mercaptoethanol

concentration of 0.01 M. In samples with a 2-mercaptoethanol concentration of 0.1 M a very weak shoulder could be identified in the 325-330 nm range. From the position of the excitonic absorption, mean particle sizes of about 4, 2, and 1.5 nm, respectively, were calculated. While formation of very small particles in samples without surfactants may appear surprising, we need to point out that our particles were most probably formed rapidly in thin water films. There was probably barely enough time and precursors available for the particle size to go past the nucleation stage. Photoluminescence spectra of planar substrates patterned with CdS are reported in Figure 4.7. Samples without capping agents had a weak, broad emission spectrum, similar to that of CdS powders,[30] indicating a large number of defects. The emission shifted towards higher energies and became narrower with increasing capping agent concentration. The emission shift towards higher energies is probably due to quantum confinement, and is consistent with the observed blue shift of the absorption with increasing capping agent concentration.
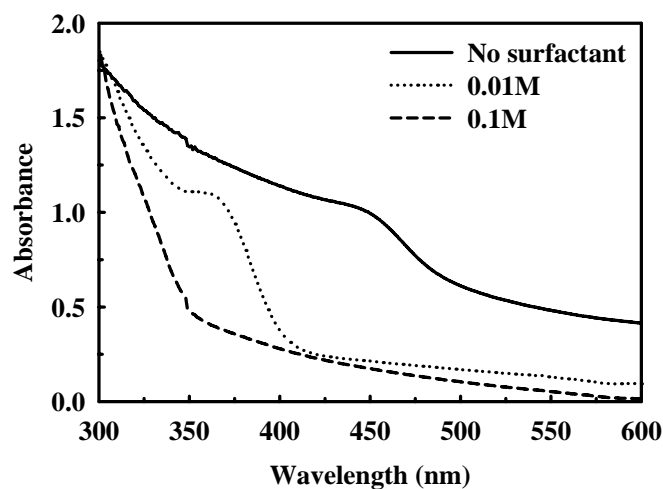
Figure 4.6. Optical absorption spectra of microscope glass slides patterned with CdS. The precursor solution contained $CdNO_3$ (0.5 mol·l^{-1}), NH_4OH (2 mol·l^{-1}), thiourea (0.5 mol·l^{-1}), and 2-mercaptoethanol concentration reported in the caption. Slides were illuminated for 3 minutes at a laser power of 1.8 W.
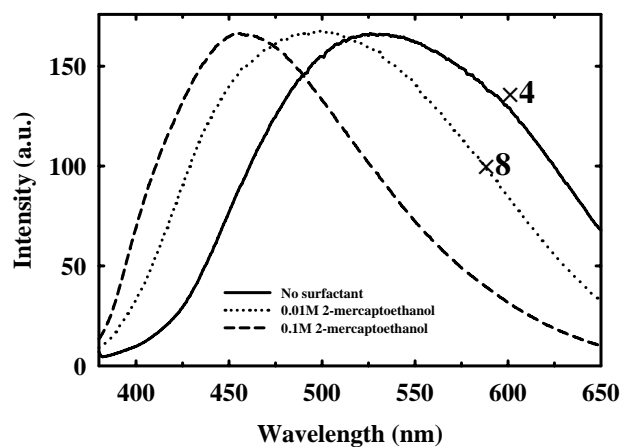
Figure 4.7. Luminescence of microscope glass slides patterned with CdS. The precursor solution contained $CdSO_4$ (0.5 M), NH_4OH (2 M), thiourea (0.5 M), and the 2-mercaptoethanol concentration reported in the caption. Slides were illuminated for 3 minutes at a power of 1.8W. The excitation wavelength was 350 nm.

XPS spectra of silicon wafers patterned with CdS are reported in Figure 4.8. Two Cd peaks were clearly evident, with binding energies of: $Cd_{3d5/2} = 405.6$ eV, and $Cd_{3d3/2} = 412.2$ eV; the sulfur peak had a maximum around 162.0 eV, which corresponded to $S_{2p3/2}$, and a shoulder around 163.2 eV, which corresponded to $S_{2p1/2}$. All these values are in excellent agreement with those previously reported for CdS nanoparticles,[31,32] and further confirm the chemical identity of the nanoparticles.
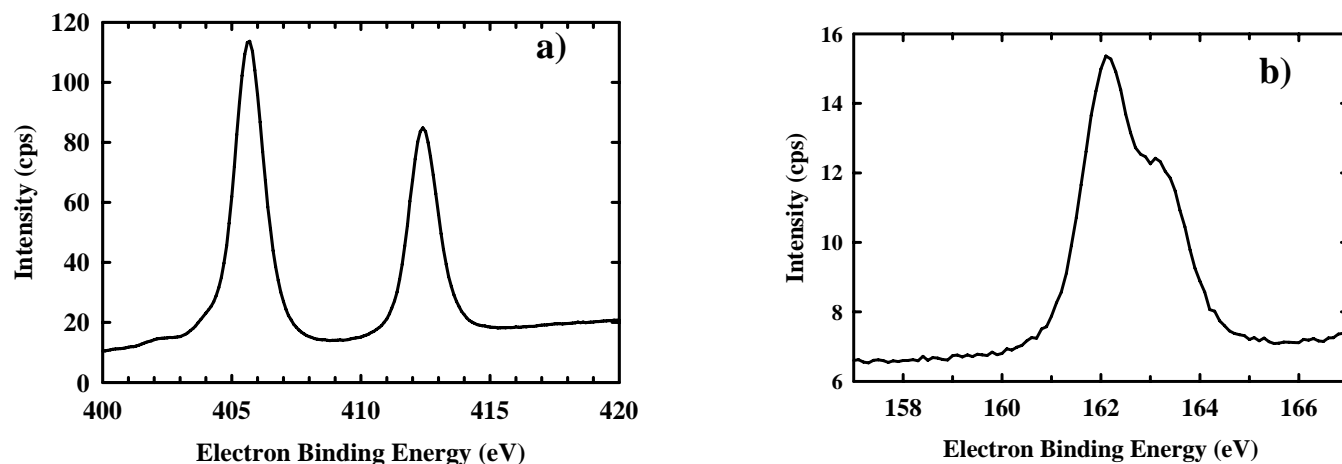
Figure 4.8. XPS spectra of CdS spots photolithographed on Si wafers. a) Cd 3d. b) S 2p. The precursor solution contained $CdNO_3$ (0.5 M), NH_4OH (2 M), and thiourea (0.5 M). Wafers were illuminated for 3 minutes at a power of 1.8 W.

4.5. CONCLUSION

In conclusion, we demonstrate a photolithographic method that can be used to fabricate two- and three-dimensional patterns of CdS quantum dots on planar and porous

matrices. Our method involves infrared radiation to dissociate thiourea, and release HS^- ions that react with Cd^{2+} and form CdS nanoparticles. Those nanoparticles are formed only in the exposed regions, and can be located either on the surface, or in the interior of silica hydrogel monoliths by merely focusing the laser beam. Furthermore, the mean size of the nanoparticles can be varied easily by using capping agents and by varying their type and concentration. Our technique is simple, extremely flexible, and compatible with existing photolithographic techniques. It allows fabrication of islands of semiconductor nanoparticles with a spatial resolution of tens of microns, comparable, for example, to that of photodiode arrays, and could be used for microfabrication purposes.

4.6. REFERENCES

[1.] V. C. Sundar, H. J. Eisler, and M. G. Bawendi *Adv Mater* **14**,739 (2002).

[2.] B. Capoen, T. Gacoin, J. M. Nedelec, S. Turrell, and M. Bouazaoui *J Mater Sci* **36**,2565 (2001).

[3.] N. Tohge, M. Asuka, and T. Minami *SPIE* **1328**, 125 (1990).

[4.] J. M. Wallace, J. K. Rice, J. J. Pietron, R. M. Stroud, J. W. Long, and D. R. Rolison *Nano Lett* **3**,1463 (2003).

[5.] M. Fukushima, H. Yanagi, S. Hayashi, N. Suganuma, and Y. Taniguchi *Thin Solid Films* **39**, 438 (2003).

[6.] S. A. Maier, M. D. Friedman, P. E. Barclay, and O. Painter *Appl Phys Lett* **86**,1103 (2005).

7. F. Stellacci, C. A. Bauer, T. Meyer-Friedrichsen, W. Wenseleers, V. Alain, S. M. Kuebler, S. J. K. Pond, Y. Zhang, S. R. Marder, and W. J. Perry *Adv Mater* **14**,194 (2002).

8. M .F. Bertino, R. R. Gadipalli, J. G. Story, C. G. Williams, G. Zhang, C. Sotiriou-Leventis, A. T. Tokuhiro, S. Guha, and N. Leventis *Appl Phys Lett* **85**, 6007 (2004).

9. (a) N. Leventis, I. A. Elder, D. R. Rolison, M. L. Anderson, and C. I. Merzbacher *Chem. Mater*. **11**, 2837(1999), (b) E. W. Bohannan, X. Gao, K. R. Gaston, C. D. Doss, C. Sotiriou-Leventis, and N. Leventis *J Sol-Gel Sci Technol* 23, 235 (2002).

10. I. Kaur, D. K. Pandya, and K. L. Chopra *J Electrochem Soc*. **127**, 943 (1980).

11. N. C. Sharma, R. C. Kainthla, D. K. Pandya, and K. L. Chopra *Thin Solid Films* **60**, 55 (1979).

12. S. C. Sahu, and S. N. Sahu *Thin Solid Films* **235**, 17 (1993).

13. P. C. Rieke, and S. B. Bentjen *Chem Mater* **5**, 43 (1993).

14. G. A. Kitaev, A. A. Uritskaya, and S. G. Mokrushin *Zhurnal Fizicheskoi Khimii* **38**, 2065 (1965).

15. A. A. Uritskaya, G. A. Kitaev, and N. S. Belova *Russian JAppl Chem* **75**, 846 (2002).

16. P. C. Rieke, and B. Bentjen *Chem Mater* **5**, 5322 (1993).

17. I. Kaur, D. K. Pandya, and K. L. Chopra *J Electrochem Soc* **127**, 943 (1980).

18. M. F. Bertino, J. F. Hund, J. Sosa, G. Zhang, C. Sotiriou-Leventis, N. Leventis, A. T. Tokuhiro, and J. Terry *J Non-Cryst Solids* 333, 108 (2004).

19. Y. Nosaka *J Phys Chem* 95, 5054 (1991).

20. P. E. Lippens, and M. Lannoo *Phys Rev B* 39, 10935 (1989).

21. H. F. De Brabander, and L. C. Van Poucke *J Coord Chem* **3**, 301 (1974), F. F. Said, and D. G. Tuck *Inorg Chem Acta* **59**, 1 (1982).

22. D. Hayes, O. I. Mitit, M. T. Nenadovit, V. Swayambunathan, and D. Meisel *J Phys Chem* **93**, 4603 (1989).

23. R. R. Gadipalli, L. A. Martin, J. G. Story, B. Heckman, M. F. Bertino, N. Leventis, P. Fraundorf, and S. Guha. *J Sol-Gel Sci Technol* **39**, 299 (2006).

24. J. Huang, K. Sooklal, C. J. Murphy, and H. J. Ploehn *Chem Mater* **11**, 3595 (1999).

25. W. H. Green, K. P. Le, J. Grey, T. T. Au, and M. J. Sailor *Science* 276, 1826 (1997).

26. V. Bekiari, and P. Lianos *Langmuir* **14**, 3459 (1998).

27. L. T. Canham, A. Loni, P. D. J. Calcott, A. J. Simons, C. Reeves, M. R. Houlton, J. P. Newey, K. J. Nash, and T. I. Cox *Thin Solid Films* **276**, 112 (1996).

28. J. O. Sintera, N. Gomeza, S. Gatzerta, C. E. Schmidt, and B. A. Korgel *Colloids and Surfaces A: Physicochem Eng Aspects* **254**, 147 (2005).

29. A. G. Rolo, L. G. Vieira, M. J. M. Gomes, J. L. Ribeiro, M. S. Belsley, and M. P. dos, Santos *Thin Solid Films* **312**, 348 (1998).

30. W. Xu, Y. Liao, and D. A. Akins, *J Phys Chem B* **106**, 11127 (2002).

31. M. Kundu, A. A. Khosravi, S. K. Kulkarni, and P. Singh *J Mater Sci* **32**, 245 (1997).

32. R. B. Khomane, A. Manna, A. B. Mandale, and B. D. Kulkarni *Langmuir* **18**, 8237 (2002).

PAPER -IV

5. QUANTUM DOTS BY ULTRAVIOLET AND X-RAY LITHOGRAPHY

Massimo F Bertino[1,7], Raghuveer R Gadipalli[1], Lane A Martin[1], Lauren E Rich[1], Alexey Yamilov[1], Brian R Heckman[2], Nicholas Leventis[3,8], Suchi Guha[4], John Katsoudas[5], Ralu Divan[6] and Derrick C Mancini[6]

[1]*Department of Physics, University of Missouri-Rolla, MO 65409, USA*

[2]*Midwest Research Institute 425 Volker Blvd. Kansas City, MO 64110, USA*

[3]*Department of Chemistry, University of Missouri-Rolla, MO 65409, USA*

[4]*Department of Physics, University of Missouri-Columbia, Columbia, MO 65211, USA*

[5] *Center for Synchrotron Radiation Research and Instrumentation, Illinois Institute of Technology, Chicago, IL 60616, USA*

[6]*Center for Nanoscale Materials, Argonne National Laboratory, 9700 S. Cass Ave., Bldg. 440 Rm. A130 Argonne, IL 60439-4812, USA*

[7] *Corresponding author. Tel.: +1-573 341 6221; fax: +1-573 341 4715. Email: Massimo@umr.edu*

[8] *Corresponding author. Tel.: +1-573 341 4391 Email: leventis@umr.edu*

5.1. ABSTRACT

Highly luminescent semiconductor quantum dots have been synthesized in porous materials with ultraviolet and X-ray lithography. For this, the pore-filling solvent of silica hydrogels is exchanged with an aqueous solution of a group II metal ion together with a chalcogenide precursor such as 2-mercaptoethanol, thioacetamide or selenourea. The chalcogenide precursor is photodissociated in the exposed regions yielding metal

chalcogenide nanoparticles. Patterns are obtained by using masks appropriate to the type of radiation employed. The mean size of the quantum dots is controlled by adding capping agents such as citrate or thioglycerol to the precursor solution, and the quantum yield of the composites can be increased to up to about 30% by photoactivation. Our technique is water-based, uses readily available reagents, and highly luminescent patterned composites are obtained in a few simple processing steps. Polydispersity, however, is high, (around 50%), preventing large-scale usage of the technique for the time being. Future developments that aim at a reduction of the polydispersity are presented.

5.2. INTRODUCTION

In the last few years, a wide array of quantum dot-based devices and composites have been proposed for applications ranging from non-linear optics[1-4] to light emitting diodes,[5,6] sensors,[7-9] and lasers.[10-12] Large-scale use of these devices and materials, however, is limited by cost and manufacturing issues. It was recognized early that applications could be made more readily available if quantum dots could be synthesized with bottom-up techniques which are compatible with conventional microfabrication methods such as photolithography.[13] However, progress in this direction has been sluggish. Only very recently patterning of substrates with quantum dots was reported, and it was obtained with a top-down approach photocorrosion of films of pre-formed quantum dots.[14]

We recently demonstrated that quantum dots can be synthesized in selected regions of porous matrices by photodissociation of appropriate precursors. In the first

demonstration of our photolithographic technique the precursors were dissociated thermally by focused infrared light (IR).[15,16] Heat diffusion, however, rendered use of masks impractical. Only relatively primitive patterns could be produced by translating the sample in front of the focused beam. We then showed that ultraviolet light (UV) could also be employed to pattern substrates with quantum dots.[17] However, photodissociation of the thiol precursors employed in the UV experiments was not very efficient. The incident light had to be tightly focused, and patterns could be produced only by translating the sample in front of a small illuminated spot as in the IR case. In addition, the composites produced with both IR and UV lithographies had a very low quantum yield, below 1%. Here we expand those methods and we show that: (i) photodissociation can be made more efficient by using a different set of precursors, allowing production of complex patterns by masking; (ii) the quantum yield of the composites can be increased to up to about 30% by photoactivation; (iii) quantum dots can be produced with X-ray lithography. Our quantum dot photolithography (QDPL) technique has therefore come a long way, and includes several attractive features, each of which has deep implications for applications. For example, we now have precursor combinations that are easily photodissociated. Thus, it may be possible to use conventional ultraviolet exposure and masking tools to produce quantum dots. The high quantum yield of the composites, combined with their porosity, may allow applications of the materials as optical materials and sensors. X-ray lithography paves the way to ultra-high spatial resolution. In our experiments, comparatively hard X-rays (8.5keV) for which masks can be realized which have a resolution of tens of microns were employed. However, it is conceivable that soft X-rays could be employed, for which masks can be fabricated with a resolution well

below 1 μm.[18] We have also observed that features produced with X-ray lithography penetrated into the bulk of the monoliths as much as 12 mm. These structures have an aspect ratio of around 200 and could conceivably be employed as waveguides. In fact, materials such as PbS have a much higher index of refraction ($n = 4.1$) than the matrix ($n = 1.1$ to 1.5) for silica gels. Addition of PbS in a concentration of as little as 0.1% by volume to a silica gel increases the index of refraction of the composite by $\Delta n \approx 5 \times 10^{-3}$, which is sufficient for waveguide applications. The main drawback of the technique, at this point, is probably polydispersity. This was estimated to be around 50% from the fwhm of the exciton peak in the absorption spectra. Polydispersity might be eliminated by using matrices with well-contolled pore size, such as MCM-41,[19] or by size-selective photocorrosion,[14, 20, 21] and this is where our research will focus in the near future.

5.3. EXPERIMENTAL

5.3.1. Sample preparation. Silica hydrogels were prepared following a conventional base-catalyzed route.[22] The hydrogels were then washed several times in methanol and water. Hydrogel cylinders were then cut into smaller cylinders of about 7 mm in diameter, and 5-7 mm in length. These cylinders were then immersed in 20 ml of a solution of a group II and a group VI precursor. To produce CdS composites with ultraviolet photolithography, the precursor solution consisted of $Cd(NO_3)_2$ in a concentration of up to 0.5 mol·l^{-1} (M) and thioacetamide (CH_3CSNH_2), or thiourea (H_2NCSNH_2), in concentrations of up to 0.5 M. The metal:sulfur mole ratio was typically kept around 1:1. To produce CdSe composites with ultraviolet photolithography, the precursor solution consisted of $Cd(ClO_4)_2·xH_2O$ (x~6), in a concentration of up to 0.1 M

and selenourea ($H_2NCSeNH_2$), also in a concentration of up to 0.1 M. The metal:chalcogenide mole ratio was kept typically around 4:1. The metal and the chalcogenide precursors tended to react at room temperature even without irradiation. To prevent spontaneous formation of metal chalcogenides, a chelating agent such as triethanolamine was added to the precursor solution, in a concentration equal to that of the metal precursor. Alternatively, the vials containing the gels and the precursor solution were cooled to 5 ^{0}C. For X-ray lithography the bathing solution contained $Cd(NO_3)_2$ or $Pb(NO_3)_2$ in a concentration between 0.01 and 0.05 M. The chalcogenide source was 2-mercaptoethanol, in a typical concentration of 1 M. The precursor solutions for X-ray lithography were stable at room temperature, and cooling was not required. In all experiments, diffusion of the precursors inside the gels was usually complete within 2 hours, at which point the gels were irradiated. Gels and bathing solution were kept under Ar during preparation and irradiation. Unreacted precursors were removed after exposure by placing the samples in a large volume (>100 ml) of cold water. This washing procedure was repeated 3-4 times. Particle size was controlled by adding a capping agent like citrate or 2-mercaptoethanol in a concentration up to 10 times higher than that of the metal ion to the bathing solutions.

5.3.2. Irradiation. <u>Ultraviolet</u> The light source for ultraviolet photolithography was a high pressure, 100 W Hg arc discharge lamp, whose light was collimated on the sample either with a long focal length lens, or with a standard collimator system. Hydrogels filled with the precursor solution were placed in a quartz cuvette, filled with some of the solution for index matching, and placed in front of the beam. To prepare masks, a pattern was printed on paper with a laser printer, and a reduced copy was transferred on an

acetate transparency with a standard copier. The mask was then placed on the outer surface of the cuvette, and the sample was irradiated.

X-Ray Irradiations were carried out at the Materials Research Collaborative Access Team (MRCAT) bending magnet beamline, at Argonne National Laboratory's Advanced Photon Source. The beamline has a beam-defining mask upstream of an 880 mm long in-vacuum platinum coated mirror held at an angle of 8 mrad used as a low pass energy filter. The low energy spectrum of the beamline is defined by 375 μm thickness of beryllium windows. The final dimensions of the collimated beam are approximately 100 mm by 6 mm. The beam was not monochromatic; the mean beam energy was 8.5 keV, and the fwhm of the energy distribution was around 6 keV. To prevent heating and damage to the gel structure, gels were translated in front of the beam at a typical speed of 20 mm/s. Hard X-Ray masks for ultradeep X-Ray lithography (UDXRL) were fabricated by electrodepositing a Au absorber layer with a thickness on the order of 50 μm on a thin (0.5 mm) graphite sheet. A detailed description of the mask fabrication procedure can be found in Ref. 23.

5.3.3. Characterization. Samples were characterized with UV-Vis optical absorption spectroscopy, photoluminescence spectroscopy, and Raman spectroscopy. Optical absorption spectra of hydrogel-quantum dot composites were taken with a CARY 5 UV-Vis-NIR spectrophotometer. Photoluminescence spectra were taken using a JY-Horiba Fluorolog 3-22 Fluorometer. Raman spectra were obtained using the 514.5 nm line of an Ar^+ laser and a SPEX 0.85 m double spectrometer equipped with a liquid N_2 cooled charge coupled device array detector, or using a Renishaw micro-Raman spectrometer with a 785 nm excitation line. Due to the challenges of PbS Raman spectroscopy, a

reference PbS powder was prepared separately. The powder was obtained by adding 0.1 M Na_2S to a 0.1 M $Pb(NO_3)_2$ solution. The precipitate was filtered and washed several times with water, methanol, and ethanol. The resulting powder was polydisperse, with grains varying from about 10 nm to a few microns.

5.3.4. Quantum Yield Measurements. Two different procedures were used to measure the quantum yield of the composites. In one case, a sample was illuminated with uncollimated UV light to produce a uniform distribution of semiconductor nanoparticles through the monolith. The emission of the composite was compared to that of a hydrogel which had the same dimensions of the composite, and where the solvent had been exchanged with a rhodamine solution. Alternatively, a CdSe spot with a diameter *ca*. 1 mm was produced in a thin (*ca*. 1 mm) hydrogel. Exposure time and lens focal length were chosen such that the CdSe pattern penetrated through the sample, giving rise to a cylindrical feature. The sample was then illuminated through a mask which had the same diameter as the CdSe pattern, and the emission was compared to that of a rhodamine-loaded sample illuminated through the same mask. For both procedures, the UV-Vis spectrum of the composite and reference monolith were measured to account for differences in absorption. To rule out sample inhomogeneity and geometry issues measurements were repeated for at least four composite samples prepared under the same conditions, and for 4-5 samples loaded with varying rhodamine concentrations.

5.4. RESULTS AND DISCUSSION

5.4.1. Pattern Generation. Figure 5.1 shows sample patterns obtained by masking. Figure 5.1(a) shows a CdSe pattern obtained with UV photolithography. The image was

taken under room lighting. Figure 5.1(b) shows the luminescence of the pattern in (a), excited by an Ar^+ laser. Figure 5.1 (c) and (d) show PbS patterns obtained with X-Ray lithography. For ease of representation, comparatively large patterns were produced. The resolution of the QDPL technique, however, is at least on the order of a few microns. A point resolution of about 3 μm was attained in our previous experiments by focusing an Ar ion laser beam on the surface of a gel with a low-magnification microscope objective. For the X-ray technique, a resolution on the order of 10 μm was obtained, which coincided with the fabrication limit of the X-ray mask.[23]
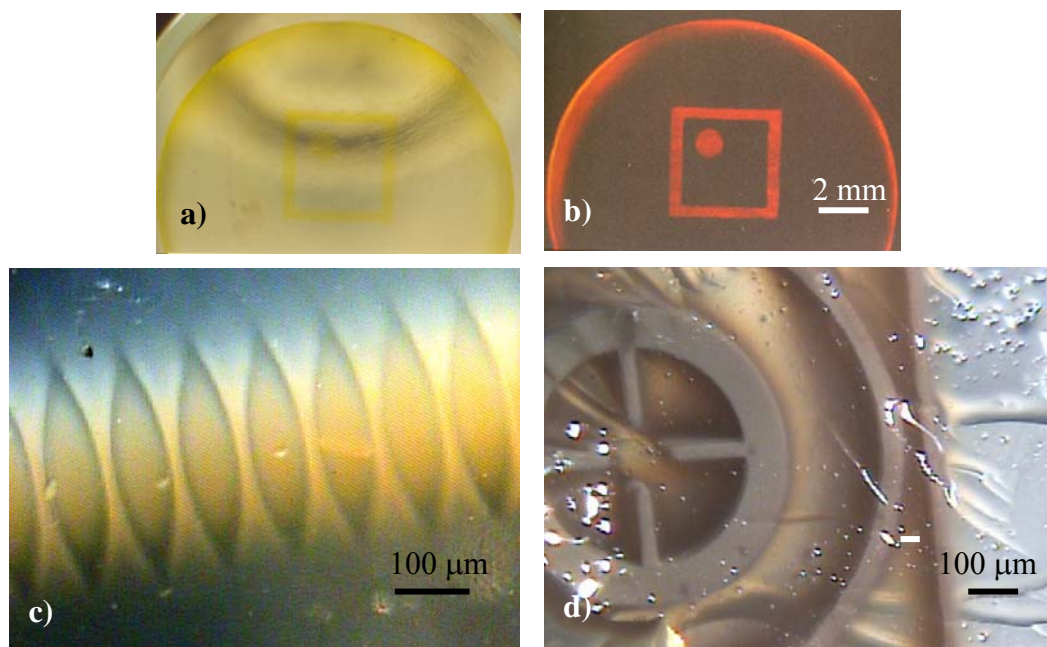
Figure 5.1. (a-b) CdSe patterns obtained with UV lithography. (b) Shows the photoluminescence of sample (a), obtained by illuminating the patterned sample with the 457.9 nm line of an Ar^+ laser. A laser goggle was interposed between the sample and the camera to filter the laser glare from the photoluminescence of the CdSe quantum dots. (c-d) PbS patterns obtained with X-Ray lithography.

5.4.2. Photodissociation and Reaction Mechanisms. <u>Ultraviolet</u>. The UV technique is based on the photodissociation of chalcogenide precursors. In our initial experiments, we employed a solution of Cd^{2+} and a thiol (RSH) like 2-mercaptoethanol.[17] Ultraviolet irradiation dissociated the thiols, yielding CdS. Photodissociation of these precursors, however, was not very efficient, and patterns could be created only by exposing matrices to tightly focused beams. In this work, we use different chalcogenide precursors which are also dissociated by UV light: thioacetamide, thiourea and selenourea. The overall reaction scheme leading to chalcogenide nanoparticles is shown in Eqs. (1) and (2) for thioacetamide.[24]

$$CH_3CSNH_2 + h\nu \rightarrow CH_3CN + H_2S \tag{1}$$

$$Cd^{2+} + H_2S \rightarrow CdS + 2H^+ \tag{2}$$

Use of selenourea as a source of selenium ions was investigated recently by other groups.[25-27] It was found that selenourea photodissociates easily, but care must be taken to avoid oxidation of Se^{2-}.[27] In our experiments, oxidation of the Se anions was prevented by the capping agents, citrate and thioglycerol, which are reducing agents.

The chalcogenide precursors employed in the present experiments were more easily photodissociated than the precursors used previously. In samples containing the same precursor concentration clearly visible patterns were formed 5-10 times more rapidly when selenourea was used instead of the 2-mercaptoethanol (RSH) used previously. In addition, the molar absorptivity at 254 nm (Hg line) of the Cd^{2+}-RSH precursor combination is 3.2×10^4 $M^{-1} \cdot cm^{-1}$,[17] the molar absorptivity of Cd^{2+}-selenourea is 1.0×10^4 $M^{-1} \cdot cm^{-1}$. When the differences in absorptivities and exposure times are

taken into account, we obtain that UV irradiation of Cd^{2+}-selenourea is 15 to 30 times more efficient than that of Cd^{2+}-RSH.

X-Ray For X-ray lithography the chalcogenide precursor was 2-mercaptoethanol. 2-mercaptoethanol is dissociated and liberates SH^- when it reacts with the solvated electrons and radicals liberated by the interaction of X-rays with water.[28,29] The overall reaction leading to metal chalcogenides is reported in Eqs. (3-5). Reduction of the metal ions by the solvated electrons, Eq. (6), was prevented by working in a large excess of thiol, typically 10-100 times the metal ion concentration.

$$H_2O + h\nu \rightarrow e^-_{(aq)} \; H^., OH^., H_3O^+, ... \tag{3}$$

$$HOCH_2CH_2SH + e^-_{(aq)} \rightarrow SH^- + {}^.CH_2CH_2OH \tag{4}$$

$$SH^- + Pb^{2+} \rightarrow PbS + H^+ \tag{5}$$

$$Pb^{2+} + 2e^-_{(aq)} \rightarrow Pb^0 \tag{6}$$

Patterns were formed readily with X-ray lithography. Typically, an exposure to 85 mA · minute was sufficient to generate clearly visible patterns. This exposure is very low when compared to more conventional X-ray lithography processes such as LIGA. These processes are usually based on radiation-induced cross-linking of polymers like poly(methyl metacrylate) (PMMA) which require extremely lengthy exposures. On our apparatus, PMMA structures were obtained after exposures on the order of 40000 mA · minute. We also noticed that the chalcogenide patterns penetrated inside the gels for several millimeters, suggesting that X-Ray lithography could be employed to fabricate three-dimensional quantum dot structures with a high aspect ratio.

5.4.3. Materials Characterization. Semiconductor nanoparticles form within the exposed regions, and do not diffuse appreciably in the unexposed regions, at least within

the limits of our measurements. The dimensions of the photolithographed features always coincided with those of the features on the masks, at least within the resolution of the optical microscope used for the measurements (~1 μm).[30] The mean particle size was most efficiently controlled by adding capping agents to the precursor solution. The effect of capping agents on the mean particle size is shown in Figure 5.2. CdSe samples capped with citrate exhibited an excitonic shoulder in the 570-580 nm range, which corresponds to a mean nanoparticle size of 5 nm.[31] Samples capped with a stronger capping agent such as thioglycerol exhibited an excitonic shoulder in the 430-440 nm range, corresponding to a mean nanoparticle size of 2.3 nm.[32] We point out, however, that the excitonic shoulders were always very broad, independent of the capping agent that we employed. The large fwhm of these shoulders is a clear indicator of polydispersity. In experiments from other groups, weak, undefined shoulders were associated with ~50% polydispersity, which is probably a realistic figure for our experiments.[20] We point out that size distribution histograms measured with transmission electron microscopy were not meaningful. In fact, for sizes below about 5 nm it is exceedingly difficult to distinguish the nanoparticles from density fluctuations of the silica matrix.
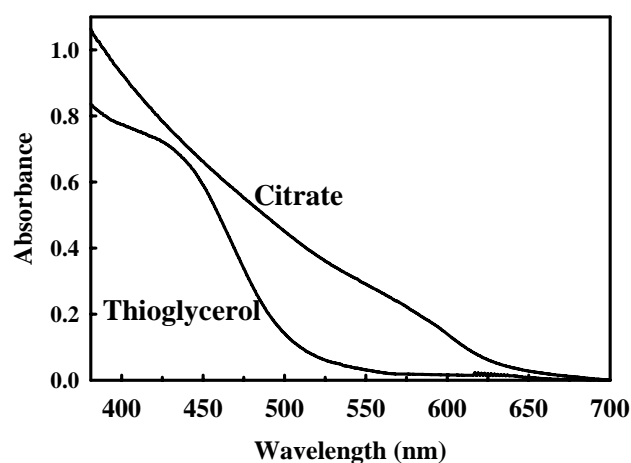
Figure 5.2. UV-Vis absorption spectra of CdSe patterns produced with UV photolithography and the indicated capping agents in a concentration of 3.5×10^{-3} M. The parent solution contained 1.6×10^{-3} M cadmium perchlorate and 4×10^{-4} M selenourea.

The as-grown composites were poorly luminescent, which is common for quantum dots grown in aqueous environment. The luminescence, however, could be increased considerably by photoactivation. For this, unreacted precursors were first washed out of the hydrogels. The samples were then exposed to a low power (~15 W) black light. Light absorption by II-VI nanoparticles can induce oxidation of the chalcogenide, Equation (7).[20,31,32] Surface defects are photooxidized preferentially, thus photoactivation is a convenient way to remove such defects and improve the photoluminescence quantum yield.[20,21,33-46]

$$CdSe + O_2 + h\nu \rightarrow Cd^{2+} + SeO_2 \tag{7}$$

Figure 5.3 reports the results of a typical photoactivation treatment of a CdSe-patterned sample. The emission of as-grown samples was very weak, but increased by more than 300 times with photoactivation. The emission maximum was around 580 nm before photoactivation, and around 560 nm at the end of the photoactivation period. The blue shift of the emission indicates that the mean size of the nanoparticles is reduced by photoactivation. Particle size reduction upon illumination has also been reported by other groups[14,20,21,32] and is not surprising, since photoactivation removes atoms preferentially, but not exclusively, from surface defects. Luminescence quantum yields were determined with two different procedures which are described in the Experimental section. The quantum yields calculated with these procedures were quite consistent and indicated that the quantum yield of citrate-stabilized quantum dot composites could be increased to up to 30%.[32] This high value of the quantum yield is in substantial agreement with recent reports of photoactivation of quantum dots. For example, citrate-capped CdSe quantum dots can be photoactivated to reach a quantum yield as high as 59%. The quantum yield of our composites is comparable or higher than the quantum yield of commercially available polymer/quantum dot composites,[40] and to the quantum yield of recently reported latex spheres decorated with quantum dots and of photonic crystals (opals) infiltrated with quantum dots.[47] All these composites have a quantum yield on the order of 10%.[48]
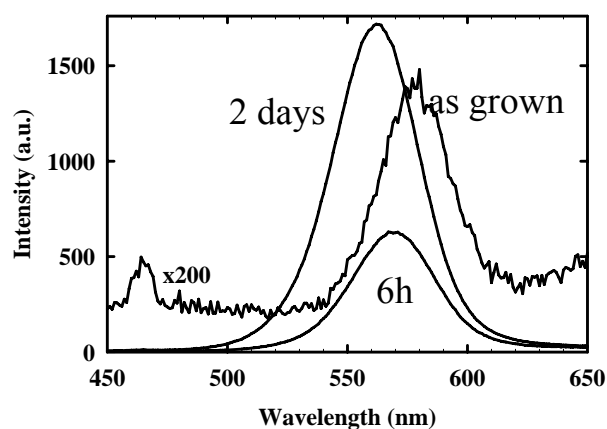
Figure 5.3. Photoactivation of a CdSe/silica composite. The parent solution contained 1.6 $\times$ 10^{-3} M cadmium perchlorate, 3.5 $\times$ 10^{-3} M sodium citrate and 4 $\times$ 10^{-4} M selenourea. Samples were photoactivated for the indicated times with a black light with a power of 15 W. Samples were excited with 400 nm light.

The chemical identity and the structure of the nanoparticles in the patterned regions were investigated in our previous reports with techniques such as Raman spectroscopy, transmission electron microscopy, X-Ray diffraction, and X-Ray photoelectron spectroscopy. All these techniques showed that the nanoparticles were free of contamination, and that they had a bulk crystalline structure. In this work, we characterized the nanoparticles with Raman spectroscopy, and the results were in agreement with our previous research.[15-17] Representative Raman spectra are shown in Figure 5.4 for CdS and PbS patterns obtained with X-Ray lithography. CdS patterns exhibited a peak at 303 cm^{-1}. This frequency is in good agreement with previous Raman measurements of CdS/silica composites, and corresponds to the first-order longitudinal optical (LO) phonon frequency of CdS.[15-17,49] The interpretation of the Raman results for

PbS is more complex. The LO phonon of crystalline PbS at ~205 cm^{-1} in normal Raman scattering is forbidden. However, using an excitation source close to the intergap energies allows the forbidden Raman bands through the Fröhlich interaction mechanism.[50] The Raman spectrum of bulk PbS contains mainly three peaks at 154, 204, and 454 cm^{-1}.[51] The 154 cm^{-1} peak is a combination of a transverse acoustic (TA) and a transverse optic (TO) phonon; the 204 peak is the first-order LO phonon and the 450 is the first overtone of the LO phonon (2LO). Our Raman measurements from a PbS powder show the first-order LO phonon at 200 cm^{-1} and a peak at 143 cm^{-1} which probably arises due to a combination of TA and TO phonons. The Raman spectrum from monoliths patterned with PbS shows the second and the third order LO phonons peaks at 440 and 610 cm^{-1}, respectively. Observation of overtones which are not detected in the bulk appears to be a common phenomenon in nanocrystals,[49] and has been reported for PbS nanoparticles with a mean size of 1.5 nm.[52] The origin of the 240 cm^{-1} is still under investigation; this could be the first-order LO phonon that has an enhanced peak position due to the size of the nanocrystal. In 2 nm PbS nanocrystals, for example, the forbidden LO phonon appears at 230 cm^{-1}.[53] We notice that a shoulder around 240 cm^{-1} is also evident in the spectra of the PbS powder.
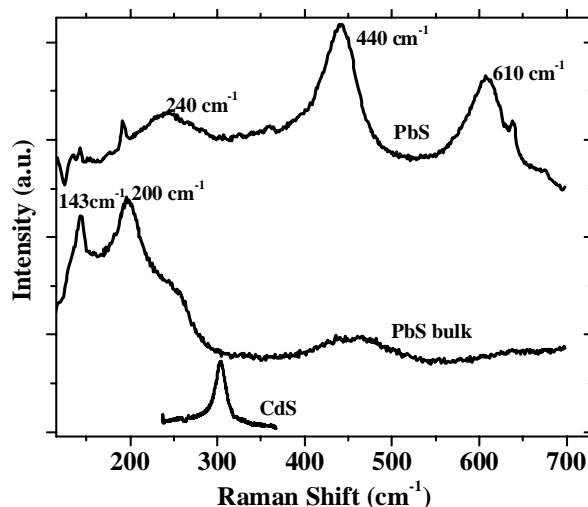
Figure 5.4. Room temperature Raman spectra of PbS and CdS produced by X-ray lithography in silica hydrogels and measured with lines at 785 nm and 514 nm, respectively. The Raman spectrum of a PbS powder is also shown for reference.

5.5. CONCLUSION

In conclusion, we have demonstrated a method of generating quantum dots with photolithography which has several important features. Quantum dots can be synthesized with UV and X-ray lithographies, which have a very high theoretical spatial resolution. The process is water-based and highly luminescent composites can be fabricated in a few steps. The quantum yield of the composites can be increased with photoactivation to up to 30%, which is comparable to the quantum yield of the best commercial quantum dot composites. The main drawback of the technique, at this point, is probably polydispersity, which was estimated to be around 50% from the fwhm of the exciton peak in the absorption spectra. Polydispersity might be eliminated by using matrices with

well-controlled pore size, or by size-selective photocorrosion, and this is where our research will focus in the near future.

5.6. ACKNOWLEDGEMENTS

5.7. REFERENCES

[1.] N. Tohge, M. Asuka and T. Minami *SPIE* **1328**, 125, (1990).

[2.] B. Capoen, T. Gacoin, J. M. Nedelec, S. Turrell and M. Bouazaoui *J. Mater. Sci*. **36**, 2565, (2001).

[3.] H. –M. Gong, X. –H. Wang, Y. –M. Du and Q. –Q. Wang *J. Chem. Phys*. **125**, 024707, (2006).

[4.] Y. Lin, J. Zhang, E. Kumacheva and E. H. Sargent *J. Mater. Sci*. **39**, 993, (2004).

[5.] S. Coe, W.K. Woo, M. G. Bawendi and V. Bulovic *Nature* **420**, 800, (2002).

[6.] L. Bakueva, S. Musikhin, M. A. Hines, T. -W. F. Chang, M. Tzolov, G. D. Scholes and E. H. Sargent *Appl. Phys. Lett*. **82**, 2895, (2003).

[7.] G. W. Walker, V. C. Sundar, C. M. Rudzinski, A. W. Wun, M. G. Bawendi and D. G. Nocera *Appl. Phys. Lett*. **83**, 3555, (2003).

8. Y. Chen and Z. Rosenzweig *Anal. Chem*. **74**, 5132, (2002).

9. K. M. Gattás-Asfura and R. M. Leblanc *Chem. Comm*. **21**, 2684, (2003).

10. V. C. Sundar, H. –J. Eisler and M. G. Bawendi *Adv. Mater*. **14**, 739, (2002).

11. V. I. Klimov, A. A. Mikhailovsky, S. Xu, A. Malko, J. A. Hollingsworth, C. A. Leatherdale, H. –J Eisler and M. G. Bawendi *Science* **290**, 314, (2004).

12. R. D. Schaller, M. A. Petruska and V. I. Klimov *J. Phys. Chem. B* **107**, 13765, (2003).

13. H. K. Schmidt *Proc. SPIE* **1758**, 396, (1992).

14. T. Torimoto, S. –Y. Murakami, M. Sakuraoka, K. Iwasaki, K. –I. Okazaki, T. Shibayama and B. Ohtani *J Phys. Chem. B* **110**, 13314, (2006).

15. M. F. Bertino, R. R. Gadipalli, J. G. Story, C. G. Williams, G. Zhang, C. Sotiriou-Leventis, A. T. Tokuhiro, S. Guha and N. Leventis *Appl. Phys. Lett*. **85**, 6007, (2004).

16. R. R. Gadipalli, L. A. Martin, B. Heckman, J. G. Story, M. F. Bertino, P. Fraundorf, S. Guha and N. Leventis *J. Sol-gel Sci. Tech*. **40**, 101, (2006).

17. M. F. Bertino, R. R. Gadipalli, L. A. Martin, J. G. Story, B. Heckman, S. Guha and N. Leventis *J. Sol-gel Sci. Tech*. **39**, 299, (2006).

18. H. I. Smith and F. Cerrina *Microlithography World* **6**, 10, (1997).

19. C. T. Kresge, M. E. Leonowicz, W. J. Roth, J. C. Vartuli and J. S. Beck *Nature* **359**, 710, (1992).

20. H. Matsumoto, T. Sakata, H. Mori and H. Yoneyama *J. Phys. Chem*. **100**, 13781, (1996).

21. T. Torimoto, H. Kontani, Y. Shibutani, S. Kuwabata, T. Sakata, H. Mori and H. Yoneyama *J. Phys. Chem. B* **105**, 6838, (2001).

22. N. Leventis, I. A. Elder, D. R. Rolison, M. L. Anderson and C. Merzbacher I *Chem. Mater*. **11**, 2837, (1999).

23. R. Divan, D. C. Mancini, S. M. Gallagher, J. Booske and D. Van der Weide *"Improvements in Graphite-Based X-ray Mask Fabrication for Ultra-Deep X-ray Lithography"* *Microsystem Technologies* **10**, 728, (2004).

24. C. Y. Wang, X. Mo, Y. Zhou, Y. R. Zhu, H. T. Liu and Z. Y. Chen *J. Mater. Chem*. **10**, 607, (2000).

25. W. –B. Zhao, J. –J. Zhu and H. –Y. Chen *Journal of Crystal Growth* **252**, 587, (2003).

26. Y. –W. Lin, M. –M. Hsieh, C. –P. Liu and H. –T. Chang *Langmuir* **21**, 728, (2005).

27. Y. –W. Chena, X. –L. Zhou, J. Tong, Y. Truong and N. Belzile *Analytica Chemica Acta* **545**, 149, (2005).

28. D. Hayes, O. I. Micic, M. T. Nenadovic, V. Swayambunathan and D. Meisel *J. Phys. Chem*. **93**, 4603, (1989).

29. M. Mostafavi, Y. P. Liu, P. Pernot and J. Belloni *Radiat. Phys. Chem*. **59**, 49, (2000).

30. M. F. Bertino, J. F. Hund, J. Sosa, G. Zhang, C. Sotiriou-Leventis, N. Leventis, A. T. Tokuhiro and J. Terry *J. Non-Cryst. Solids* **333**, 108, (2004).

31. Y. Wang, Z. Tang, M. A. Correa-Duarte, I. Pastoriza-Santos, M. Giersig, N. A. Kotov, and L. M. Liz-Marzan *J. Phys. Chem. B* **108**, 15461, (2004).

32. A. L. Rogach, A. Kornowski, M. Gao, A. Eychmüller and H. Weller *J. Phys. Chem. B* **103**, 3065, (1999).

33. D. Meissner, R. Memming and B. Kastening *J . Phys. Chem*. **92**, 3476, (1988).

34. D. Meissner, I. Lauermann, R. Memming and B. Kastening *J. Phys. Chem*.**92**, 3484, (1988).

35. C. E. Bunker, B. A. Harruff, P. Pathak, A. Payzant, L. F. Allard and Y.-P. Sun *Langmur* **20**, 5642, (2004).

36. W. G. J. H. M. van Sark, P. L. T. M. Frederix, D. J. Van den Heuvel, H. C. Gerritsen, A. A. Bol, J. N. J. van Lingen, C. de Mello Donega and A. Meijerink *J. Phys. Chem. B* **105**, 8281, (2001).

37. V. P. Kunets, N. R. Kulish, M. P. Lisitsa and V. P. Bryksa *Semiconductors* **38**, 447, (2004).

38. J. A. Kloepfer, S. E. Bradforth and J. L. Nadeau *J. Phys. Chem. B* **109**, 9996, (2005).

39. A. van Dijken, A. H. Janssen, M. H. P. Smitsmans, D. Vanmaekelbergh and A. Meijerink *Chem. Mater.* **10**, 3513, (1998).

40. J. O. Winter, N. Gomez, S. Gatzert, C. E. Schmidt and B. A. Korgel *Colloids and Surfaces A: Physicochem. Eng. Aspects* **254**, 147, (2005).

41. Y. Wang, Z. Tang, M. A. Correa-Duarte, L. M. N. A. Liz-Marzan and Kotov *J. Am. Chem. Soc.* **125**, 2830, (2003).

42. M. Jones, J. Nedeljkovic, R. J. Ellingson, A. J. Nozik and G. Rumbles *J. Phys. Chem. B*. **107**, 11346, (2003).

43. S. R. Cordero, P. J. Carson, R. A. Estabrook, G. F. Strouse and S. K. Buratto *J. Phys. Chem. B*. **104**, 12137, (2000).

44. A. A. Bol and A. Meijerink *J. Phys. Chem. B*.**105**, 10203, (2001).

45. L. Manna, E. C. Scher, L.-S. Li and A. P. Alivisatos *J. Am. Chem. Soc.* **124**, 7136, (2002).

46. Y. C. Cao and J. Wang *J. Am. Chem. Soc.* **126**, 14336, (2004).

47. G. R. Maskaly, M. A. Petruska, J. Nanda, I. V. Bezel, R. D. Schaller, H. Htoon, J. M. Pietryga and V. I. Klimov *Adv. Mater*. **18**, 343, (2006).

48. W. Sheng, S. Kim, J. Lee, S.-W. Kim, K. Jensen and M. G. Bawendi *Langmuir* **22**, 3782, (2006).

49. A. G. Rolo, L. G. Vieira, M. J. M. Gomes, J. L. Ribeiro, M. S. Belsley and M. P. dos Santos *Thin Solid Films* **312**, 348, (1998).

50. M. Reedyk, C. Thomsen, M. Cardona, J. S. Xue and J. E. Greedan *Phys. Rev. B* **50**, 13762, (1994).

51. G. D. Smith, S. Firth, R. J. H. Clark and M. Cardona *J. Appl. Phys*. **92**, 4375, (2002).

52. T. D. Krauss and F. W. Wise *Phys. Rev. B* **55**, 9860, (1997).

53. T. D. Krauss, F. W. Wise and D. B. Tanner *Phys. Rev. Lett*. **76**, 1376, (1996).

PAPER-V

6. THREE-DIMENSIONAL SEMICONDUCTOR PATTERNING

R.R. Gadipalli[1], L.A. Martin[1], L.E. Rich[1], J.G. Story[1], A. Yamilov[1], M.F. Bertino[2,*],

B. Heckman[3], N. Leventis[4,*], S. Guha[5]

[1]*Department of Physics, University of Missouri-Rolla, MO 65409, USA*

[2]*Department of Physics, Virginia Commonwealth University, Richmond, VA*
Email: Massimo@umr.edu
* Corresponding author. Tel.: +1-573 341 6221; fax: +1-573 341 4715.

[3]*Midwest Research Institute 425 Volker Blvd. Kansas City, MO 64110*

[4]*Department of Chemistry , University of Missouri-Rolla, MO 65409, USA E-mail: leventis@umr.edu*
* Corresponding author. Tel.: +1-573 341 4391.

[5]*Department of Physics, University of Missouri-Columbia, Columbia, MO 65211, USA*

6.1. ABSTRACT

Three-dimensional patterns of semiconductor nanoparticles were produced inside silica hydrogels by multiphoton ionization. The pore-filling solvent of silica hydrogels was exchanged with an aqueous solution of a group II metal ion and 2-mercaptoethanol or selenourea. Metal chalcogenide nanoparticles were formed in the spots where the light of a pulsed laser was focused. The lithographed features had an elongated shape with a minimum diameter of 30 microns and a minimum length of 60 microns. Optical, photoluminescence and Raman spectroscopies confirmed the chemical identity of the nanoparticles in the patterned regions. The mechanism of formation was investigated, and it was established that the process is at least 2-photon in nature and that patterning can be

achieved with either femtosecond or nanosecond pulses. The experiments also suggested that chalcogenide anions were not liberated by direct dissociation of the chalcogenide. Rather, the chalcogenide dissociated after capturing solvated electrons and radicals liberated by multi-photon ionization of water.

6.2. INTRODUCTION

In the last few years, a considerable amount of research has focused on the three-dimensional fabrication of contacts and electronic devices,[1-19] on the fabrication of quantum dot devices,[20-31] and on the fabrication of three-dimensional (3D) optical integrated circuits.[32-43] We present here a technique that allows 3D fabrication of semiconductor nanoparticles which is of potential relevance for these seemingly unrelated fields. For example, three-dimensional (3D) fabrication techniques that employ pulsed lasers have been reported, but they were limited until now to metals.[1-19] We show here that pulsed lasers can be applied also to fabricate 3D semiconductor patterns which might be employed to fabricate 3D opto-electronic circuitry that includes passive and active components. We also show that it is possible to pattern monoliths with high index materials such as PbS. We present estimates showing that the index of refraction of the patterned regions can be considerably higher than that of the matrix. Thus, our technique might also be employed for the fabrication of three-dimensional, all-optical circuitry that includes optically active materials. The technique could be used in its present form for applications that do not require monodisperse nanoparticles, or a high luminescence quantum yield. We anticipate that the technique might be also applied for 3D quantum dot fabrication. In fact both polydispersity and quantum yield can be controlled by

photocorrosion, as repeatedly demonstrated by several groups.[44-49] For example, we recently demonstrated that the quantum yield of CdSe quantum dots produced with UV lithography could be increased from ≤ 1% to up to about 30% by photoactivation.[49]

6.3. EXPERIMENT

Silica hydrogels were prepared following a conventional base-catalyzed route.[50] The hydrogels were then immersed in a solution of a group II and a group VI precursor. To produce sulfides, the bathing solution contained $Cd(NO_3)_2$ or $Pb(NO_3)_2$ in a concentration between 0.01 and 0.05 mol·l^{-1} (M), and 2-mercaptoethanol or thioglycerol in a concentration of 1 M. To produce selenides, metal concentrations were on the order of 4×10^{-3} M, and selenourea was used in a concentration on the order of 1×10^{-3} M. Precursors diffused inside the gels in 1-2 hours, and after this time the samples were removed from the solution and exposed. Unreacted precursors were removed after exposure by repeatedly bathing the samples in distilled water. Most irradiations were carried out using the frequency-doubled output ultraviolet light (532 nm) from a pulsed ND:YAG laser (Continuum Surelite I, q-switched). Pulses of 5 ns duration with a 20 Hz repetition rate were used. The energy per pulse was 200 mJ, producing a time averaged power of 1.1 Watts. The beam was focused down to a spot of 30 μm in diameter, and the estimated power in the focal region was on the order of 1 TW·cm^{-2}. For some experiments, a beam was employed from a Ti:Sapphire laser femtosecond (fs) laser at the Kansas Light Source, Kansas State University. This beam had a pulse length of 30 fs, a repetition rate of 1 kHz and an energy of 0.14 mJ per pulse. Hydrogels filled with precursor solutions were placed in a quartz cuvette, filled with some of the solution for

index matching, placed in front of the beam, and moved in front of the beam with precision, two-axis translation stages. The light was focused on the samples typically by a 10X, 0.25 numerical aperture objective.

Samples were characterized with UV-Vis optical absorption spectroscopy, photoluminescence spectroscopy, and Raman spectroscopy. Optical absorption spectra of hydrogel-quantum dot composites were taken with a CARY 5 UV-Vis-NIR spectrophotometer. Photoluminescence spectra were taken using a JY-Horiba Fluorolog 3-22 Fluorometer. Raman spectra were obtained using the 514.5 nm line of an Ar^+ laser and a SPEX 0.85 m double spectrometer equipped with a liquid N_2 cooled charge coupled device array detector, or using a Renishaw micro-Raman spectrometer with a 785 nm excitation line.

6.4. RESULTS AND DISCUSSION

Figure 1(a) and (b) show the top view and respectively the side view of PbS patterns obtained with ns pulses. The patterned regions are clearly at different depths within the monolith, and complex patterns could be easily obtained, as shown in figure Figure 1(c). Damage of the gel matrix was often observed when the laser was operated at powers higher than $0.1 \ TW \cdot cm^{-2}$. In figure 1(d) we show a typical patterned region, which was obtained at a laser power slightly above the damage threshold. The beam was incident from the top. We notice some damage in the focal region, and an elongated dark feature extending in the direction of the beam axis. The elongated shape of the patterns is in agreement with previous reports of patterning with multiphoton ionization, and has been attributed to beam self-focusing induced by an increased refraction index in the

exposed region.[43, 51, 52] The diameter and length of the patterns could be varied from a minimum of 30×60 µm to up to 200×600 µm by decreasing the magnification of the microscope objective or by increasing the exposure time.
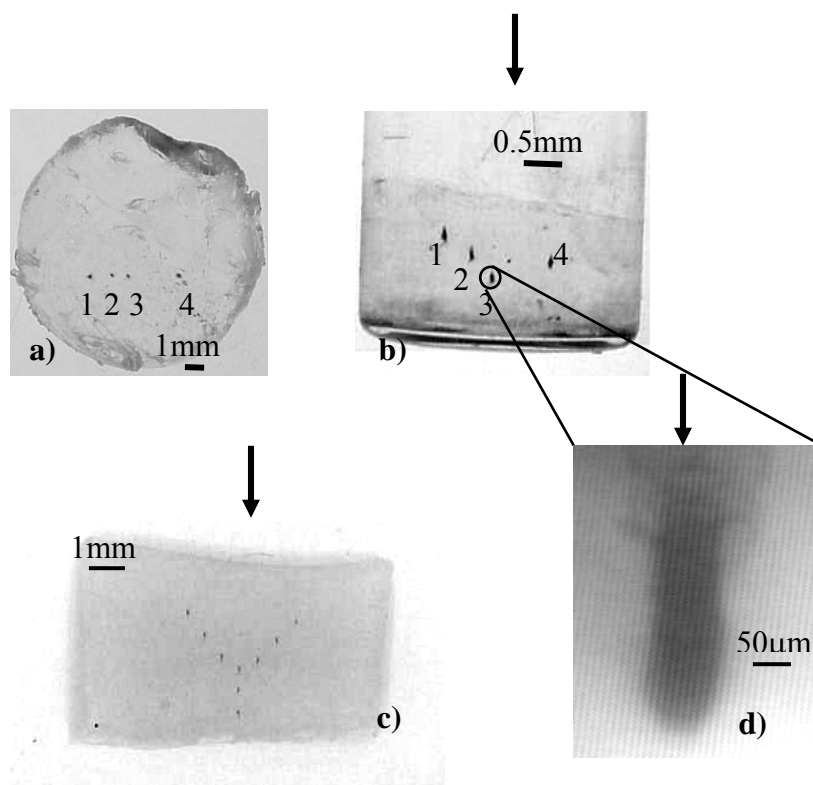
Figure 6.1. (a) top view and (b) side view of sample PbS patterns. The side view of a pattern obtained by mounting a sample on a precision x-y-z translation stage is shown in (c). (d) Optical microscope image of a patterned region. Arrows indicate the incident beam direction.

The chemical identity of the nanoparticles in the patterned regions was determined with standard characterization techniques such as optical absorption, photoluminescence and Raman spectroscopy. Absorption spectra showed a monotonic

increase of the absorbance with decreasing wavelength and broad excitonic shoulders, as

shown in figure 2a) for PbS and in figure 2b) for CdSe. From the positions of the

excitonic shoulders a mean particle size around 5 nm was estimated for both PbS and

CdSe.[53-55] We point out, however, that the broadness of the shoulders indicates that the

samples were quite polydisperse and therefore the mean particle size should only be

regarded as a rough estimate.
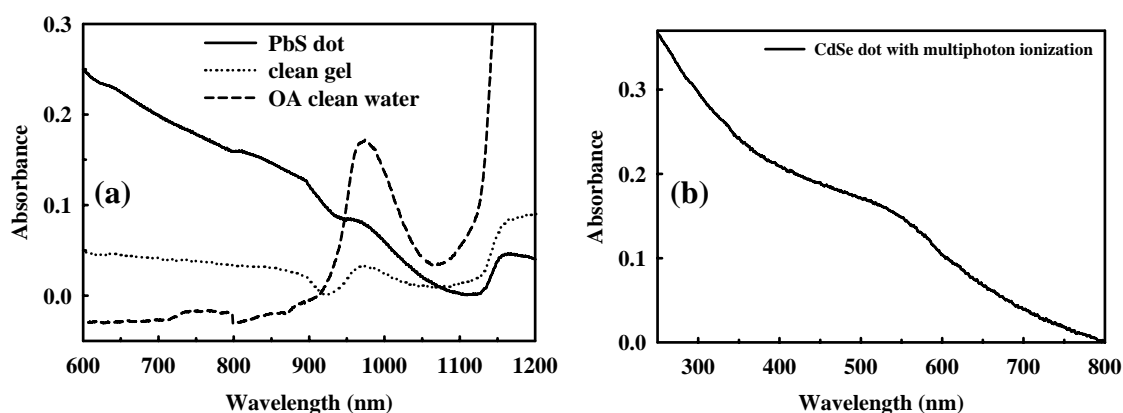
Figure 6.2. Optical absorption of a) PbS-patterned samples, and b) CdSe-patterned

samples. In a), sepactra were taken from wet hydrogel monoliths, and overtones of water

vibrations were measured at ~975 nm and ~1160 nm.

Photoluminescence spectra were measured for CdS-patterned samples and a

representative spectrum is reported in figure 3a). A very broad emission peak dominated

the spectrum in the 450-700 nm region, consistent with surface trap recombination. Two

sharp peaks around 400 and, respectively, 425 nm were also evident in the spectrum. The

peak at 400 nm can be reconciled with the emission from defects in silica gels,[21, 56-60]

while the peak at 425 nm is probably due to the intrinsic luminescence of

quantum-confined CdS nanoparticles.[21] Overall, the emission spectrum of figure 3a) is consistent the conventional picture of water-based quantum dot synthesis, which is known to yield polydisperse, defect-rich nanoparticles. Raman spectra are reported in figure 3b) for a CdS-patterned sample and show a peak around 310 cm^{-1} which is in overall agreement with the frequency of the first order longitudinal optical mode of bulk CdS.[15, 61-67] The characterization experiments showed therefore that polydisperse metal chalcogenide nanoparticles were formed in the patterned regions.
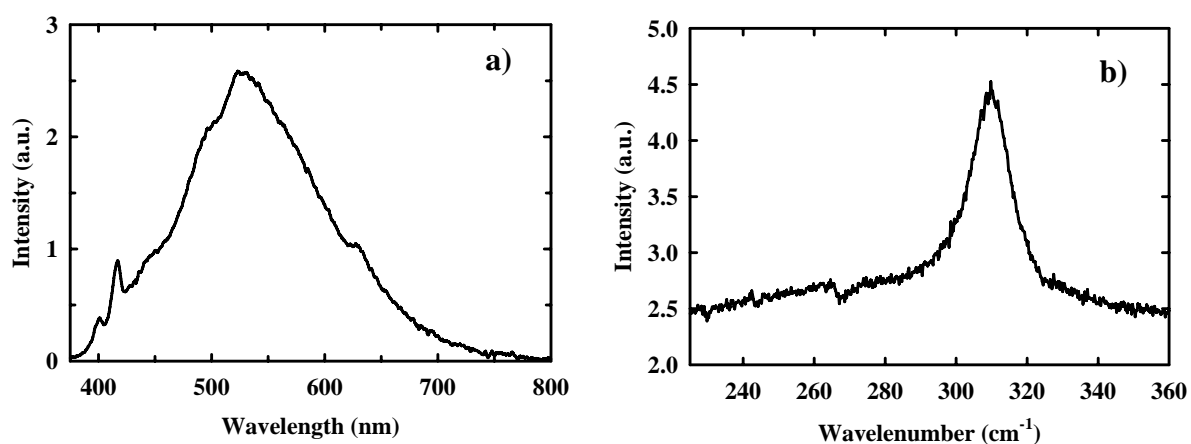
Figure 6.3. a) Room temperature photoluminescence spectrum of a CdS-patterned sample. The excitation wavelength was 352 nm. b) Raman spectrum of a CdS-patterned sample.

The mechanism of nanoparticle formation in the exposed regions was investigated with a series of control experiments. To rule out single-photon photochemical reactions we exposed samples to the 488 nm and, respectively, 532 nm lines of a continuous-wave Ar ion laser. The illuminated spots remained transparent and patterns did not form even when laser powers were employed which were sufficient to damage the gels. We then

exposed samples to the focused light of a 2W, continuous-wave Nd:YAG laser emitting at an infrared wavelength of 1064 nm. No particles formed in the illuminated spots, ruling out thermally induced chemical reactions. We concluded that the chemical process was two- or multi-photon in character. To make sure that the sulfur precursor was not directly dissociated by the incident light we replaced the sulfur source, 2-mercaptoethanol, with other precursors which are often used to generate metal sulfides such as thioacetamide and thiourea. None of these precursors generated nanoparticles, suggesting that multiphoton dissociation of sulfur-containing organic molecules does not play a relevant role. Dissociation of the sulfur precursors likely followed an indirect path and was probably triggered by the radicals liberated by water ionization. The power in the focal spot was between 0.01 and 0.1 TW $\cdot$ cm^{-2}, which is sufficient to ionize water, and it is known that 2-mercaptoethanol liberates SH^{-} after scavenging solvated electrons.[68-70] A possible overall reaction scheme is reported in Eqs. (1-3). To confirm our conjecture, we added an electron scavenger such as 2-propanol to the parent solution and noticed that nanoparticles were not formed.

$$H_2O + h\nu \rightarrow e^{-}_{(aq)}, \overset{\cdot}{H}, \overset{\cdot}{OH}, H_3O^{+}, \ldots \tag{1}$$

$$HOCH_2CH_2SH + e^{-}_{(aq)} \rightarrow SH^{-} + \overset{\cdot}{C}H_2CH_2OH \tag{2}$$

$$SH^{-} + Pb^{2+} \rightarrow PbS + H^{+} \tag{3}$$
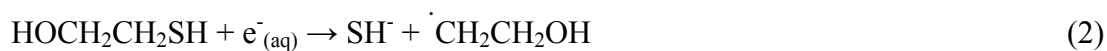
The mechanism of formation of selenide nanoparticles probably also did not proceed via direct dissociation of selenium compounds. Irradiation of monoliths loaded

only with selenourea did not yield elemental selenium nanoparticles which are the typical by-product of selenourea dissociation.[71,72] The fact that chalcogenide nanoparticles formed with selenourea and not with thiourea as a precursor is probably reconcilable with the higher reactivity of selenourea. For example, recent experiments have shown that selenourea scavenges radicals 6-7 times more efficiently than thiourea,[71] and our own group showed that chalgodenide nanoparticles are formed 5-10 times more efficiently by ultraviolet irradiation when selenourea is used instead of thiourea or 2-mercaptoethanol.[49] The higher reactivity of selenourea is confirmed by the current experiments, where selenide nanoparticles formed 5-10 times more rapidly than sulfides. Oxidation of selenium anions to elemental selenium was probably prevented by the addition of citrate, which acted both as a surfactant and as a reducing agent.

The concentration of PbS nanoparticles was estimated from the optical absorption spectra of figure 2. Recent work[54] has shown that the extinction coefficient σ of PbS depends strongly the radius r of the nanoparticles. An extinction coefficient was calculated in Ref. [54] by integrating absorption spectra in the visible and near infrared ranges and was found to depend exponentially on the radius:

$$\sigma\,(\mathrm{M^{-1} \cdot cm^{-1}}) = 5.15 \times 10^5\, r^{4.08} \tag{4}$$

The extinction coefficient was calculated from Eq.(4) assuming a particle radius r = 2.5 nm and the absorbance α was calculated by integrating the spectrum of figure 2a). The patterns in the sample used for optical absorption had a depth d = 0.7 mm, and a PbS particle concentration was obtained:

$$c_{opt} = \frac{\alpha}{\sigma d} = 3.5 \times 10^{-5}\ \mathrm{M} \tag{5}$$

This nanoparticle concentration is very close to the one that can be estimated from the precursor concentration. The parent solution had a Pb^{2+} concentration $c_0 = 0.05$ M; the molecular weight of PbS is $MW = 239.25$, and the density is $\rho = 7.5$ g $\cdot$ l^{-1}; assuming a mean particle size $r = 2.5$ nm, the particle concentration is

$$c = \frac{c_0 MW}{\frac{4}{3}\pi r^3 \rho} = 4 \times 10^{-5} \text{ M} \qquad\qquad (6)$$

The concentration of CdSe nanoparticles was also calculated from absorption spectra and was also found in fair agreement with the concentration of the parent solution. The molar absorptivity of polydisperse CdSe quantum dots is $\sigma = 4 \times 10^{-5}$ $M^{-1} \cdot cm^{-1}$,[45,46] the absorbance of the excitonic shoulder in figure 2b) is $\alpha = 0.14$ and the depth of the patterns was $d = 0.7$ mm. From Eq. (5), we obtain a nanoparticle concentration $c_{opt} = 5 \times 10^{-6}$ M. The parent solution of the samples in figure 2b) had a selenourea concentration $c_0 = 1.2 \times 10^{-3}$ M; CdSe has a molecular weight $MW = 191.38$ and a density $\rho = 5.81$ g $\cdot$ l^{-1}; for a mean particle size $r = 2.5$ nm, Eq.(6) yields $c = 1.0 \times 10^{-6}$ M. These concentration estimates are approximate, especially considering that the uncertainty in the mean particle radius is probably very large. However, they consistently show that the particle concentration calculated from the optical absorption is comparable to that estimated from the concentration of the parent solution. Based on the estimated nanoparticle concentration we can also estimate the index contrast in the patterned regions. In experiments with PbS, the precursor concentration was $c_0 = 0.05$ M. The volume fraction is $f = \frac{V_{PbS}}{V_{matrix}} = \frac{c_0 MW}{\rho} = 0.16\%$. The corresponding change in the dielectric constant is $\varepsilon_{composite} = (1 - f)\varepsilon_{matrix} + f\varepsilon_{PbS}$, and the refractive index of the

composite is $n_{composite} = \sqrt{\varepsilon_{composite}}$. If PbS nanoparticles with a dielectric constant $\varepsilon_{PbS} =$ 17.0 were embedded in a xerogel (or aerogel) matrix with a dielectric constant $\varepsilon_{matrix} \sim$ 1.69 ($n_{matrix} = 1.310$) the index of the composite would be $n_{composite} = 1.310$, or $\Delta n = 0.01$. Thus, the index contrast that is theoretically attainable with our technique is 2-5 times higher than the index contrast $\Delta n = 1\text{-}4 \times 10^{-3}$ that is typically obtained by densification of glasses with fs pulses.[32, 34, 37, 43]

6.5. CONCLUSION

In conclusion, we have shown that chalcogenide nanoparticles can be produced in the bulk of porous sol-gel materials such as silica hydrogels. Patterning is obtained by focusing a pulsed laser beam inside the bulk of a monolith, and can be achieved with femtosecond-pulsed lasers but also with cheaper and simpler with nanosecond-pulsed lasers. The process is multi-photon in character, and is probably induced by the scavenging of solvated electrons by chalcogenide-containing organic molecules. These molecules dissociate liberating chalcogenide anions that react with the metal cations. The nanoparticle concentration in the exposed regions was estimated from absorption spectra and was found comparable to the density estimated from the precursor concentration in the parent solution. The estimated index contrast is 2-5 times higher than the contrast commonly obtained by fs-pulse induced glass densification and is sufficient for light guiding applications. Our technique allows three-dimensional patterning with semiconductor nanoparticles and could be used for a variety of applications, ranging from construction of three-dimensional, quantum-dot based electronic applications to the fabrication of optically active photonic crystals and optical circuitry.

6.6. ACKNOWLEDGEMENTS

6.7. REFERENCES

1. Pu-Wei, W. Cheng, I. B. Martini, B. Dunn, B. J. Schwartz, and E. Yablonovitch, *Adv. Mater*. **12**, 1438 (2000).

2. A. Ishikawa, T. Tanakaa, and S. Kawata, *Appl. Phys. Lett*. **89**, 113102, (2006).

3. Y. S. Chen, A. Tal, D. B. Torrance, and S. M. Kuebler, *Advanced Functional Materials* **16**, 1739, (2006).

4. C. N. LaFratta, D. Lim, K. O'Malley, T. Baldacchini, and J. T. Fourkas, *Chemistry Of Materials*, **18**, 2038, (2006).

5. J. H. Moon, J. Ford, and S. Yang, *Polymers For Advanced Technologie,s* **17**, 83, (2006).

6. I. Pastoriza-Santos, J. Perez-Juste, G. Kickelbick, and L. M. Liz-Marzan, *Journal Of Nanoscience And Nanotechnology* **6**, 453, (2006).

7. T. Tanaka, A. Ishikawa, and S. Kawata, *Appl. Phys. Lett*. **88**, 081107, (2006).

8. F. Formanek , N. Takeyasu, T. Tanaka , K. Chiyoda, A. Ishikawa, and S. Kawata, *Optics Express* **14**, 800, (2006).

9. J. H. Moon, and S. Yang *Journal Of Macromolecular Science-Polymer Reviews C*, **45**, 351, (2005).

10. J. Perez-Juste, I. Pastoriza-Santos, L. M. Liz-Marzan, and P. Mulvaney *Coordination Chemistry Reviews* **249**, 1870, (2005).

11. A. S. Korchev, T. S. Shulyak, B. L. Slaten, W. F. Gale, and G. Mills *J. Phys. Chem. B*, **109**, 7733, (2005).

12. H. B. Sun, and S. Kawata *Advances In Polymer Science*, **170**, 169, (2004).

13. T Baldachin, A. C. Pons, J. Pons, C. N. LaFratta, J. T. Fourkas, Y. Sun, and M. J. Naughton *Optics Express*, **13**, 1275, (2005).

14. J. F. Hund, M. F. Bertino, G. Zhang, C. Sotiriou-Leventis, and N. Leventis, *Journal Of Non-Crystalline Solids* **350**, 9, (2004).

15. M. F. Bertino, R. R. Gadipalli, J. G. Story, C. G. Williams, G. Zhang, C. Sotiriou Leventis, A. T. Tokuhiro, S. Guha, and N. Leventis *Appl. Phys. Lett*, 85, 6007, (2004).

16. V. I. Boev, J. Perez-Juste, I. Pastoriza-Santos, C. J. R. Silva, M. D. J. M. Gomes, and L. M. Liz-Marzan, *Langmuir* **20**, 10268, (2004).

17. O. L. A. Monti, J. T. Fourkas, D. J. Nesbitt *J. Phys. Chem. B*, **108**, 1604, (2004).

18. M. F. Bertino, J. F. Hund, J. Sosa, G. Zhang, C. Sotiriou-Leventis, N. Leventis, A. T. Tokuhiro, and J. Terry, *Journal Of Non-Crystalline Solids*, **333**, 108, (2004).

19. F. Stellacci, C. A. Bauer, T. Meyer-Friedrichsen, W. Wenseleers, V. Alain, S. M. Kuebler, S. J. K. Pond, Y. D. Zhang, S. R. Marder, and J. W. Perry, *Adv. Mater.* **14**, 194, (2002).

20. N. Tohge, M. Asuka, and T. Minami, *SPIE*, **1328**, 125 (1990).

21. B. Capoen, T. Gacoin, J. M. Nedelec, S. Turrell, and M. Bouazaoui, *J. Mater. Sci.* **36**, 2565 (2001).

22. H.-M. Gong, X.-H. Wang, Y.-M. Du, and Q.-Q. Wang, *J. Chem. Phys.* **125**, 024707, (2006).

23. Y. Lin, J. Zhang, E. Kumacheva, and E. H. Sargent, *J. Mater. Sci*. **39**, 993, (2004).

24. S. Coe, W.-K. Woo, M. G. Bawendi, and V. Bulovic, *Nature*, **420**, 800, (2002).

25. S. Bakueva, S. Musikhin, M. A. Hines, T.-W. F. Chang, M. Tzolov, G. D. Scholes and E. H. Sargent, *Appl. Phys. Lett*. **82**, 2895, (2003).

26. G. W. Walker, V. C. Sundar, C. M. Rudzinski, A. W. Wun, M. G. Bawendi, and D. G. Noceraa, *Appl. Phys. Lett*. **83**, 3555, (2003).

27. Y. Chen, and Z. Rosenzweig, *Anal. Chem*., **74**, 5132, (2002).

28. K. M. Gattás-Asfura, and R. M. Leblanc, *Chem. Comm*., **21**, 2684, (2003).

29. V. C. Sundar, H.-J. Eisler, and M. G. Bawendi, *Adv. Mater*. **14**, 739 (2002).

30. V. I. Klimov, A. A. Mikhailovsky, S. Xu, A. Malko, J. A. Hollingsworth, C. A. Leatherdale, H.-J. Eisler, and M. G. Bawendi, *Science* **290**, 314 (2004).

31. R. D. Schaller, M. A. Petruska, and V. I. Klimov, *J. Phys. Chem. B*, **107**, 13765, (2003).

32. J. W. Chan, T. R. Huser, S. H. Risbud, J. S. Hayden, D. M. Krola, *Appl. Phys. Lett.* **82**, 2371, (2003).

33. J. W. Chan, T. R. Huser, S. H. Risbud, and D.M. Krol, *Appl. Phys. A*, **76**, 367, (2003).

34. V. R. Bhardwaj, E. Simova, P. B. Corkum, and D. M. Rayner C. Hnatovsky R. S. Taylor B. Schreder, M. Kluge, and J. Zimmer, *J. Appl. Phys.* **97**, 083102, (2005).

35. Q.-Z. Zhao, J.-R. Qiu, X.-W. Jiang, C.-J. Zhao, and C.-S. Zhu, *J. Appl. Phys.* **96**, 7122, (2004).

36. G. Cheng, Y. Wang, J. D. White, Q. Liu, W. Zhao, and G. Chen, *J. Appl. Phys.* **94**, 1304, (2003).

37. A. Saliminia, N. T. Nguyen M.-C. Nadeau, S. Petit, S. L. Chin, and R. Valle´e, *J. Appl. Phys.* 93, 3724, (2003).

38. K. Miura, J. Qiu S. Fujiwara, S. Sakaguchi, and K. Hirao, *Appl. Phys. Lett.* **80**, 2263, (2002).

39. J. Qiu, *Chemical Record*, **4**, 50, (2004).

40. N. Takeshima, Y. Narita, S. Tanaka, Y. Kuroiwa, and K. Hirao, *Optics Letters*, **30**, 352, (2005).

41. N. Takeshima, Y. Narita, T. Nagata, S. Tanaka, and K. Hirao, *Optics Letters*, **30**, 537, (2005).

42. N. Takeshima, Y. Kuroiwa, Y. Narita, S. Tanaka, K. Hirao, *Optics Express*, **12**, 4019, (2004).

43. E. N. Glezer, and E. Mazur *Appl. Phys. Lett.* **71**, 882, (1997).

44. H. Matsumoto, T. Sakata, H. Mori, and H. Yoneyama, *J. Phys. Chem.*, **100**, 13781, (1996).

45. T. Torimoto, H. Kontani, Y. Shibutani, S. Kuwabata, T. Sakata, H. Mori, and Hiroshi Yoneyama, *J. Phys. Chem. B*, **105**, 6838, (2001).

46. T. Torimoto, S.-Y. Murakami, M. Sakuraoka, K. Iwasaki, K.-I. Okazaki, T. Shibayama, and B. Ohtani, *J.Phys. Chem. B*, **110**, 13314, (2006).

47. Y. Wang, Z. Tang, M. A. Correa-Duarte, I. Pastoriza-Santos, M. Giersig, N. A. Kotov, and L. M. Liz-Marzan, *J. Phys. Chem. B*, **108**, 15461, (2004).

48. M. Jones, J. Nedeljkovic, R. J. Ellingson, A. J. Nozik, and G. Rumbles, *J. Phys. Chem. B*, **107**, 11346, (2003).

49. M. F. Bertino, R. R. Gadipalli, L. A. Martin, L. E. Rich, A. Yamilov, B. R. Heckman, N. Leventis, S. Guha, J. Katsoudas, R. Divan, and D. C. Mancini, *Nanotechnology*, **18**, 315603, (2007).

50. N. Leventis, I. A. Elder, D. R. Rolison, M. L. Anderson, and C. I. Merzbacher, *Chem. Mater*. **11**, 2337 (1999).

51. G. Cheng, Y. Wang, J. D. White, Q. Liu, W. Zhao, and G. Chen, *J. Appl. Phys*. **94**, 1304, (2003).

52. S. Kanehira, J. Si, J. Qiu, K. Fujita, and K. Hirao, *Nano Letters*, **5**, 1591, (2005).

53. B. Capoena, A. Martuccib, S. Turrell, and M. Bouazaoui, *Journal Of Molecular Structure*, **651**, 467, (2003).

54. L. Cademartiri, E. Montanari, G. Calestani, A. Migliori, A. Guagliardi, and G. A. Ozin, *J. Am. Chem. Soc*. **128**, 10337, (2006).

55. V. Sukhovatkin, S. Musikhin I. Gorelikov S. Cauchi, L. Bakueva E. Kumacheva, and E. H. Sargent, *Optics Letters*, **30**, 171, (2005).

56. J. R. Lakowicz, I. Gryczynski, Z. Gryczynski, and C. J. Murphy, *J. Phys. Chem. B*, **103**, 7613, (1999).

57. N. De La Rosa-Fox, M. Pinero, R. Litran, and L. Esquivias, *J. Sol-Gel Sci. Techn*. **26**, 947 (2003).

58. T. Iwami, K. Tadanaga, M. Tatsumisago, and T. Minami, *J. Am. Ceram. Soc*. **78**, 1668 (1995).

59. V. Hornebecq, M. Antonietti, T. Cardinal, and M. Treguer-Delapierre, *Chem. Mater*. **15**, 1993 (2003).

60. D. Lawless, S. Kapoor, P. Kennepohl, D. Meisel, and N. Serpone, *J. Phys. Chem*. **98**, 9619 (1994).

61. R. R. Gadipalli, L. A. Martin, B. Heckman, J. G. Story, M. F. Bertino, P. Fraundorf, S Guha, N. Leventis, *J. Sol-gel Sci. Tech*., **40**, 101, (2006).

62. M. F. Bertino, R. R. Gadipalli, L. A. Martin, J. G. Story, B. Heckman, S. Guha, N. Leventis, *J. Sol-gel Sci. Tech*., **39**, 299, (2006).

63. A. G. Rolo, L. G. Vieira, M. J. M. Gomes, J. L. Ribeiro, M. S. Belsley, and M. P. dos Santos, *Thin Solid Films***, 312**, 348 (1998).

64. M. Reedyk, C. Thomsen, M. Cardona, J. S. Xue, amd J. E. Greedan, *Phys. Rev. B***, 50,** 13762 (1994).

65. G. D. Smith, S. Firth, R. J. H. Clark, and M. Cardona, *Phys. Rev. B*, **92**, 4375 (2002).

66. T. D. Krauss and F. W. Wise, *Phys. Rev. B*, **55**, 9860 (1997).

67. T. D. Krauss, F. W. Wise, D. B. Tanner, *Phys. Rev. Lett*. **76**, 1376 (1996).

68. D. Hayes, O. I. Mitit, M. T. Nenadovit, V. Swayambunathan, and D. Meisel, *J. Phys Chem*. **93**, 4603 (1989).

69. M. Mostafavi, Y. P. Liu, P. Pernot, and J. Belloni, *Radiat. Phys. Chem*. **59**, 49 (2000).

70. M. F. Bertino, J. F. Hund, J. Sosa, G. Zhang, C. Sotiriou-Leventis, N. Leventis, A. T. Tokuhiro, and J. Terry, *J. Non-Cryst. Solids*, **333**, 108 (2004).

71. B. Mishra, D. K. Maity, K. I. Priyadarsini, H. Mohan, and J. P. Mittal, *J. Phys. Chem. A* **108**, 1552 (2004).

72. K. I. Priyadarsini, B. Mishra, D. Maity, and H. Mohan, *Phosphorus, Sulfur and Silicon and the Related Elements*, **180**, 985, (2005).

CONCLUSIONS

We have presented a method where porous sol-gel materials and planar substrates can be patterned with semiconductor quantum dots using photolithography. Silica gels and planar substrates are patterned with infrared, ultraviolet, X-rays and multi-photon ionization radiation. Our photolithographic method is a bottom-up method where we can position semiconductor quantum dots and nanoparticles at the required positions in the porous materials and on planar substrates. Arrays of quantum dots are usually fabricated on the surfaces of silica hydrogels. However, by focusing the laser beam inside the monolith, the arrays can be extended into the bulk of silica gels. Arrays of quantum dots can be patterned on planar substrates by focusing a light source on a thin film of a precursor solution. The quantum dot size distribution can be improved, and its mean size reduced by adding capping agents like sodium hexametaphosphate, 2-mercaptoethanol, thioglycerol and sodium citrate, and also by varying the concentration of capping agent. We will now briefly describe the characteristics of the lithographic techniques.

Infrared photolithography allowed patterning the surface and bulk of silica hydrogels and the surface of planar substrates. The diameter of the smallest pattern is 40 μm, which extended inside the silica hydrogel for up to 4 mm. Focusing the IR beam on the surface of the silica hydrogel for shorter times allowed patterning only the surface of the hydrogel, and longer times allowed extending the pattern inside the hydrogel. This infrared photolithography can be employed to pattern silica hydrogels and planar substrates with other inorganic semiconductor quantum dots like CdSe, PbS, PbSe, ZnS and ZnSe, metal nanoparticles like silver and magnetic nanoparticles like Fe_3O_4. The main challenge of our method concerns the choice of the precursors. These must not

react rapidly at room temperature, otherwise the composites will by uniformly loaded with the active phase. The reaction cannot require high temperatures, because this necessitates high laser powers that can damage the host matrix. In the IR patterning of CdS quantum dots, the reaction rate is tuned by varying the NH_4OH concentration. When the concentration of NH_4OH is too low, most of the Cd precipitates as $Cd(OH)_2$ and does diffuse inside the hydrogel. $Cd(OH)_2$ also catalyzes hydrolysis of thiourea, and CdS forms rapidly even in cold samples. At high NH_4OH concentrations, $Cd(NH_3)_4^{2+}$ complexes are formed. These complexes are water soluble, and they diffuse inside the matrix. They also do not catalyze hydrolysis of thiourea as strongly as $Cd(OH)_2$. Temperatures of the order of 35-60 ^0C are required to hydrolyze thiourea at an appreciable rate, and these temperatures are easily reached with IR radiation. This technique is simple, extremely flexible, and compatible with existing photolithographic techniques. It allows fabricating islands of semiconductor nanoparticles with a spatial resolution of tens of microns, comparable, for example, to that of photodiode arrays, and could be used for microfabrication purposes. The main limitation, however, is spatial resolution, which cannot be better than about 40 μm because of heat diffusion.

Ultraviolet photolithography can also be employed for patterning porous matrices and planar substrates. This method is based on photodissociation of metal thiolate precursors of CdS. The Cd precursor is a water-soluble salt such as $CdSO_4$, and the chalcogenide source can be 2-mercaptoethanol, thioacetamide (CH_3CSNH_2), or thiourea (H_2NCSNH_2). cadmium perchlorate hexahydrate ($Cd(ClO_4)_2.6H_2O$) and selenourea ($H_2NCSeNH_2$) were employed as precursors for CdSe formation and sodium citrate or thioglycerol were used as capping agents. The minimum pattern diameter attained in this

method was a few microns. In the future the spatial resolution might be brought to the diffraction limit by employing more elaborate photolithographic set-ups. Since heat diffusion is not an issue with UV, masking could be employed. CdSe patterns produced by employing thioglycerol as a capping agent were highly luminescent without further photoactivation. When sodium citrate was employed as a capping agent then the quantum yield of CdSe quantum dots can be further improved by photoactivation to reach a value as high as 30%. The composites could be employed to fabricate highly stable quantum dot ion sensors, since the porous matrix prevents coagulation and leaching of the nanoparticles in the environment. They can also be used to fabricate sophisticated devices, such as photonic crystals and quantum dot lasers.

X-ray lithography paves the way to ultra-high resolution lithography. A resolution on the order of 10 μm was obtained, which coincided with the fabrication limit of the X-ray mask.Silica hydrogels were patterned with CdS and PbS quantum dots by employing X-rays. $Cd(NO_3)_2$ and $Pb(NO_3)_2$ were used as metal ion precursors and 2-mercaptoethanol was used as a sulphur ion precursor. In this method comparatively hard X-rays were employed, for which masks can be realized which have a resolution of tens of microns. Masks with a resolution well below 1 μm can be employed when soft X-rays are used. Features patterned with X-ray lithography penetrated into the bulk of silica hydrogels as much as 12 mm, suggesting that X-ray lithography could be employed to fabricate three-dimensional quantum dot structures with a high aspect ratio. Our structures have an aspect ratio of around 200 and could conceivably be employed as waveguides. In fact PbS has a higher index of refraction (n=4.1) than the silica hydrogel (n=1), so the addition of PbS in a concentration as low as 0.1% by volume to a silica

hydrogel increases the index of refraction of the hydrogel by $\Delta n \approx 5 \times 10^{-3}$. This is sufficient for waveguide applications.

Multi-photon ionization photolithography can also be employed to pattern silica hydrogels with different semiconductor nanoparticles and quantum dots. A spatial resolution of as low as 10 μm was obtained. PbS, PbSe, CdS and CdSe quantum dots were patterned. $Pb(NO_3)_2$ and $Cd(ClO_4)_2.6H_2O$ were used as Pb and Cd precursors respectively. 2-mercaptoethanol was used as a sulphur precursor in the patterning of PbS. Selenourea was used as a selenium precursor in the patterning of PbSe and CdSe. Thiogycerol was used as a sulphur precursor in the patterning of CdS, and thioglycerol was used as a capping agent in the patterning of CdSe. Translation of the silica hydrogel in front of the multi-photon ionization beam allowed patterning of sophisticated integrated optical components.

VITA

Raghuveer Reddy Gadipalli was born on August 14, 1976, in 8 Incline colony (Godavarikhani), India. He received his primary school education in Singareni Collories High School Sector-III and high school education in Aditya Residential Junor college, Hyderabad. His undergraduate degree in Mathematics, Physics and Chemistry was received in 1996 from Bharatiya Vidhyabhavan's Bhavan's New Science College, affiliated with Osmania University. In 1998, Raghuveer received his Masters Degree in Physics with the specialization is Opto-electronics from Andhra Vidyalaya College of Arts and Science, affiliated with Osmania University. Following the completion of his Masters Degree, Raghuveer worked at Brilliant Junior college, Hyderabad, India for 4 years as a Lecturer for High School students and in Sri Ventakeshwara Junior College, Karimnagar, India for 1 year as a Lecturer for High School students before going to the United States.

In August 2003, he enrolled in the University of Missouri − Rolla (UMR) to obtain his Ph.D. in Physics with the specilaziation of Photolithography of Quantum dots, under the guidance of Dr. Massimo F. Bertino. While pursuing his doctoral studies, he held a Teaching Assistantship in the Physics Department of UMR, and also awarded a Research Assistantship, supported by the Department of Energy and Missouri Research Board.

He has been an active member of the American Physical Society (APS) and American Chemical Society (ACS).

LIST OF PUBLICATIONS

1. M F Bertino, R R Gadipalli, J G Story, C G Williams, G Zhang, C Sotiriou-Leventis, A T Tokuhiro, S Guha, and N Leventis "Laser Writing of Semicnoductor Nanoparticles and Quantum dots", *Appl. Phys. Lett*., , **85**, 6007 (2004).

2. M F Bertino, R R Gadipalli, L A Martin, J G Story, B Heckman, S Guha and N Leventis, 'Patterning porous matrices and planar substrates with quantum dots', *J. Sol-gel Sci. Tech*., , **39**, 299 (2006).

3. R R Gadipalli, L A Martin, B Heckman, J G Story, M F Bertino, P Fraundorf, S Guha and N Leventis, "Infra red quantum dot photolithogrpahy ," *J. Sol-gel Sci. Tech*., **40**, 101 (2006).

4. Massimo F Bertino, Raghuveer R Gadipalli, Lane A Martin, Lauren E Rich, Alexey Yamilov, Brian R Heckman, Nicholas Leventis, Suchi Guha, John Katsoudas, Ralu Divan and Derrick C Mancini, "Quantum dots by ultraviolet and X-ray lithogrpahy", *Nanotechnology* **18**, 315603, (2007).

5. M.F.Bertino, R.R.Gadipalli, L.A.Martin, B. Heckman, N.Leventis S.Guha, J. Katsoudas, R. Divan, and D. C. Mancini, "X-ray lithography of metal and semiconductor nanoparticles", *J. Vaccu. Sci. & Technol.*, (accepted).

6. R.R. Gadipalli, L.A. Martin, L.E. Rich, J.G. Story, A. Yamilov, M.F. Bertino, B. Heckman, N. Leventis, S. Guha, "Three-dimensional semiconductor patterning", (to be published).

7. Michael D. Hoffmann, Emilio A. Nanni, Raghuveer R. Gadipalli, Massimo F. Bertino, Nicholas Leventis, and Akira T. Tokuhiro, "*Quantum dot - gamma ray interaction*", (to be published).